The geochemistry of conglomerates, chert and silica veins from the Fig Tree Group, Barberton Greenstone Belt: implications for Paleoarchean silicification processes

Earth Structure & Dynamics MSc thesis (2022)

Liadh Keogh

1st Supervisor: Prof. Dr. P.R.D Mason (Utrecht University)

2nd Supervisor: Dr. D.L. Roerdink (University of Bergen)

Cover: Fig Tree age conglomerate from Puddingstone Hill.

Photograph by Kimberly Myers (2020)

Universiteit Utrecht

Abstract

Considerable disagreement surrounds the causes of silicification and barite formation in Paleoarchean greenstone belts. Determining the mechanisms responsible for the primary precipitation of these chemical sediments could help identify how these rocks record the evolution of the early oceans, biosphere and geosphere. This thesis focuses on silicified conglomerates, chert and silica veins from three different localities of the ~3.26 Ga Fig Tree Group of the Barberton Greenstone Belt: 1) Eastern Barite Valley 2) the Masenjane Barite Workings and 3) Puddingstone Hill. Chert, jaspilite and ferruginous sediment conglomerate clasts display Rare Earth Element & Yttrium (REE+Y) patterns of heavy REEs enriched over light REEs (HREE>LREE), variably positive Eu anomalies and often super-chondritic Y/Ho ratios. These patterns are consistent with precipitation of these chemical sediments from fluids derived from Archean seawater. Eu anomalies in some of these clasts are more positive than those expected from contemporaneous seawater. This has been used to conclude that low-temperature hydrothermal venting was occurring in some segments of the basin whilst silicification was occurring. Silicified sediments are also represented by some of the conglomerates clasts. These sediments often display REE+Y patterns which deviate from the flat REE+Y patterns expected from sedimentary material. Instead, they also exhibit REE+Y patterns consistent with Archean marine waters. Similar REE+Y patterns are observed in the matrix material of the conglomerates. These results have been used to conclude that sedimentary sequences in the Fig Tree Group were silicified by seawater-derived fluids. REE+Y patterns of some silica veins found in the Eastern Barite Valley and Masenjane Barite Workings also imply formation from a seawater-derived fluid. Mafic signatures observed in these samples also disagree with previous interpretations that these silica veins represent silicified felsic ash. Instead, elevated Cr values indicate relatively deep circulation of a silicifying-fluid through the underlying Onverwacht strata caused these silica veins to form.

Table of Content

1. Introduction

1.1. Background Geology

Representing one of the oldest and best-preserved volcano-sedimentary sequences on Earth, the ~3.552-3.219 Ga Barberton Greenstone Belt (BGB) offers an excellent potential to study the composition, tectonic-style and surface processes of the Early Earth (eg. Viljoen, 1969; Lowe & Byerley, 1999). Located on the eastern margin of the Kaapvaal Craton, South Africa, the NE-SW striking belt of supracrustal rocks is categorised into 3 stratigraphic units.

The oldest of these units, the Onverwacht Group, is composed primarily of ~3.55 to 3.3 Ga komatiites and basalt with a minor felsic component (Stiegler, 2009). Onverwacht volcanism was likely the product rifting and possibly subduction processes, with the presence of subordinate amounts of layered cherts marking hiatuses in submarine volcanic activity (Lowe, 1999c). During the Onverwacht period, surface relief was severely limited and composed of small build-ups of felsic complexes (de Wit et al., 1987).

Following the 300 million years of anorogenic ultramafic to mafic Onverwacht volcanism, there was a major transition in the tectonic style operating in the BGB. This change is recorded by the occurrence of the ~3.225 Ga primarily sedimentary sequence of the Fig Tree Group (de Ronde et al., 1994; Drabon et al., 2019; Stoll et al., 2021). The transitional boundary between the volcanism-dominated Onverwacht environment to the sedimentary Fig Tree regime is marked by the ~3.33-3.26 Ga Mendon Formation (Decker et al., 2015). The Mendon Formation is punctuated by numerous meteorite-impact related spherule layers (Lowe, 2013; Decker et al., 2015). Sedimentation was initiated in the Fig Tree Group in the 3.28–3.23 Ga Mapepe Basin (Heinrichs, 1980; Drabon et al., 2019). The temporal correlation between meteorite spherule beds and Mapepe Basin sedimentation has been used to argue that meteorite bombardment may have been responsible for the initiation of widespread tectonic uplift and the termination of komatiitic volcanism in the BGB (Byrley et al., 1996; Lowe, 2013).

The stratigraphy of the Fig Tree Group is divided based on its location north or south of the Inyoka Fault (Fig. 1). The northern portion of the Fig Tree Group shows lithologies representative of deposition in a predominantly deep water setting such as banded cherts

and carbonaceous mudstone (Reimer, 1983). However, located to the south of the Inyoka Fault, the Mapepe Basin shows a sequence of laminated shales and siltstones in the lower unit, which transition to fine-grained volcaniclastics in the middle of the unit, and further coarsen upwards to detrital barite deposits, chert and conglomerates in the upper-most units (Lowe et al., 1999). The variable lithologies of the Mapepe Formation are indicative of deposition in various environments, ranging from deep marine to alluvial settings (Lamb & Paris, 1988; Lowe et al., 1999). Continuous local uplift of the underlying supracrustal rocks, erosion of terrigenous material, and periodic felsic volcanism would have allowed for fan deltas flanked by these deep-water basins to develop during this time (Drabon, et al. 2019). The southern portion of the Fig Tree Group therefore offers an excellent example to study Paleoarchean basin dynamics and tectonics. This is further strengthened by the fact that metamorphic grade has not exceeded lower greenschist facies, and in most places primary sedimentary structures remain well preserved (Condie et al., 1970).

The youngest member of the BGB, the ~3.22-3.10 Ga Moodies Group, is composed primarily of a quartz-rich sedimentary sequence that reaches up to 3700 m in thickness (Heubeck et al., 1972; Heubeck et al. 1994). The lower Moodies Group contains a fining upwards sequence from conglomerates representing alluvial setting to tidal and deltaic sandstones to shelf deposits, interpreted to having been deposited in an extensional basin (Heubeck et al,. 1994; Hessler & Lowe, 2006). The upper Moodies Group was deposited in a foreland basin which was shorted to incorporate most of the BGB into a fold and thrust belt (Heubeck et al., 1994).

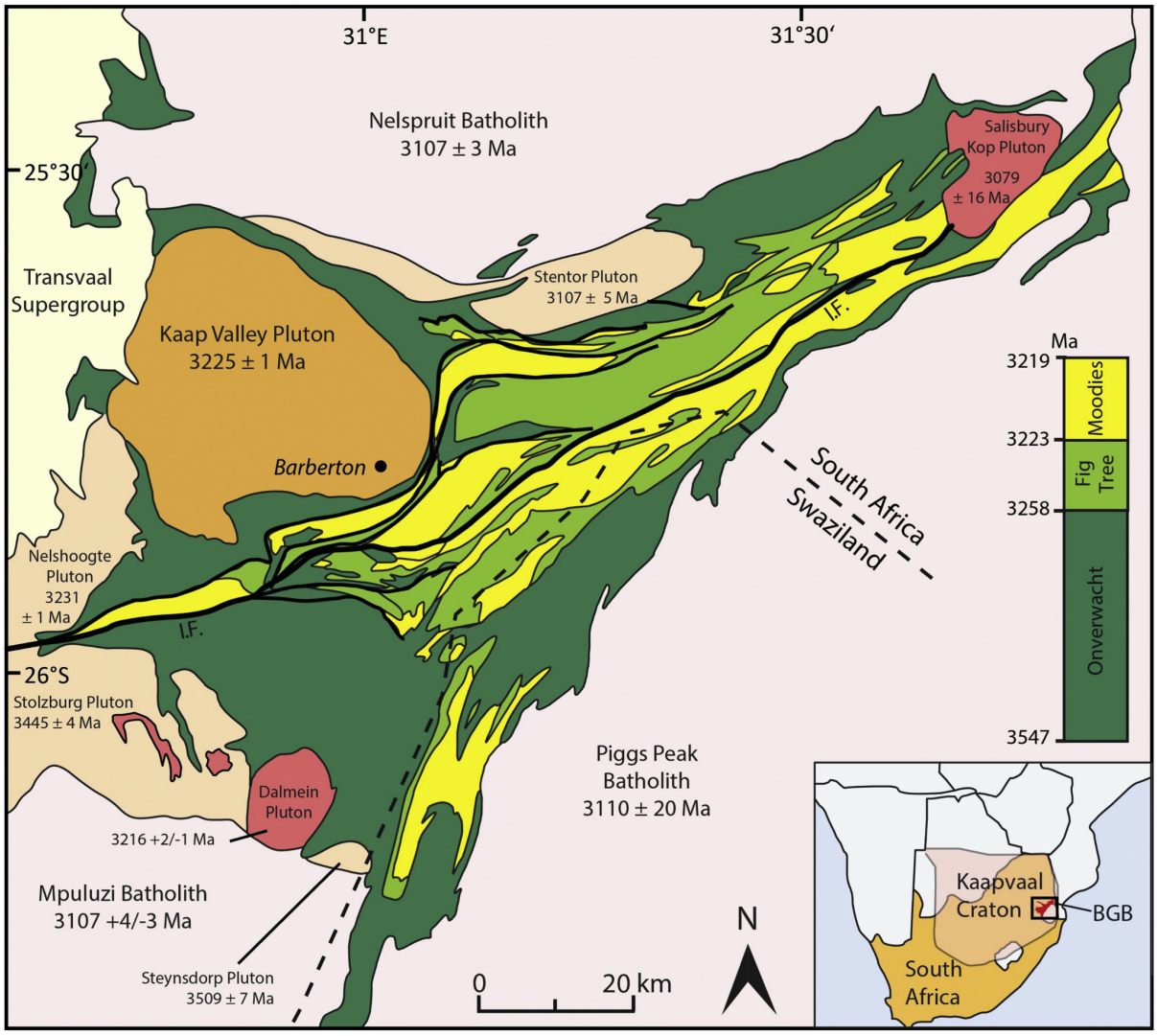

Figure 1: Geological map of the Barberton Greenstone Belt showing the relationship between the Onverwacht Group, Fig Tree Group and Moodies Group and plutons. The Fig Tree Group is compositionally different north and south of the Inyoka Fault (thick black line). For sample locations discussed in this study see Tables 1, 2 and 3. (Homann, 2019)

1.2. Paleoarchean silicification and barite deposition

Widespread silicification in the form of chert, chert dykes and silica alteration zones are conspicuous features of many Paleoarchean (3.5-3.2 Ga) units in greenstone belts (eg. Duchac & Hanor 1987; Sugitani et al., 1998; Van den Boorn et al., 2007; Hofmann & Harris, 2008). Debate surrounds the cause of Paleoarchean silicification processes, with contrasting lines of thought including: *1)* post-depositional metasomatism on the Archean seafloor as a result of low-temperature hydrothermal venting (de Wit et al. 1982;

Paris et al. 1985; Duchac et al. 1987; Nijman et al., 1998; Orberger et al., 2006); or *2)* silicification as a result of the interaction of sediments and shallow seawater leading to marine weathering of volcanic flow tops (Lowe & Byerley, 1986; Lowe et al., 1999). In the BGB, field based observations have been used to support (and reject) both hypotheses, with chert filled veins and dykes within and below chert horizons and brecciated cherts lending evidence for hydrothermal activity (eg. Hofmann, 2005); and the lack of other hydrothermally associated features such as alteration zones and massive sulphide deposits lending favour against this (Lowe, 2013). Although convincing evidence for hydrothermal activity, Lowe and colleagues (1989; 2003; 2013) have used the association with Mendon-age spherules and the chert dykes to interpret that the dykes were generated due to closely spaced meteorite impacts. In this so-called '*Neptunian-dyke*' hypothesis, meteorite impact-events would have fractured the crust. Fractures in the crust would then have filled with soft or unlithified sediments. Fluids moving upward through the fractures would then have vented onto the seafloor to silicify the sediments into chert 'dykes'.

Prior to the oxygenation of the atmosphere (~2.4-2.0 Ga) the ocean is expected to have been undersaturated with respect to sulphate. However, in Paleoarchean greenstone belts primary barite ($BaSO_4$) deposits are sometimes found. When occurring, this barite is closely associated with silicified zones; inferring contemporaneous precipitation of sulphate and silica. Similar to silicification processes, debate surrounds the formation of Paleoarchean barite. There is currently no agreement in the literature as to whether hydrothermal fluids, ambient seawater, meteoric water or a mixture of sources were the host fluids from which the barite precipitated (eg. Buick et al., 1990; Nijman et al., 1998; Huston et al, 2004; Lowe et al., 2019). Due to their close spatial association, determining the origin of chert and silica veins which are found in the Fig Tree Group may also provide information as to how proximal barite formed.

Variations in sulfate mineral occurrences and abundances have proven to be powerful tools in inferring the evolution of the atmosphere, geosphere and oceans (eg. Canfield 1998; Kah et al. 2004; Fike et al. 2006; Roerdink et al., 2022). Furthermore, hydrothermal vent settings and sulphate increases in the Paleoarchean may have provided nutrient fluxes for the earliest microbial sulfate metabolisers (Pinti et al., 2009; Schopf, 1993).

Figuring out which process(es) caused silicification and barite deposition 3.5-3.2 Ga thus has potential to provide information regarding the evolution of the early oceans, landmasses and atmosphere as well as hosting critical information regarding which geological phenomena were responsible for the advent of microbial life.

1.3. Conglomerates as an indicator of basin conditions

Conglomerates host powerful paleoenvironmental reconstruction potential (eg. Graham et al., 1986; Hidaka et al., 2002; Wandres et al., 2004). This has been demonstrated by Hessler & Lowe (2006) who have used the geochemistry of Moodies Group conglomerates from the BGB to infer sediment sources and weathering rates which prevailed ~3.2 Ga. Conglomerate lenses found interbedded with silicified and baritic units are also well documented in the Fig Tree Group of the BGB (eg. Nocita & Lowe, 1990; Lowe et al., 1999; Hofmann, 2005). There is a general agreement that the likely source of such Fig Tree conglomerates was the shallow uplift of basin-proximal material (Lowe & Nocita, 1999; Hofmann, 2005; Drabon et al., 2019). Analysis of such conglomerates could therefore host valuable information regarding the cause of silicification of the lower portions of the Fig Tree Group, the sediment influx into the Mapepe basin during the time of silicification and/or barite formation; and the environmental conditions prevailing during Mapepe basin sedimentation. Despite this, little to no detailed geochemical analyses of Mapepe Formation conglomerates currently exists in the literature.

This thesis will offer one of the first detailed studies of Mapepe basin conglomerates and in doing so will attempt to answer the following questions:

1) *What was the type of materials influxed into the ~3.26 Ga Mapepe basin?*
2) *What was the cause of silicification in these conglomerates?*
3) *What was the composition of seawater in the ~3.26 Ga Mapepe Basin?*

These results will then be compared with trace element analysis of silica vein and chert samples collected from the Eastern Barite Valley, Puddingstone Hill and Masenjane Barite Working sites in order to attempt to reconstruct the processes controlling silica vein formation and silicification in the ~3.26 Ga Fig Tree Group.

2. Materials and methods

2.1. Sample locations

Samples were collected from 3 locations of the Mapepe Formation in the southern Fig Tree Group: The Eastern Barite Valley, Puddingstone Hill and the Masenjane Barite Workings. For exact sample locations, refer to Tables 1, 2 and 3. A total of 18 samples are discussed in this study. Samples include Mapepe Formation conglomerates, black, white, and grey silica veins, grey/green chert, black chert and green chert, and older black-and-white banded Mendon Formation chert.

2.1.2. Barite Valley

The sampling site falls within Barite Valley, which is well-reported in the literature due to the excellent preservation of morphologically diverse primary barite, abundant chert dykes, meteorite-impact spherule layers, and the relatively easy field access that the site offers (Heinrichs & Reimer, 1997; Lowe et al., 2013; Roerdink et al., 2013; Ledevin et al., 2015; Lowe, 2019).

The Mapepe Formation stratigraphy exhibits 2 different lithologies based on its location east or west of an unnamed fault in the Barite Valley. The samples described in this study were collected from the eastern limb of Barite Valley (EBV), which is a 400 m thick sequence of mudstone, siltstone, sandstone, dacitic tuff, barite, chert, and jasper lenses (Drabon, 2018; Drabon et al., 2019). The base of the EBV is marked by a spherule bed, with barite occurring 1-75 m above the spherule layer. Above the spherule layer the Mapepe Formation has been classified into Members 1, 2, 3, 4 and 5 (Drabon, 2019). Members 1, 2 3, and lower Member 4 represent a mud-rich basin which shoals upwards into a subtidal setting. Upper Member 4 and Member 5 represent a deep water turbidite. Tabular to irregular grey, green, black carbonaceous and tuffaceous chert veins ranging in size from a few centimetres to <8 m cross-cut the EBV. For a more detailed description of the Eastern Barite Valley readers are directed to Lowe (2019).

Table 1:

Sample descriptions and locations of the Barite Valley samples.

Sample	Rock type	Description	Location	Elevation (m)
18-BV-13	Silica vein	Uppermost portion of large silica vein	(-25.902661, 31.061609)	1211
18-BV-15	Silica vein	Middle part of large silica vein	(-25.092779, 31.061658)	1216
18-BV-18	Silica vein	Lower part of of large silica vein	(-25.902862, 31.061695)	1223
18-BV-26	Green chert	Found close to barite	(-25.882851, 31.103651)	1372
18-BV-30	Green chert	Found below barite lenses. Cuts through layered black and white chert.	(-25.882449, 31.102777)	1403
18-BV-32	Green/grey chert	Found below barite	(-25.882319, 31.102849)	1396

2.1.3. Puddingstone Hill

Puddingstone Hill is the informal name which has been given to a conglomerate quarry which lies approximately 3 km NE of the EBV. No published data exists on the locality to date. The location is characterised by abundant 'Puddingstone conglomerates' which in places overlay baritic chert and wave-structured barite sand. Towards the north-western portion of the site, Puddingstone conglomerates are replaced by black cherts and minor occurrences of jasper which in some cases are brecciated. In some portions of the section, barite horizons and silica veins are found in contact with black banded chert, marking a boundary between the Mapepe and Mendon Formations.

Table 2:

Sample descriptions and locations of the Puddingstone Hill samples. Blank fields represent no data given.

Sample	Rock Type	Description	Location	Elevation (m)
19-PS-01	Black chert	Black silica vein. Cross-cuts Mendon chert.	(-25.882630, 31.103296)	1395
19-PS-02	Chert	Black/white banded Mendon chert	(-25.882636, 31.103378)	1391
19-PS-03	Black chert	Black silica vein. Found downhill from 19-PS-01	(-25.882636, 31.103378)	1389
19-PS-04	Grey/green chert	Found between barite and conglomerate.	(-25.882770, 31.103474)	1384
TSA	Conglomerate	Translucent silicified matrix. Matrix supported. Rounded to subrounded jaspilite, banded jasper, chert, lithic clasts (2-4 cm)		
MMT	Conglomerate	Translucent silicified matrix. Matrix supported. Rounded to subrounded jaspilite, banded jasper, chert, lithic clasts (2-4 cm)		
MSA15-CQ-10	Conglomerate	Translucent silicified matrix. Matrix supported. Parallel fractures. Rounded to subrounded jaspilite, banded jasper, chert, lithic clasts (2-4 cm)		
MSA15-CQ-1	Conglomerate	Dark grey silicified matrix. Subrounded to subangular chert and lithic fragment clasts. (1-4 cm).		

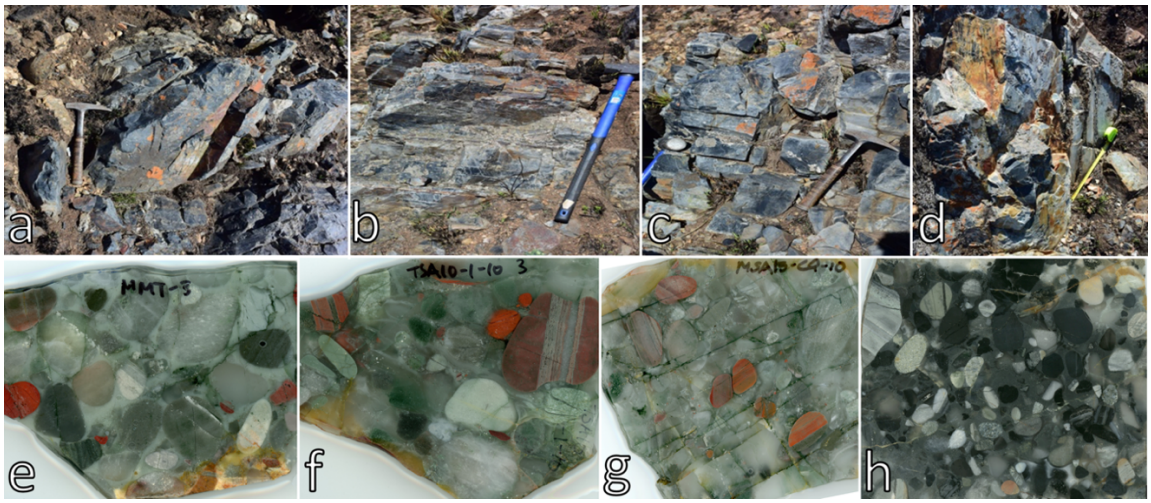

Figure 2: Samples from the Puddingstone Hill site. **a)** 19-PS-01; **b)** 19-PS-02 **c)** 19-PS-03 **d)** 19-PS-04 **e)** MMT **f)** TSA **g)** MSA15-CQ-10 **h)** MSA15-CQ-1 Note: **e-f)** are representative examples of portions of the conglomerate slabs. Photographs **a-d)** credit: Desiree Roerdink. Photographs **e)- f)** credit: Kimberly Myers.

2.1.4. Masenjane Barite Workings

Located in the central portion of the BGB, the Masenjane Barite Workings lie on the southern flanks of Masenjane mountain, to the east of the Puddingstone Hill locality. The samples discussed in this study were collected from shallow quarries which lie at the Mendon/Fig Tree contact from which no published data exists.

Table 3:

Sample descriptions, pit number sampled and locations of the Masenjane Barite Workings samples.

Sample	Rock Type	Description	Location	Elevation (m)
19-MB-19	Grey chert	Found in Pit 02. Possible silica vein.	(-25.872419, 31.112107)	1464
19-MB-21	Chert	Black/white banded Mendon chert found in Pit 02.	(-25.872936, 31.111923)	1479
19-MB-22	Black chert	Found in Pit 02 at the trench of the pit. Base of chert is in contact with domal barite.	(-25.873204, 31.111645)	1480
19-MB-24	Grey chert	Found in Pit 02 between barite in a barite block.	(-25.873444, 31.111392)	1461
19-MB-01	White chert vein	Pit 05: Barite (mostly bladed) on both sides and bottom of the pit. Vein cuts through barite.	(-25.869693, 31.110631)	1490

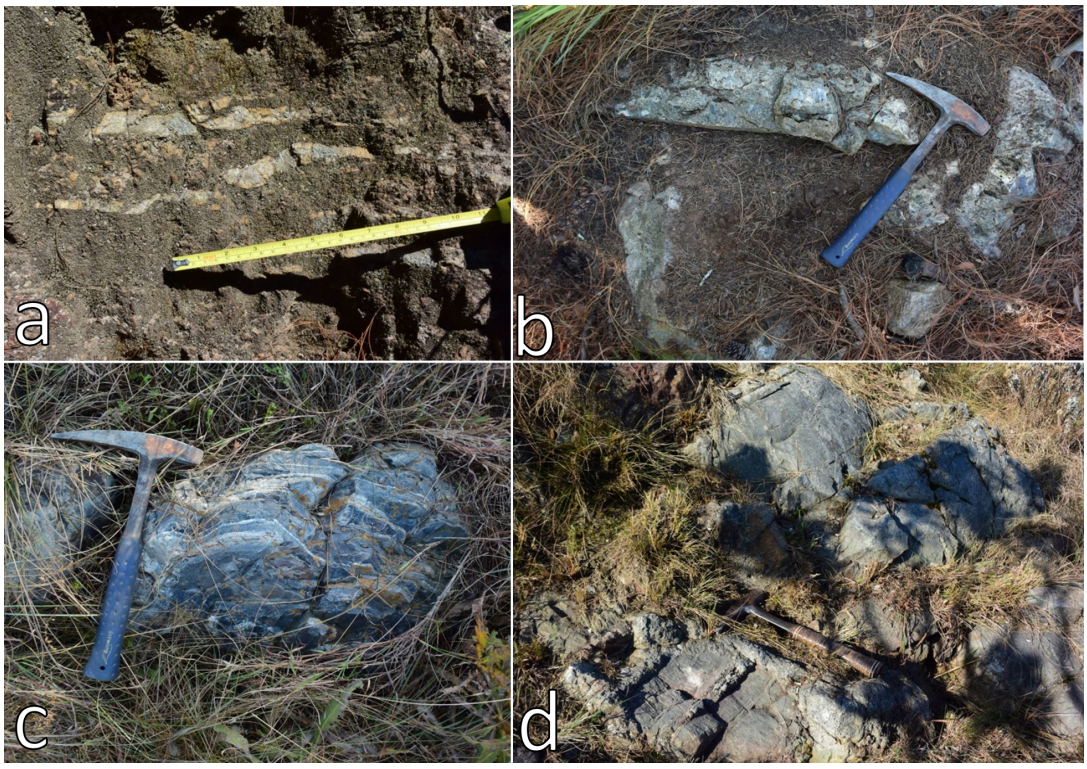

Figure 3: Outcrop photos of samples **a)** 19-MB-01 **b)** 19-MB-19 **c)** 19-MB-21 **d)** 19-MB-24. Photographs credit of Desiree Roerdink.

2.2. Analytical techniques

Fresh rock fragments and conglomerate clasts were carefully chosen to avoid weathered and inclusion-rich material. Offcuts were then made of each sample.

Trace element and rare earth element concentrations were determined using a Lambda Physik 193 nm wavelength COMPex 102 ArF excimer laser ablation instrument connected to a Thermo Scientific X-Series 2 ICP-MS at Utrecht University. The mass spectrometer was operated in low-resolution mode. A 20 Hz laser pulse repetition rate was used with a fluence of 5 to 10 Jcm^{-2}. Each measurement included an 80 second background interval followed by 100 seconds of ablation.

The data was reduced using GLITTER software. NIST-SRM-612 was used as a calibration standard. BCR-2G was used as a secondary standard to check the daily accuracy of the calibration. Results for BCR-2G were typically within 1-15% of published values (GeoReM database, Jochum et al., 2005).

SiO_2 was used as the internal standard. For the Puddingstone conglomerate clasts, SiO_2 values were previously obtained by XRF (unpublished data of Kimberly Myers, 2020). For the conglomerate matrix, SiO_2 values of 95 wt% were arbitrarily chosen as deemed most suitable to represent the almost entirely silicified matrix. For the Masenjane and Puddingstone chert and silica veins, SiO_2 values were obtained using a JEOL JXA-8530F Hyperprobe Field Emission Electron probe microanalyser (EMPA) at Utrecht University (Esemee Wardenburg, unpublished MSc data 2020).

The analysis of ultra-low trace element concentrations by LA-ICP-MS can be challenging. This was observed in this study as many of the samples showed trace element values below the detection limit. Furthermore, the heterogeneous nature of many of the samples could lead to erroneous representations of provenance if an average composition was considered. In order to address these issues several precautionary methods were systematically used: *1)* in order to ablate as much sample volume as possible, the laser aperture was removed to allow for the maximum crater size possible (approximately 150 µm diameter spot size); *2)* at least 3 - and up to 7 - spots per sample were measured; *3)*

ablation points were preliminarily considered separately in order to assess sample heterogeneities; *4)* when samples were found to be homogenous, mean data were reported in order to produce representative averages. However, when samples were heterogeneous individual ablation points were considered separately.

Many of the silica vein and chert samples were heavily weathered. If indicators of weathering such as anomalous negative Ce values (indicative of extreme post-depositional oxidative weathering eg. Bonnand et al., 2020) were observed, these values were discarded as it was assumed other trace element values could be compromised. The values for individual analyses are given in Appendices A and B.

Thin sections of samples the Puddingstone and Masenjane chert were analysed using a digital ZEISS Axio Imager 2 Pol polarised light microscope.

2.3. Data quality

Several analytical problems can affect the accuracy of the laser ablation results, especially at the ultra-low concentrations (<1 ppm) of trace elements measured in the cherts. BaO can cause significant spectral interference with Eu (eg. Jarvis et al., 1989; Smirnova et al., 2006). However, the lack of correlation of Eu/Eu* and Ba (R^2 = -0.05) for the Puddingstone clasts (Fig. 4) determined that any europium anomalies were unlikely to be influenced by spectral interference between $^{135}Ba^{16}O$ with ^{151}Eu.

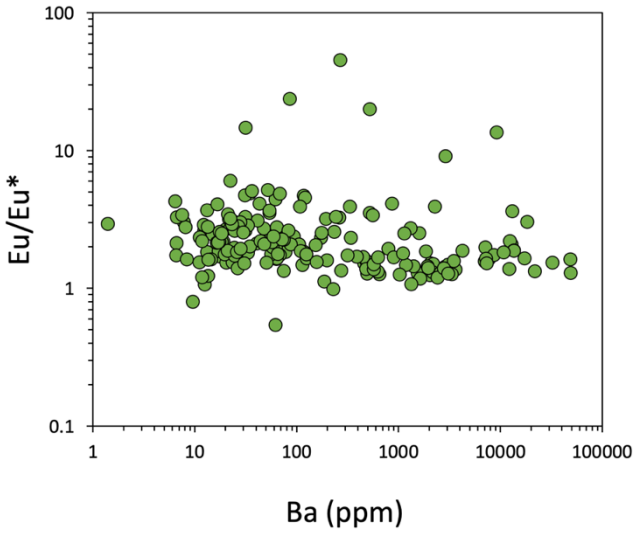

Figure 4: The lack of correlation between the europium anomaly (Eu/Eu*) and barium concentration rules out BaO interference as affecting Eu anomaly. Note: both axes are in log scale.

Lanthanum values deemed to be erroneously high were measured for many of the samples. Sample 19-MB-19 was reanalysed in the University of Bergen and in this

analyses no lanthanum spike was reported. This analysis was used to confirm that La spikes were due a specific problem with the mass spectrometer settings used Utrecht University, as opposed to being a naturally occurring anomaly or due to sample preparation. As a result, lanthanum was removed from the reported REE+Y plots.

2.4. Seawater REE+Y systematics - a brief review

Due to their unique and predictable behaviour in aqueous solutions, REE+Y patterns are often used to infer the fluid composition from which hydrogenous sediments were precipitated (eg. Bau and Dulski, 1996; Kamber & Webb, 2001; Lawrence and Kamber, 2006; Johannesson et al., 2006; Planavsky et al., 2010). Shale-normalised REE+Y plots of seawater sediments display characteristic patterns of positive slopes towards the HREEs; positive La and Y anomalies; and negative Ce anomalies (Bau & Moller, 1993; Bolhar et al., 2002; Bolhar et al., 2004; Hofmann & Bolhar, 2007; Shields & Webb, 2004; Van Kranendonk et al., 2003). These patterns are a result of the behaviour of REE+Y in marine settings which causes the following solution-particle interactions:

1) Increasing atomic mass is associated with decreasing particle complexation and preferential retention in solution. This causes the HREEs to become preferentially enriched in seawater thereby leading to HREE>LREE (Lee & Byrne, 1993).
2) The configuration of the inner 4f electrons of La leads to more stable solution complexation when compared to its neighbouring elements. This provides a positive shale-normalised La anomaly in marine precipitates (Bau et al., 1995).
3) Due to their identical charge and similar ionic radius, Yttrium and Holmium are regarded as 'geochemical twins' (Pack, 2007). They are rarely fractionated by any terrestrial processes and thereby are found in chondritic (~28) ratios in volcanic and clastic sediments (Pack, 2007). However, Y and Ho exhibit differences in complexation behaviour which allows them to become fractionated in hydrous settings, thereby leading seawater to have Y/Ho ratios well above chondritic values (Bau & Dulski, 1996).
4) When Ce^{3+} is oxidised to Ce^{4+}, its solubility is decreased causing it to be preferentially adsorbed onto particulate matter. This leads to its relative depletion in the oxic water-column and a resulting negative Ce anomaly (Sholkovitz et al., 1994).

5) Eu^{3+} changes valence state to Eu^{2+} under high temperature and strongly reducing conditions. Therefore, a modern marine positive Eu anomaly is characteristic of oceanic input influenced by hydrothermal solutions (Bau, 1991; Douville et al., 1999; Derry & Jacobsen, 1990).

It has been shown in numerous studies that the marine REE+Y signature has remained relatively consistent throughout time for both carbonates (Kamber et al., 2004; Kamber & Webb, 2001; Nothdurft et al., 2004) and chemical sediments such as BIFs and chert (Sugitani, 1992; Bau & Moeller, 1993; Derry & Jacobson, 1990). This has allowed REE+Y patterns to successfully fingerprint hydrous settings in Archean settings. However, the lack of free O_2 in the atmosphere combined with the higher heat flux from the mantle causes some key observations to be considered when using REE+Y systematics to infer Archean marine conditions.

In an absence of free O_2, Ce remains in its trivalent state, therefore remaining in solution. As a result, a negative Ce anomaly is not to be typically expected from Archean marine precipitates (Holland, 2005). In the oxygenated modern ocean, REEs are scavenged by Mn and Fe oxyhydroxides immediately following discharge from a hydrothermal vent. This allows for terrestrial material to be the primary source of REEs to the modern oceans (Taylor & McLennan, 1985; Bau & Dulski, 1999). However, in an Archean Ocean devoid of free O_2 with higher heat flow, REEs were not scavenged at their discharge site by oxygenated species and hydrothermal activity was more intense. This allowed hydrothermal activity to be the primary source of the oceanic REE budget during the Archean (Danielson et al., 1992). Therefore Eu-enrichment (ie. a positive Eu anomaly) is a consistent feature of Archean marine precipitates (Danielson et al., 1992, Tice and Lowe, 2006a, Tice and Lowe, 2006b), with Eu/Eu* <2 not being considered a significant indicator of hydrothermal activity in Archean settings (Sugahara et al., 2010). However, he magnitude of Eu/Eu* in Archean seawater is less well-constrained, and it may have changed significantly through time.

2.4.2. REE standardisation and terminology

MuQ (Kamber, 2005) was chosen as the normalisation factor for this study rather than the commonly used Post Archean Average Shale (PAAS) of Taylor & McLennan (1985). The rationale behind this choice was that MuQ incorporates a high contribution of

basaltic as well as felsic material, and therefore most accurately represents the bimodal mafic and felsic lithology as would characterise the Archean greenstone crust (Kamber, 2005).

REE anomalies are derived from the ratio of the measured trace element value divided by the value of its 2 neighbouring elements. This allows for the relative enrichment/depletion of the element to be quantified. The expression of a REE anomaly is generally calculated by (Taylor & McLennan, 1985):

$$REE_n/REE_n^* = 2REE_n/(REE_n\text{-}1 + REE_n\text{+}1)$$

Where REE_n is the shale-normalised REE; and n = 1,2,3,4… represents the REE position in the lanthanide series (eg. Ce-1 = La).
Due to variable stabilities of Gd in solution, Gd anomalies are common in marine settings (De Baar et al., 1985). As a result, Tb is used to calculate the Eu anomaly in place of Gd.

When discussing REE anomalies the following calculations were used:

1) Europium anomaly (Bau & Dulski, 1996):

$$Eu/Eu^* = Eu_{MuQ}/[(Sm_{MuQ}*0.67)+(Tb_{MuQ}*0.33)]$$

Eu∗ represents the concentration that trivalent Eu would have. When Eu is depleted, Eu/Eu∗ <1 and vice versa.

2) The slope of the REE pattern:

Yb_{MuQ}/Pr_{MuQ}

A positively sloped REE profile in which HREEs are enriched when compared to LREEs will be represented as Yb_{MuQ}/Pr_{MuQ} >1 and vice versa.

3. Results and Discussion

3.1.1. Data filtering: determining a hydrogenous signature

A silica-precipitating fluid should have extremely low trace element concentrations (Ledevin, 2015). However, many of the Puddingstone conglomerate clasts show

enrichments in Al, Cr, Ni, Pb and HFSEs. This indicates that many of the conglomerate clasts represent silicified sediments; or that detrital material was incorporated into a precursor silica gel before being lithified to chert. As little as <1 wt% detrital material is able to obscure an originally hydrogenous REE+Y pattern (Bau, 1993). Therefore, before the composition of the Mapepe Basin water or a silicifying fluid could be inferred, the role of contamination by terrestrial matter in the Puddingstone conglomerates requires critical assessment.

As sedimentary and volcaniclastic materials are enriched in aluminium, Al was used as a proxy mineral for detrital contamination. In order to determine the influence of detrital material on the composition of the Puddingstone conglomerate clasts and matrix material, Al was plotted against selected trace elements (V, Ti, Sc, Cs) and the Eu anomaly for each individual LA-ICP-MS measurement (Fig. 5). For V, Ti, Sc and Cs there is a clear correlation with Al when Al concentrations exceed approximately 1,100 ppm (Figs. 5a-d). Similarly, the Eu anomaly found within the Puddingstone clasts and matrix material are much more variable and generally higher when Al concentrations are below approximately 1,100 ppm (Fig. 5e). Significant positive Eu anomalies are generally absent from Archaean shales and volcanic material (Taylor and McLennan, 1985). Therefore, the elevated Eu anomalies captured in many of the conglomerate clasts and matrix material when Al concentrations are <1,100 ppm may record signatures directly derived from a silica-precipitating fluid. This interpretation must be met with caution, as the variability in Eu/Eu* may arise as a result of degraded LA-ICP-MS precision at the low REE count rates observed in these samples. Nonetheless, the lack of correlation between Al and V, Ti, Sc and Cs indicates that <1,100 ppm Al detrital material has no influence on trace element concentrations. Therefore, it is reasonable to conclude that samples with <1,100 ppm Al may record the composition of the silica-precipitating fluid. The majority of the clasts which contain <1,1000 ppm Al are jaspelites, translucent chert, ferruginous sediments and the matrix material. This is to be expected if these chemical sediments were directly precipitated from Mapepe Basin waters.

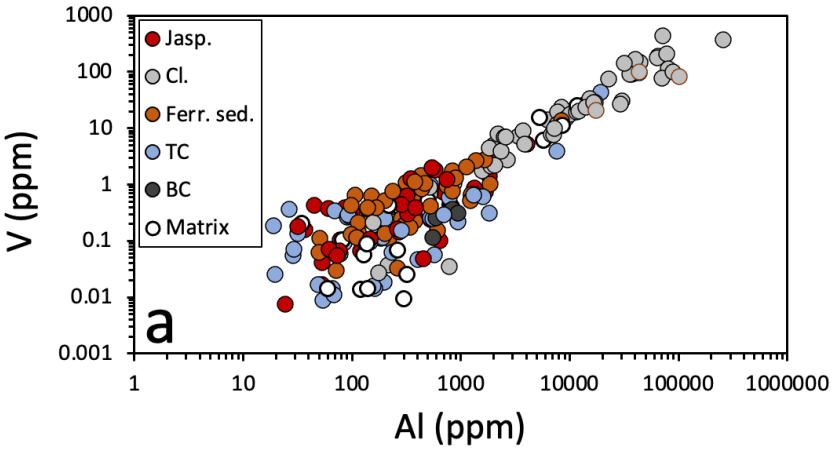
Jasp.
Cl.
Ferr. sed.
TC
BC
Matrix
a
V (ppm)
Al (ppm)
1000
100
10
1
0.1
0.01
0.001
1
10
100
1000
10000
100000
1000000

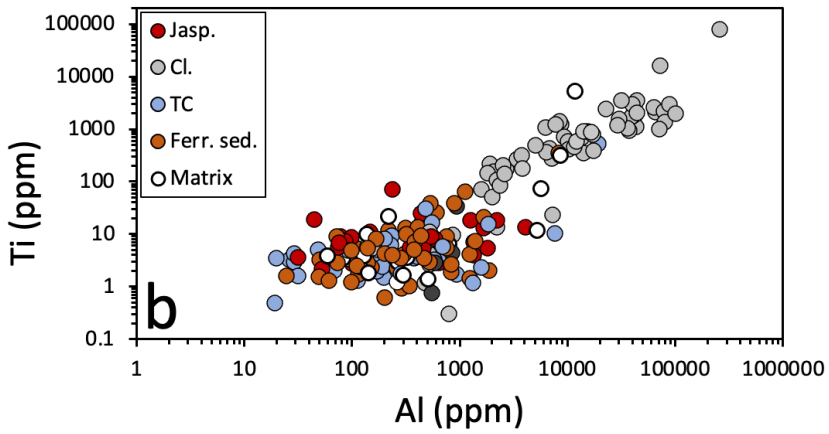
Jasp.
Cl.
TC
Ferr. sed.
Matrix
b
Ti (ppm)
Al (ppm)
100000
10000
1000
100
10
1
0.1
1
10
100
1000
10000
100000
1000000

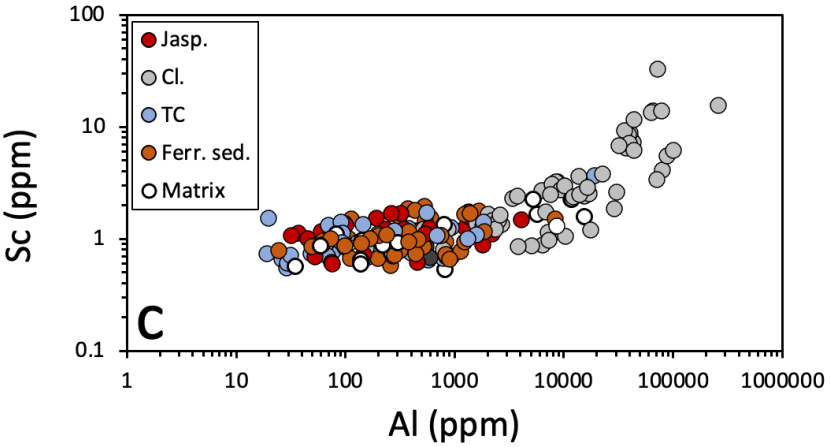
Jasp.
Cl.
TC
Ferr. sed.
Matrix
c
Sc (ppm)
Al (ppm)
100
10
1
0.1
1
10
100
1000
10000
100000
1000000

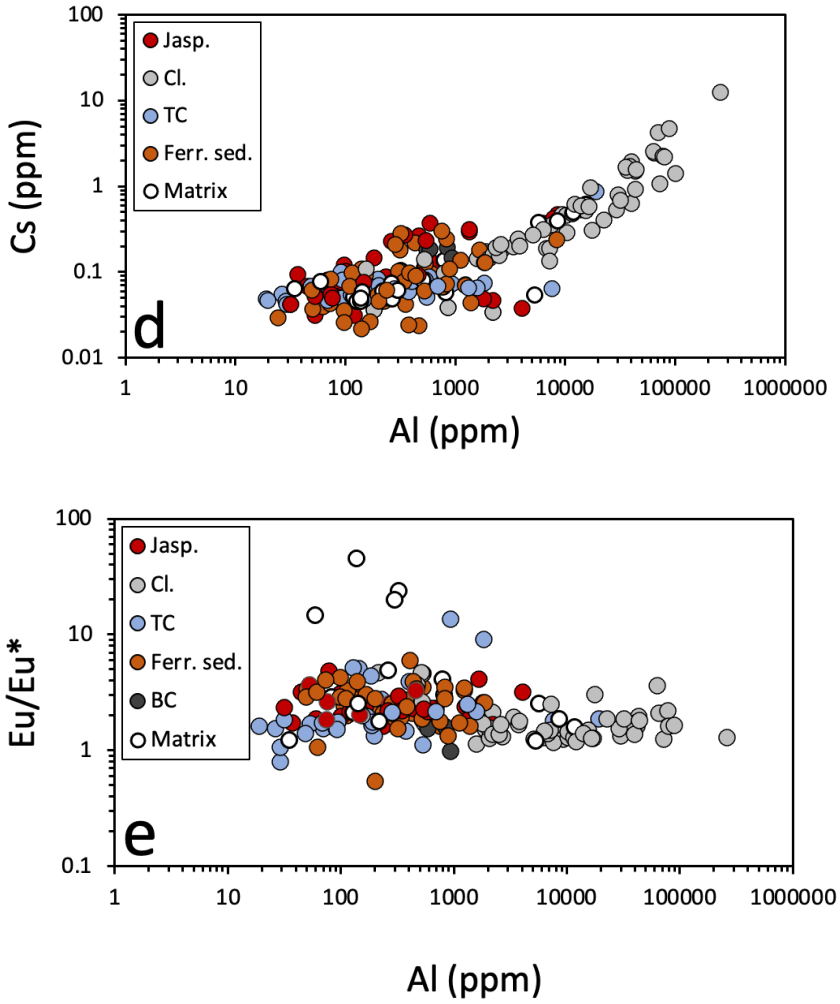

Figure 5: Individual LA-ICP-MS analyses for the Puddingstone conglomerate clasts and matrix. **a)** V vs Al **b)** Rb vs Al **c)** Sc vs Al **d)** Ti vs Al **e)** Cs vs Al **f)** Eu/Eu* vs Al. **a)** – **e)** Trace element abundances correlate with Al >1,100 ppm Al. **f)** Eu/Eu* is more variable and generally higher <1,100 ppm Al. *Jasp.* = jaspilite; *Cl.* = clastic sediment; *TC* = translucent chert; *Ferr. Sed.* = ferruginous sediment; *BC* = black chert.

3.1.2. Conglomerate clasts as an indicator of basin-fluid composition

As determined in *Section 3.1.*, Puddingstone conglomerate clasts with <1,100 ppm Al may record the composition of a silica-precipitating fluid. Furthermore, these clasts are depleted in other elements which may be considered as a detrital or volcaniclastic component (Ti, Zr, Th, Hf, Pb; see Table 4). Instead, these clasts are primarily composed of SiO_2 (and in some cases Fe_2O_3) which may have been directly precipitated from ancient seawater. As precipitates deposited in the water column are well-documented in the Mapepe stratigraphy (Drabon et al., 2019; Stoll et al., 2021), analysis of such clasts may allow the conditions prevailing in the Mapepe Basin to be inferred.

Phosphate minerals such as apatite and monazite may also significantly alter REE+Y patterns of hydrogenous sediments (Thurston et al. 2012). Although less U was dissolved in the Archean oceans prior to the Great Oxidation Event, Th/U ratios of 3-5 can still be used to distinguish the presence of phosphate minerals (Condie, 1993). To further ensure that the discussed REE+Y patterns may record those of a primary fluid, the presence of REE-bearing phosphates entrained in the Puddingstone clasts was considered. As all the discussed clasts have Th/U < 3, the possibility of phosphate minerals being the carrier of REE+Y patterns can be discounted (Table 4). When REE values were below the detection limits such analyses were also discounted.

3.1.3. REE+Y patterns of the chemical-sedimentary Puddingstone clasts

The data in Fig. 6 represent the Puddingstone jaspilite, chert and ferruginous sediment clasts which were deemed to contain minimal detrital contamination. All of the plotted samples consistently display REE+Y characteristics of well-established Archean hydrogenous marine sediments (e.g. Bolhar et al., 2004; Van Kranendonk et al., 2003). This signature is illustrated when compared to jasper from the 3.45 Ga Strelley Pool Formation (Van Kranendonk et al., 2003) which can be seen as an accurate proxy for Paleoarchean seawater. All samples show LREE depletion, positive Eu anomalies and (mostly) super-chondritic Y/Ho ratios which characterise Archean seawater-derived hydrogenous sediments. This result allows it to be concluded that the clasts host information surrounding water chemistry of the early Mapepe Basin.

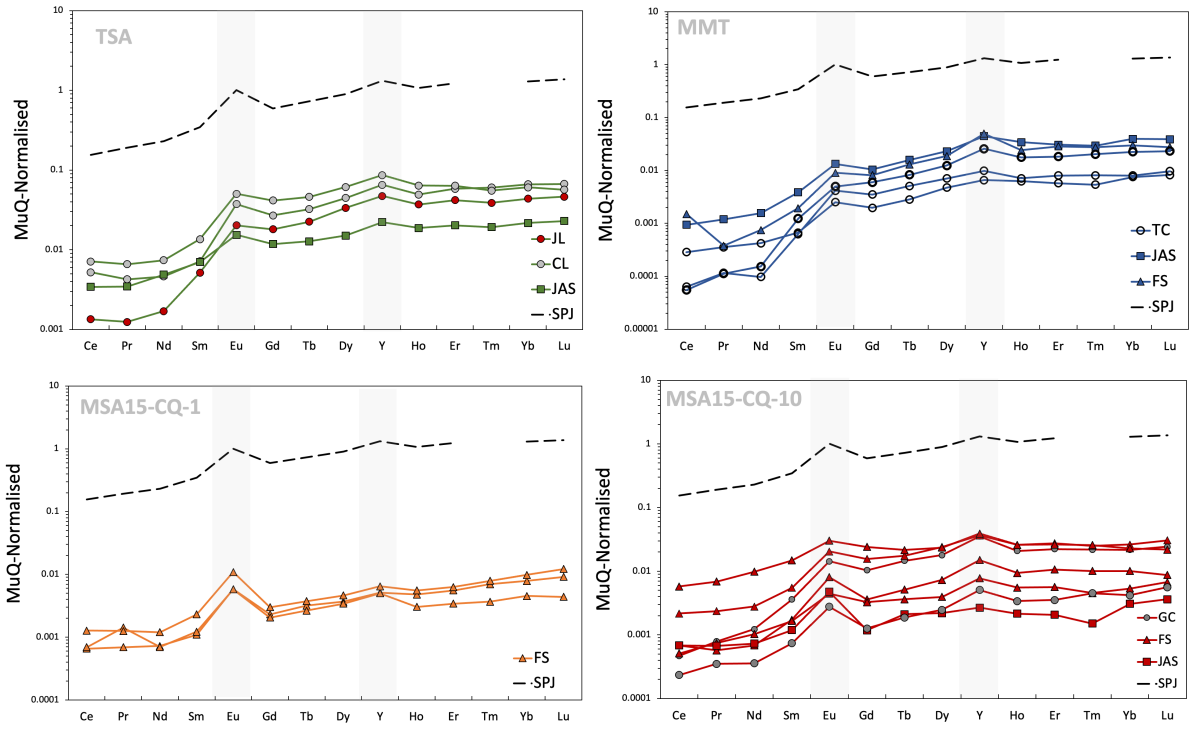

Figure 6: REE+Y profiles of the inferred hydrogenous sediments from the Puddingstone conglomerates. *JL* = jasper lamination (of a banded clast); *CL* = chert lamination (of a banded clast); *JAS* = jaspilite; *TC* = translucent chert; *FS* = ferruginous sediment; *GC* = grey chert. Compared to 3.45 Ga hydrogenous jasper ($X10^{-1}$) (Van Kranendonk et al., 2003).

An intriguing feature of the results is that although REE+Y patterns are variable, they are similar throughout each conglomerate sample - with an exception being MSA15-CQ-10 where there is some inter-sample variation. Such a result may be an artefact of the Mapepe Basin being segmented allowing for varying degrees of marine and/or hydrothermal solutions being present in different portions of the basin. Another interpretation is that each sample may offer insight into secular changes of the Mapepe basin geochemistry.

In sample TSA Eu/Eu* values range between 1.7 and 2.4, whilst the Eu/Eu* values found in the MMT clasts is slightly lower at 1.4-2. These ranges both fall into those expected from contemporaneous seawater (Sugahara et al., 2010). Eu/Eu* values in MSA15-CQ-10 are much more variable, ranging between 1.8 and 3.2. The overall REE concentrations in MSA15-CQ-10 are also variable, with concentrations varying by an order of magnitude between clasts. The Eu anomalies and REE concentrations vary together, with lower REE concentrations being associated with higher Eu anomalies and vice versa. As

hydrothermal effluent is associated with low REE concentrations, such patterns may represent an environment in which there was a mix of an ambient seawater-component (lower Eu/Eu*, higher REE) and more hydrothermally influenced-component (higher Eu/Eu*, lower REE). The more-variable REE+Y patterns in sample MSA15-CQ-10 possibly representing a segmented basin geometry. Such an interpretation is consistent with earlier studies which have concluded that as the Mapepe Basin matured, the environment changed from a relatively deep marine setting to shallow, segmented water bodies enclosed by zones of local uplift (Heinrichs & Reimer, 1977).

Unlike the rest of the samples, MSA15-CQ-1 has consistently high Eu/Eu* values of 3.3 - 3.9. Although a positive Eu anomaly is a conspicuous feature of Archean marine precipitates, these values are above those that are expected from Archean seawater (Sugahara et al., 2010), whilst remaining far below those expected from high-temperature hydrothermal fluids (eg. Bau & Dulski, 1996). The conclusion can therefore be drawn that an increase in low-temperature hydrothermal activity effected the chemistry of the Mapepe Basin prior to silicification.

Y/Ho ratios are quite variable between the clasts (27-54). However, this trend of Y/Ho variability likely represents fractionation processes between solution and particulate matter rather than solely representing basin chemistry (Nozaki et al., 1997). This is observed in the results as the clasts which contain carbonaceous matter exhibit larger Y/Ho ratios.

Table 4:

Major and trace element composition of the Puddingstone clasts which have ultra-low levels of trace elements and display hydrogenous REE+Y profiles. Empty fields represent measurements which were below the detection limit. SiO_2, Fe_2O_3, MnO, Na_2O and P_2O_3 were obtained by Bulk XRF (Kimberly Myers, unpublished data). ΣHFSE: sum of Zr, Hf, Nb, Ta and Y; ΣLILE: sum of Cs, Rb and Ba. Calculation of Eu/Eu* is given in *Section 2.4.2.*

Sample	**TSA**				**MMT**					**MSA15-CQ-1**			**MSA15-CQ-10**						
Clast	**E6**	**E6**	**E10**	**E11**	**E14**	**E20**	**E24**	**E26**	**E27**	**E31**	**E34**	**E36**	**E39**	**E40**	**E43**	**E45**	**E46**	**E47**	**E51**
Description	*Chert lam.*	*Jasper lam.*	*Chert lam.*	*Jaspelite*	*Translucent chert*	*Carbonaceous jaspelite*	*Translucent chert*	*Carbonaceous ferruginous sed.*	*Transulcent chert*	*Ferruginous sed.*	*Carbonaceous ferruginous sed.*	*Ferruginous sed.*	*Carbonaceous chert*	*Carbonaceous ferruginous sed.*	*Ferruginous sed.*	*Carbonaceous ferruginous sed.*	*Ferruginous sed.*	*Carbonaceous jaspilitic sed.*	*Ferruginous sed.*
Element (wt%)																			
SiO2	85.772	85.772	85.722	85.417	84.318	85.372	83.602	85.410	83.597	85.73	85.42	85.09	85.59	81.53	85.72	85.70	83.86	85.80	85.46
Al2O3	0.253	0.035	0.082	0.007	0.006	0.016	0.032	0.012	0.009	0.02	0.01	0.03	0.03	0.16	0.06	0.11	0.14	0.01	0.25
Fe2O3	2.751	2.751	3.393	2.547	1.599	12.518	0.508	2.004	0.226	10.01	4.29	3.78	2.02	2.27	3.35	7.28	16.14	5.26	1.55
MnO	0.020	0.009	0.017	0.004	0.040	0.146	0.001	0.018	-	0.03	0.01	0.26	0.00	0.02	0.14	0.01	0.03	0.00	0.01
MgO	-	-	-	-	-	0.619	-	-	-	-	0.13	-	-	0.18	0.31	-	0.83	-	-
CaO	0.046	0.041	0.076	-	0.038	0.054	0.019	0.057	0.016	0.04	0.03	-	0.03	0.04	0.04	0.05	0.08	0.03	0.04
Na2O	0.292	0.292	0.371	0.116	0.271	0.472	0.247	0.358	0.215	0.43	0.41	0.27	0.35	0.39	0.45	0.40	0.53	0.31	0.30
P2O5	0.138	0.138	0.128	0.116	0.128	0.149	0.124	0.158	0.129	0.15	0.12	0.12	0.14	0.06	0.14	0.13	0.16	0.12	0.13
(ppm)																			
Cs	0.291	0.145	0.219	0.093	0.042	0.076	0.057	0.039	0.068	0.097	0.037	0.022	0.109	0.073	0.078	0.369	0.303	0.078	0.065
Ba	57.440	25.050	106.080	6.600	13.220	18.030	62.770	14.500	26.400	6.700	7.520	2292.100	58.050	26.920	28.220	57.520	65.420	22.360	18.470
Rb	0.064	0.045	0.151	-	0.038	0.034	0.224	0.037	0.071	0.027	0.025	0.024	0.225	0.073	0.036	0.077	0.064	0.028	0.024
Th	-	0.009	0.020	-	-	0.002	-	0.001	-	0.003	0.003	0.005	0.004	0.007	0.002	0.016	0.007	0.001	0.001
U	-	0.024	0.032	0.007	0.025	0.014	-	0.009	0.019	0.007	0.004	0.003	0.014	0.006	0.003	0.013	0.024	0.006	0.001
Nb	0.057	0.021	0.085	-	0.006	0.017	0.002	0.008	0.005	0.020	0.004	0.019	0.006	0.004	0.004	0.041	0.031	0.006	0.002
Ta	0.003	0.002	0.005	-	-	0.001	-	-	-	0.001	0.000	0.001	-	0.001	-	0.003	0.001	-	0.001
Pb	2.310	0.551	9.750	0.608	0.011	3.490	-	0.534	-	0.507	5.150	6.430	34.390	10.920	0.727	1.750	13.300	0.278	0.111
Sr	17.320	6.570	24.810	9.400	1.360	4.360	2.110	2.590	2.030	2.950	2.420	9.030	2.100	3.350	4.230	12.110	19.380	4.440	2.410
Zr	0.186	0.161	0.329	-	0.011	0.085	0.050	0.078	0.048	0.052	0.088	0.118	0.067	0.063	0.040	0.278	0.266	0.024	0.024
Hf	0.004	0.003	0.006	-	-	0.001	-	0.001	-	0.001	0.002	0.003	-	0.002	0.001	0.007	0.004	0.001	0.001
Ti	7.10	7.890	14.780	-	1.590	7.380	1.920	2.390	5.050	1.690	3.300	5.470	5.350	2.630	1.010	7.990	5.460	1.293	1.175
Sc	1.750	0.827	1.799	1.131	0.712	1.192	0.974	0.959	0.732	0.823	0.831	0.907	0.824	0.724	0.971	1.232	1.076	0.887	0.997
V	0.866	0.229	1.467	0.157	0.137	0.385	0.129	0.062	0.017	0.208	0.112	0.394	0.212	0.758	0.174	1.828	1.226	0.071	0.640
Cr	1.451	0.660	2.790	-	0.917	1.181	0.578	0.578	0.743	2.620	0.923	0.924	1.244	1.653	1.041	8.250	1.430	16.480	1.213
Co	4.650	0.850	17.270	0.580	0.239	3.390	0.104	1.112	0.023	16.910	6.050	6.190	8.290	13.210	0.940	2.810	8.350	0.941	0.104
Ni	21.350	5.020	91.680	2.560	1.870	16.650	2.080	2.460	0.781	107.340	40.520	40.310	60.690	39.620	9.060	23.900	96.740	4.870	6.240
As	128.410	20.530	1356.860	25.970	1.490	283.520	2.920	22.580	1.610	12.670	503.230	4650.020	1958.010	864.780	171.120	50.720	673.850	7.920	5.380
La	2.450	0.045	0.342	-	2.860	1.242	1.490	0.010	4.900	0.017	0.151	1.590	0.556	0.037	1.880	0.097	0.154	0.026	0.311
Ce	0.370	0.095	0.505	0.243	0.020	0.067	0.005	0.107	0.004	0.047	0.049	0.091	0.033	0.049	0.036	0.154	0.408	0.048	0.017
Pr	0.036	0.010	0.056	0.029	0.003	0.010	0.001	0.003	0.001	0.006	0.012	0.011	0.007	0.005	0.006	0.020	0.058	0.006	0.003
Nd	0.152	0.056	0.243	0.160	0.014	0.052	0.003	0.025	0.005	0.024	0.023	0.039	0.040	0.022	0.034	0.092	0.324	0.024	0.012
Sm	0.049	0.035	0.093	0.048	0.005	0.027	0.004	0.013	0.009	0.008	0.008	0.016	0.025	0.012	0.011	0.038	0.102	0.008	0.005
Eu	0.059	0.032	0.079	0.024	0.004	0.021	0.007	0.014	0.008	0.009	0.009	0.017	0.023	0.013	0.007	0.032	0.047	0.007	0.004
Gd	0.171	0.115	0.263	0.075	0.013	0.066	0.022	0.052	0.038	0.015	0.013	0.019	0.066	0.023	0.021	0.099	0.153	0.008	0.008
Tb	0.032	0.022	0.046	0.013	0.003	0.016	0.005	0.013	0.008	0.003	0.003	0.004	0.014	0.005	0.004	0.017	0.021	0.002	0.002
Dy	0.262	0.197	0.361	0.089	0.028	0.136	0.042	0.111	0.073	0.022	0.020	0.027	0.106	0.043	0.023	0.142	0.138	0.013	0.015
Ho	0.060	0.045	0.078	0.023	0.008	0.042	0.009	0.029	0.022	0.006	0.004	0.007	0.025	0.011	0.007	0.032	0.032	0.003	0.004
Y	2.070	1.500	2.750	0.706	0.210	1.416	0.313	1.590	0.822	0.163	0.159	0.205	1.126	0.476	0.246	1.162	1.240	0.085	0.162
Er	0.196	0.141	0.214	0.068	0.019	0.104	0.027	0.096	0.062	0.019	0.012	0.021	0.075	0.036	0.019	0.092	0.089	0.007	0.012
Tm	0.031	0.020	0.028	0.010	0.003	0.015	0.004	0.014	0.010	0.004	0.002	0.004	0.011	0.005	0.002	0.013	0.013	0.001	0.002
Yb	0.215	0.142	0.197	0.070	0.025	0.128	0.026	0.097	0.073	0.026	0.015	0.032	0.070	0.033	0.017	0.086	0.075	0.010	0.014
Lu	0.033	0.023	0.028	0.011	0.004	0.019	0.005	0.014	0.011	0.004	0.002	0.006	0.012	0.004	0.003	0.015	0.011	0.002	0.003
∑HFSE	2.320	1.687	3.174	0.706	0.227	1.520	0.365	1.677	0.875	0.24	0.25	0.34	1.20	0.55	0.29	1.49	1.54	0.12	0.19
∑LILE	57.795	25.240	106.450	6.693	13.300	18.141	63.051	14.576	26.539	6.82	7.58	2292.15	58.38	27.07	28.33	57.97	65.79	22.47	18.56
Y/Ho	34.558	33.186	35.347	30.965	27.344	33.876	36.018	54.082	37.880	28.1	42.7	30.2	44.3	41.5	36.4	36.8	39.2	32.6	39.2
Eu/Eu*	2.416	1.864	2.077	1.731	1.828	1.695	1.972	1.615	1.393	3.3	3.4	3.9	2.0	2.8	1.9	2.2	1.8	3.2	2.5
Yb/PrSN	15.546	35.237	9.207	6.237	21.258	32.976	69.327	78.903	199.752	11.4	3.2	7.8	27.4	17.7	7.2	11.1	3.3	4.6	11.9
Th/U		0.4	0.6			0.2		0.1		0.4	0.7	1.6	0.3	1.1	0.6	1.2	0.3	0.2	0.6

3.2. Sediment input to the Mapepe Basin

In this section of the thesis, the provenance of the conglomerate clasts which contain >1,100 ppm Al is determined. This allows for the source of detrital material which eroded into the Mapepe Basin to be inferred.

3.2.1. Immobile elements

Due to the pervasive silicification of Fig Tree rocks, the analysis of fluid-immobile elements offers the most suitable indicator of provenance as it has been shown that Al, Ti, Zr, Cr, Th, and Sc remained immobile during metasomatism of rocks from the BGB (Pearce & Cann, 1973; Hessler & Lowe, 2006). Th, Sc and Cr are commonly used to identify the detritus source of sediments, with Cr/Th vs Th/Sc being regarded as the most robust indicators of local provenance and tectonics (Hallberg, 1984; Condie and Wronkiewicz, 1990). Higher Cr/Th and lower Th/Sc ratios are indicative of a more mafic contribution; whilst differentiation in igneous rocks and their associated sediments will cause Cr/Th ratios to decrease with an increased Th/Sc ratio (Taylor & McLennan, 1995).

Shale represents an accurate representation of the average terrigenous input into basins (Bolhar et al., 2005). In order to analyse how the sampled conglomerate differed from overall sedimentation at the time, the data were compared to the average southern facies Fig Tree Group Shale (Hofmann, 2005). Silicified komatiites of the Mendon Formation (M5v and M3v2, Decker et al., 2015) and ~3.4 Ga dacite of the Hooggenoeg Formation (H6, Drabon et al., 2019) were also added to the immobile element plots as a means to constrain a mafic/ultramafic or felsic source respectively.

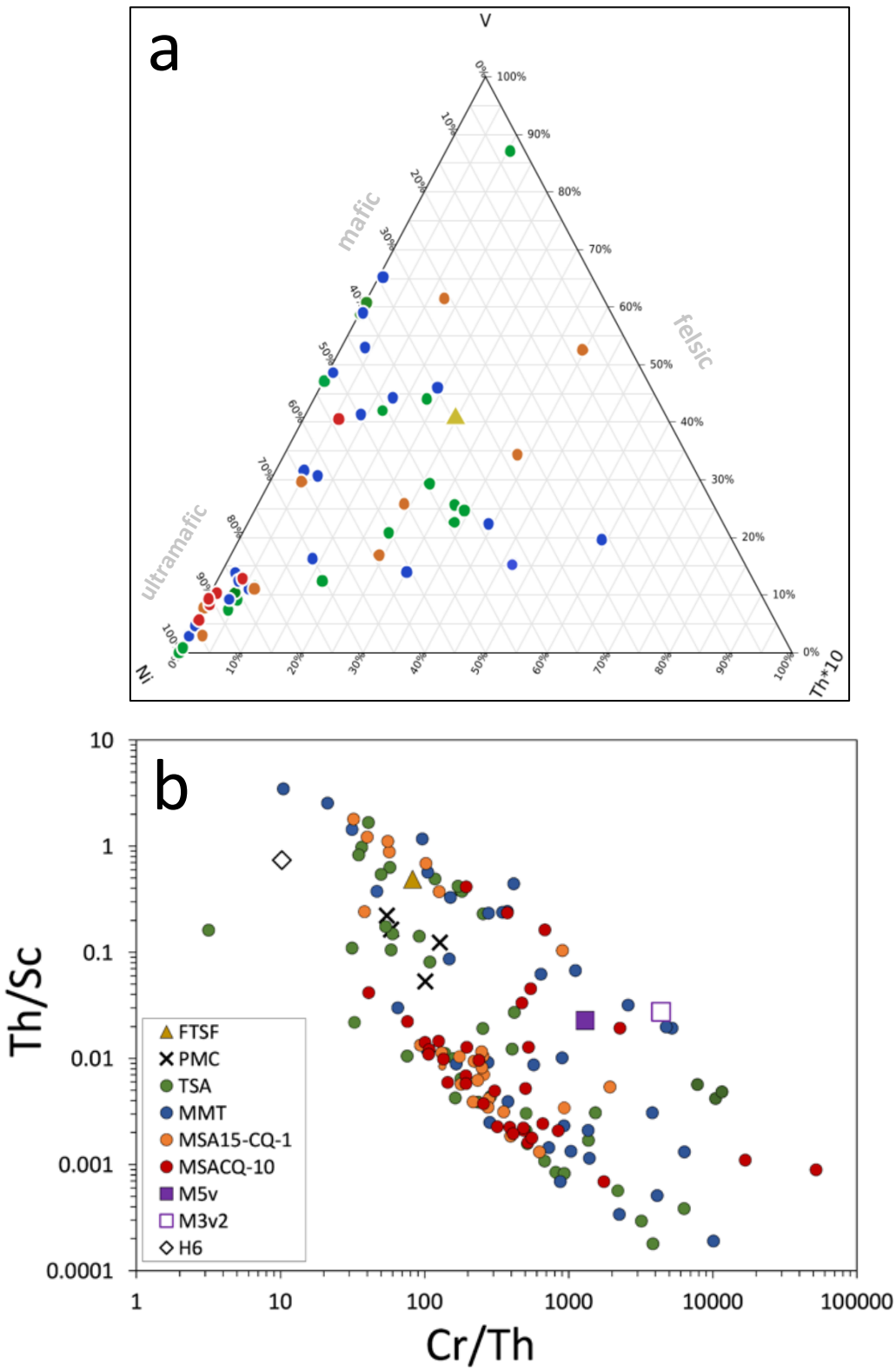

Figure 7: a) Ni-V-Th ternary plot and **b)** Th/Sc vs Cr/Th plot of the Puddingstone sedimentary clasts. Fig Tree south facies shale composition (FTSF: Hofmann, 2005); ~3.4 Ga dacite of the Hooggenoeg Formation (H6: Drabon et al., 2019), silicified komatiites of the Mendon Formation (M5v, M3v2: Decker et al., 2015); and Mendon chert found in the Puddingstone Hill site (PMC) were added as comparison material. Note: axes of Th/Sc vs Cr/Th plot are in log scale. Points represent individual ablation points.

The Ni-V-Ti ternary diagram and Cr/Th vs Th/Sc plots imply a variable provenance for the detrital material which constitutes the conglomerate clasts. Most notably the material of MSA15-CQ-10 clusters more tightly on both diagrams when compared to the rest of the samples. The ternary diagram implies that all of the detrital material from which the clasts of MSA15-CQ-10 (n = 10) are composed of was derived from an ultramafic source. The immobile element graph agrees with this in that most of the material has Th/Sc ratios below that which is expected for a mafic source (0.02; Condie & Wronkiewicz, 1990). However, Cr/Th ratios <500 for much of the material does identify a more intermediate composition. This is indicative of some degree of sediment differentiation rather than direct uplift of ultramafic material provided the material for the clasts in MSA15-CQ-10. As sedimentation only began after inception of the Mapepe Basin, the material entrained in the MSA15-CQ-10 must therefore be of Mapepe age. As much of the Mapepe sediments were derived from the uplift and exposure of underlying Mendon komatiite and cherts, the interpretation is that the clasts of MSA15-CQ-10 are derived from shallow uplift of previously formed Mapepe sediments which were reworked into the conglomerate.

In contrast to sample MSA15-CQ-10, the detrital material in samples MSA15-CQ-1 (n = 9), MMT (n = 21) and TSA (n = 13) are much more variable. A few clasts, mostly from TSA, have a composition which plots near the Mendon chert which was collected from the Puddingstone Hill Site (PMC). Much of the material also plots in the ultramafic field on both the ternary and Cr/Th vs Th/Sc plots. A few clasts - E9 (TSA), E15 (MMT) - which have a homogenous composition, plot as more felsic than the average Fig Tree shale (Cr/Th > 83; Th/Sc >0.5). Similar to MSA15-CQ-10, MMT and TSA also contain material of intermediate compositions (Th/Sc <0.2; Cr/Th <500).

MSA15-CQ-1 has a distinctly less mafic signature than the rest of the conglomerates, with Cr/Th ratios rarely exceeding that expected of basalt (Cr/Th < 500; Condie, 1980). This indicates that more felsic detritus was entrained in the MSA15-CQ-1 source. The hand specimen-scale appearance of MSA15-CQ-1 is also distinctive from the other samples (Fig. 2 h). Many of the clasts are smaller and fragmented in nature and less-well rounded than those of the other conglomerates. These features combined with the less sorted nature of the clasts indicates deposition in a higher energy environment more proximal to the source.

3.2.2. Trace element diagrams

In order to more accurately constrain the composition of the Puddingstone sediment clasts, trace element compositions were plotted on shale-normalised diagrams (Fig. 8). The average south facies Fig Tree Shale (Hofmann, 2005) was again plotted as a comparison material in order to constrain how sediment influx may have differed than the background sedimentation occurring at the time.

Plotted data was chosen based on analyses which showed all elements above the detection limit. For homogenous samples averages were taken. However, when sample heterogeneities occurred, more than 1 data point from a single sample were plotted in order to constrain the variable provenance. The graphed data is shown in Table 4.

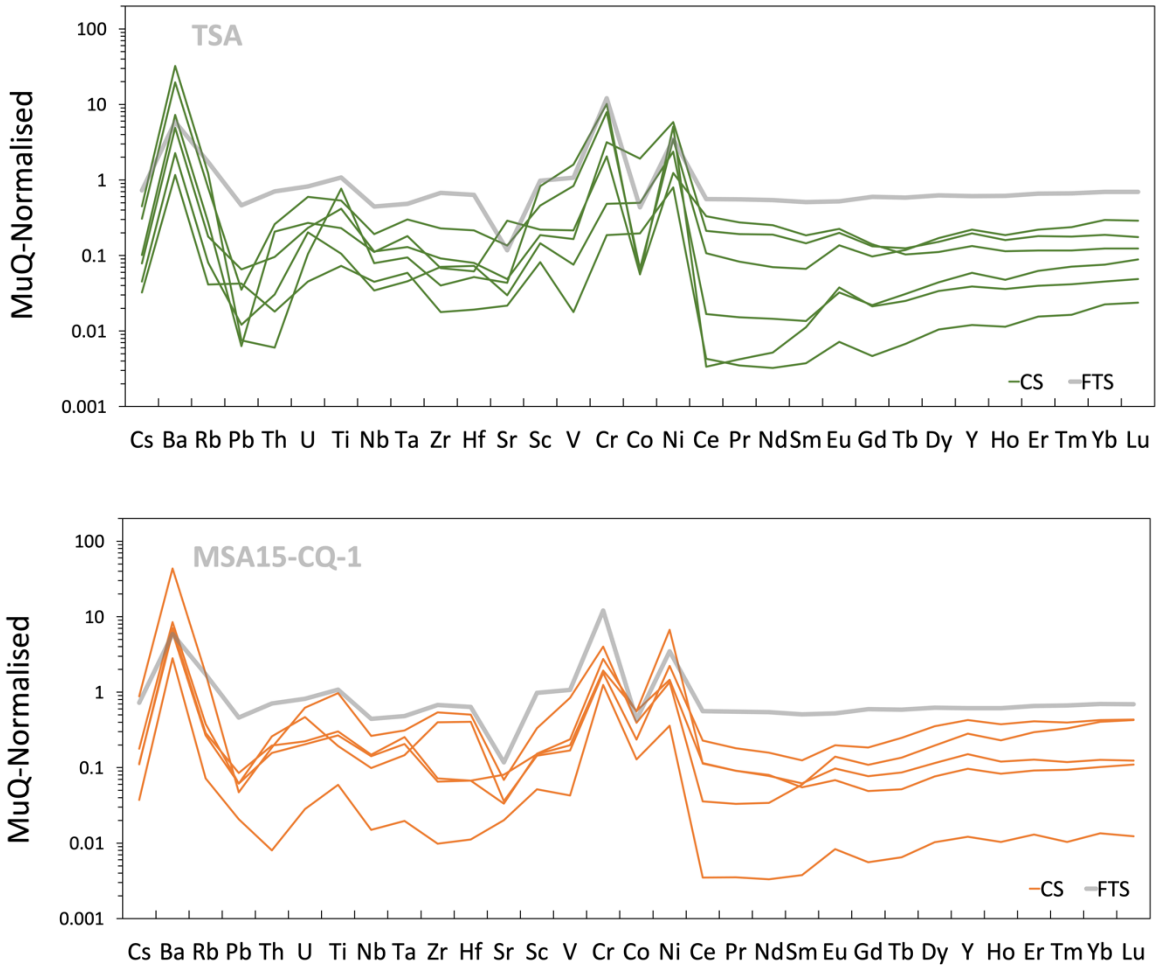

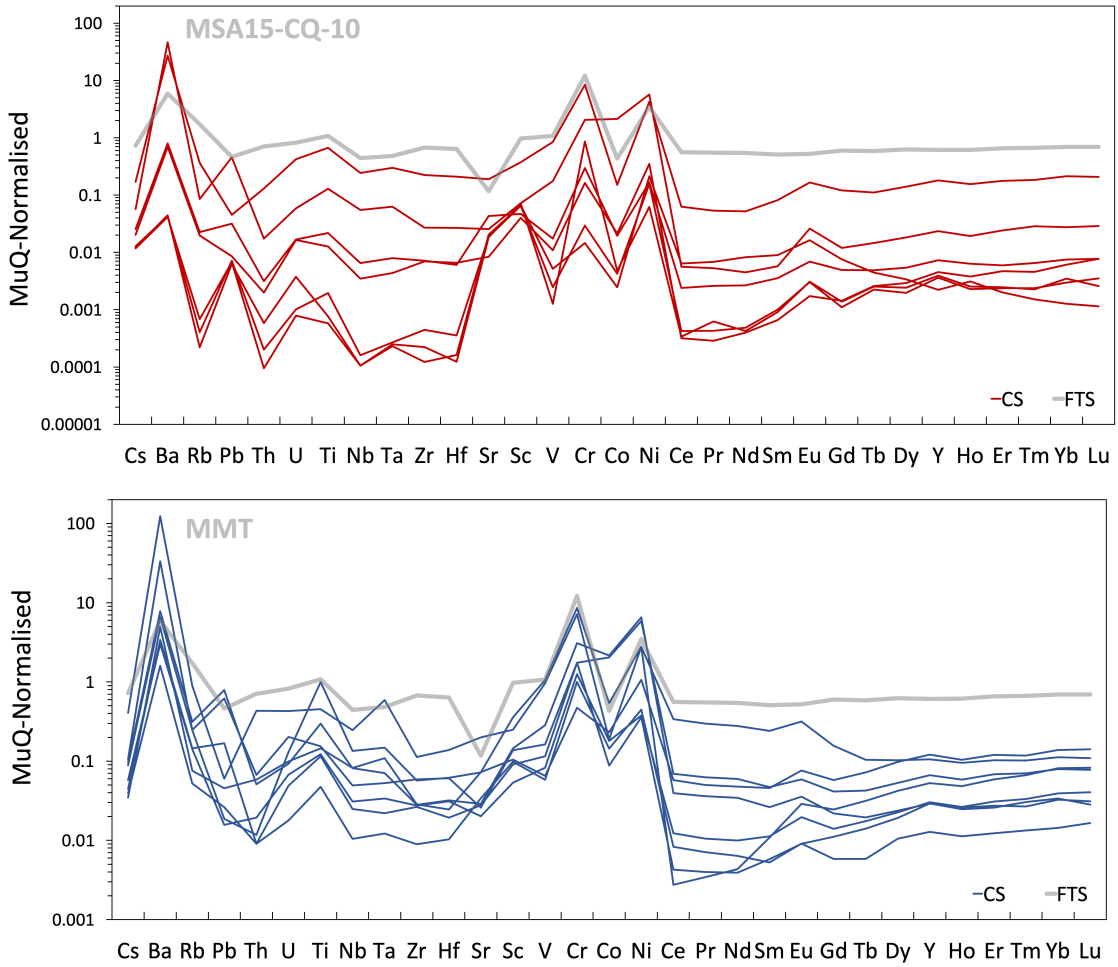

Figure 8: Shale-normalised (MuQ) trace element plots of the clastic sediments (*CS*) of the Puddingstone conglomerates. Comparison is made with the average Fig Tree South Facies shale (FTS, Hofmann, 2005) in order to determine how Mapepe sedimentation may have differed from the average sedimentation expected at the time.

As is the case for the average south facies Fig Tree shale (Hofmann 2005), most of the samples are enriched in Cr when normalised to MuQ. This is to be expected from Paleoarchean sediments, as the majority of material influx into basins would have retained the signature of ultramafic to mafic volcanism which characterised the early Archean (Sun, 1984). Exceptions to this are seen in some samples of TSA and MMT. These samples also display LREE enrichment and V depletion which further attests to their representation as a (minor) felsic contribution. All samples – including those that have been identified as a felsic component - are enriched in Ni, an element associated with mafic lithologies. An explanation for prevalent Ni enrichment could be that a silicifying fluid circulated through underlying Ni-rich strata (ie. the Mendon Formation) leaving all

of the conglomerate clasts relatively Ni-enriched. However, this interpretation must be met with caution, as Ni can readily adsorb onto sediment particles during transport and deposition, an effect which is well reported in Archean successions (Balistrieri and Murray, 1984; Condie and Wronkiewicz, 1990).

Unlike the pattern observed in the average Fig Tree south facies shale, Th is consistently depleted by up to 2 orders of magnitude for the majority of the Puddingstone conglomerate clasts. This attests to the fact that the sampled clasts derive their provenance from more mafic (ie. older) material that had only a minor felsic (Th-bearing) mineral input when compared to younger Fig Tree sediments.

Perhaps the most striking feature on the trace element plots is the deviation of the REE+Y patterns from that of the flat shale-normalised pattern characteristic of sedimentary material. Flat HREEs characterise the sedimentary rocks of the Fig Tree Group, whereas Fig Tree igneous source rocks typically have depleted HREEs (Hofmann, 2005). Furthermore, significant positive Eu anomalies are generally absent from Archaean shales and volcanic material (Taylor and McLennan, 1985). These expected REE+Y patterns strongly contrast with the observed patterns from many of the Puddingstone sedimentary clasts. Most of the clasts display distinctly seawater-like signatures, with HREE enrichment ($Yb/Pr_{SN} > 1$) and slightly positive Eu anomalies ($Eu/Eu^* > 1$) (Table 4). Furthermore, many of the clasts exhibit Y/Ho ratios over the chondritic values of ~27, which is only possible due to fractionation in hydrogenous settings (Pack, 2007).

As the southern portion of the Fig Tree Group has not exceeded metamorphic grades of lower greenschist facies, metamorphic effects can be ruled out as having fractionated the REEs in the conglomerate clasts (Condie et al., 1970). Furthermore, as igneous and sedimentary rocks contain orders of magnitude (approximately $10^5 – 10^6$) more REEs than primary chemical sediments, their signatures should easily overwhelm a fluid signature (Van den Boorn et al., 2007). Although REE+Y patterns should generally retain the signature of their source (Taylor & McClennan, 1985), it has been shown that when fluid rock ratios are high, fluids can impart their REE patterns on igneous or sedimentary lithologies (Elderfield & Sholkovitz, 1987; Migdisov et al., 2016). Furthermore, heavy-REE bearing minerals may be removed from mafic-derived materials due to weathering and transport effects, causing them to not represent source provenance (Cullers et al., 1993). As the detrital REE+Y signature would obscure the original fluid composition

which silicified the clasts, no direct interpretation of a silicifying fluid composition can be made. However, the significant departure from the expected provenance-derived REE+Y pattern of many of the Puddingstone sedimentary clasts may be used as *prima facie* evidence that a seawater-derived fluid caused silicification of the sedimentary material which makes up many of the Puddingstone conglomerate clasts.

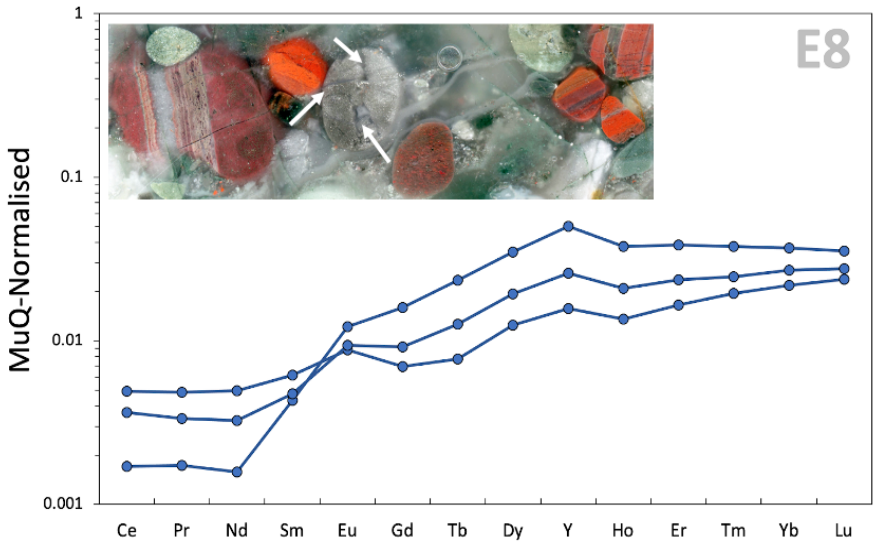

Figure 9: Sample TSA. Arrows point to 3 Si-filled fractures which are infilled in clast E8. Eu/Eu* = 1 - 1.5 and Y/Ho = 30-35 are indicative of the rare earth element and Yttrium component of the sample being primarily supplied by an Archean seawater-derived fluid. (Photograph credit of Kimberly Myers).

3.2.3 Barium enrichment in the conglomerate clasts

As is characteristic of many Fig Tree sediments, the Puddingstone sedimentary and hydrogenous clasts are variably enriched in barium. The correlation between Ba and Al_2O_3 ($R^2 = 0.8$) is to be expected from preferential incorporation of Ba into phyllosilicates and the clastic fraction (Zhang et al., 2001). This is further illustrated when Ba is plotted against other fluid-mobile elements such as Cs and Sr (Fig. 10). These plots show that elevated Ba concentrations are associated with elevated Cs and Sr concentrations. However, 2 'low-Ba' and 'high-Ba' categories develop in which the clastic conglomerate clasts are associated with the latter. These plots also illustrate that as Ba was being mobilised so were the other fluid mobile elements. However, Ba concentrations are generally much higher than the other mobile elements. This is a result of the silicifying fluid being more rich in Ba – either as a result of mobilising Ba from surrounding Ba-rich rocks, or having originated as a Ba-rich fluid.

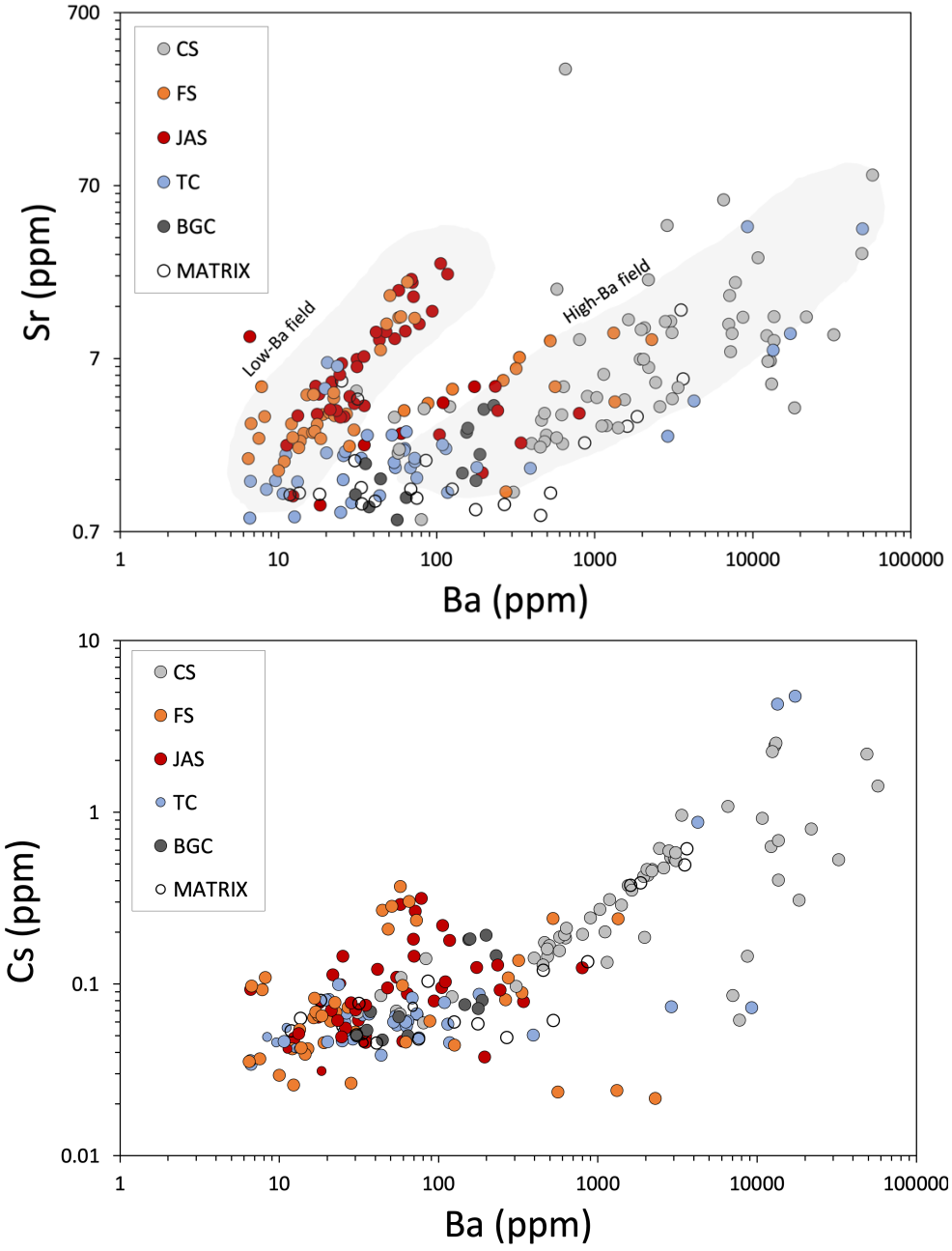

Figure 10: Sr vs Ba plot. Ba and Sr correlate as they were both mobilised by a fluid. Group into 2 separate "Low-Ba" and "High-Ba" fields due to preferential incorporation of Ba into phyllosilicates and onto clay minerals. *CS* = clastic sediment; *FS* = furriginous sediment; *JAS* = jaspilite; *TC* = translucent chert; *BGC* = black/grey chert.

Table 5:

Major and trace element composition of the sedimentary Puddingstone conglomerate clasts. Empty fields represent measurements which were below the detection limit. *n* = number of ablation points averaged. For some heterogeneous clasts multiple points were plotted. SiO_2, Fe_2O_3, MnO, Na_2O and P_2O_3 were obtained by Bulk XRF (Kimberly Myers, unpublished data). ΣHFSE: sum of Zr, Hf, Nb, Ta and Y; ΣLILE: sum of Cs, Rb and Ba. Calculation of Eu/Eu* is given in *Section 2.4.2.*

Sample	**TSA**						**MMT**								**MSA15-CQ-1**					**MSA15-CQ-10**							
Clast	**E2**	**E5**	**E8**	**E9**	**E12**	**E13**	**E15**	**E17**	**E18**	**E19**	**E22**	**E22**	**E26**	**E28**	**E32**	**E37**	**E37**	**E38**	**E38**	**E40**	**E40**	**E41**	**E41**	**E41**	**E51**	**E51**	**E51**
Extra info.																*Carbonaceous*		*Carbonaceous*		*Carbonaceous*		*Inclusion-rich*				
n	1	3	1	1	1	3	1	1	3	1	1	1	1	1												
Element (wt%)																										
SiO2	82.03	85.64	85.48	85.56	85.76	82.91	81.52	84.79	84.94	84.95	84.17	84.17	85.41	83.59	68.93	85.03	85.03	84.80	84.80	81.53	81.53	80.44	80.44	80.44	85.46	85.46	85.46
Al2O3	7.83	1.47	0.36	2.57	0.71	13.01	15.09	1.28	5.95	1.20	2.90	2.19	1.58	0.49	16.76	2.30	3.23	2.65	0.72	0.21	0.17	8.25	8.25	3.32	0.05	0.30	0.13
Fe2O3	4.24	0.63	0.39	0.74	0.24	5.23	-	1.49	4.27	6.67	1.03	1.03	2.00	0.44	1.72	0.59	0.59	1.54	1.54	2.27	2.27	2.28	2.28	2.28	1.55	1.55	1.55
MnO	0.01	-	-	-	-	0.01	0.02	0.09	0.02	0.01	-	0.00	-	-	0.005	0.001	0.001	0.002	-	-	-	0.011	0.011	0.001	0.002	0.002	0.004
MgO	-	-	-	-	-	-	0.13	-	0.13	-	-	-	-	-	0.95	-	-	-	-	0.18	0.18	0.38	0.38	0.38	-	-	-
CaO	0.11	0.08	0.06	0.10	0.07	0.19	0.20	0.08	0.10	0.06	0.09	0.09	0.10	0.07	0.21	0.07	0.08	0.07	0.05	0.03	0.02	0.12	0.12	0.08	0.06	0.06	0.05
Na2O	0.50	0.28	0.25	0.29	0.30	0.46	0.44	0.33	0.45	0.35	0.34	0.34	0.36	0.25	0.49	0.33	0.33	0.37	0.37	0.39	0.39	0.34	0.34	0.34	0.30	0.30	0.30
P2O5	0.07	0.11	0.13	0.12	0.10	0.09	0.08	0.14	0.10	0.15	0.13	0.13	0.16	0.14	0.43	0.10	0.10	0.12	0.12	0.06	0.06	0.04	0.04	0.04	0.13	0.13	0.13
(ppm)																											
Cs	1.65	0.42	0.17	0.55	0.24	2.41	2.18	0.19	0.57	0.31	0.52	0.47	0.24	0.21	4.74	0.62	0.96	0.60	0.20	0.14	0.11	0.92	0.92	0.31	0.06	0.07	0.07
Ba	7740.93	1936.35	461.31	2874.07	897.81	12834.10	48942.91	1965.35	13159.06	1186.27	3093.91	2587.96	1342.03	634.56	17295.09	2432.26	3357.45	2795.67	1111.09	317.87	274.04	10763.74	10763.74	18342.13	16.43	17.52	16.96
Rb	62.41	14.19	3.28	21.84	6.39	96.46	70.50	6.03	19.41	11.24	25.00	19.70	11.53	4.15	140.69	21.25	30.18	22.94	5.72	1.80	1.57	29.03	29.03	6.82	0.05	0.02	0.03
Th	2.89	1.07	0.20	2.30	0.34	0.07	4.80	0.65	0.13	0.22	0.57	0.75	0.10	0.10	2.05	2.89	1.74	2.19	0.09	0.04	0.02	1.45	1.45	0.19	0.001	0.01	0.002
U	1.69	0.66	0.13	0.76	0.57	0.30	1.21	0.28	0.37	0.19	0.26	0.57	0.14	0.05	1.76	1.32	0.58	0.63	0.08	0.05	0.05	1.20	1.20	0.17	0.002	0.01	0.003
Nb	2.95	1.73	0.69	1.71	0.53	1.21	3.76	1.26	2.07	0.47	1.25	0.76	0.38	0.16	4.04	1.52	2.17	2.28	0.23	0.10	0.05	3.72	3.72	0.84	0.002	0.002	0.002
Ta	0.34	0.14	0.07	0.20	0.05	0.11	0.66	0.12	0.17	0.04	0.08	0.06	0.02	0.01	0.35	0.16	0.23	0.28	0.02	0.01	0.00	0.34	0.34	0.07	0.0003	0.0003	0.0003
Pb	0.72	1.34	0.87	0.13	0.25	0.15	1.23	0.93	0.38	0.32	16.15	12.64	3.44	0.54	0.96	1.26	1.26	1.74	0.42	0.65	0.18	0.92	0.92	9.33	0.14	0.13	0.15
Sr	19.23	6.94	3.08	41.13	4.24	6.18	28.30	10.31	10.22	2.87	4.10	3.69	3.94	4.81	9.78	5.09	4.75	11.45	2.86	6.12	1.19	26.80	26.80	3.63	2.62	2.91	2.66
Zr	45.40	18.25	3.55	13.58	14.04	7.97	22.49	5.66	11.29	5.50	5.61	11.75	5.27	1.78	107.11	79.62	13.03	14.30	1.96	1.43	1.38	44.40	44.40	5.39	0.04	0.02	0.09
Hf	1.14	0.43	0.10	0.33	0.39	0.28	0.74	0.13	0.33	0.17	0.17	0.32	0.10	0.05	2.68	2.15	0.36	0.36	0.06	0.03	0.04	1.12	1.12	0.14	0.00	0.00	0.00
Ti	1601.66	1245.90	218.33	689.83	316.31	2310.27	1361.44	434.55	2978.17	367.89	890.22	463.79	346.37	141.98	2919.71	581.33	802.21	908.31	177.56	65.28	38.03	2013.96	2013.96	387.14	1.74	2.29	5.83
Sc	7.57	3.06	1.34	3.63	2.40	13.63	4.10	1.73	5.89	0.89	2.39	2.26	1.50	1.63	5.48	2.37	2.53	2.48	0.85	0.77	0.66	6.16	6.16	1.19	1.18	1.10	1.07
V	100.01	19.73	2.13	25.74	9.08	192.47	115.32	7.80	126.84	9.93	34.06	19.59	13.85	6.98	100.86	20.24	28.42	23.70	5.15	2.09	1.31	101.52	101.52	21.02	0.15	0.62	0.30
Cr	511.33	203.65	12.05	132.19	31.27	656.45	462.02	30.40	555.28	80.63	198.35	112.58	112.61	64.68	258.48	115.54	178.07	124.86	80.40	19.05	10.46	543.45	543.45	132.41	55.29	0.94	1.89
Co	1.50	42.97	4.40	1.27	11.12	1.26	4.23	5.20	12.06	4.02	48.34	45.82	1.97	3.23	8.82	5.26	12.46	12.63	2.89	0.44	0.48	3.39	3.39	47.99	0.11	0.06	0.09
Ni	108.94	184.76	25.11	39.05	74.76	160.26	87.29	33.56	88.18	11.93	207.09	185.21	11.27	14.11	42.77	70.46	211.52	46.23	11.31	5.30	11.06	134.41	134.41	180.15	1.96	6.77	4.97
As	5.18	357.78	83.93	4.56	131.10	1.77	11.03	15.15	48.61	12.87	424.57	630.59	15.92	22.61	67.62	125.13	413.84	103.73	21.14	5.80	11.05	9.62	9.62	172.53	9.20	3.51	3.65
La	4.42	7.54	2.67	14.50	20.55	0.07	13.08	4.05	0.30	2.64	1.36	5.65	0.12	1.14	1.31	8.87	4.42	4.63	0.94	3.15	2.84	2.45	2.45	1.27	0.02	0.27	0.01
Ce	7.62	15.05	0.31	23.53	1.19	0.24	24.13	4.09	0.20	0.88	2.81	4.94	0.30	0.59	2.53	16.26	8.04	8.17	0.25	0.17	0.02	4.46	4.46	0.40	0.02	0.45	0.03
Pr	0.70	1.62	0.03	2.31	0.13	0.04	2.51	0.42	0.03	0.09	0.31	0.53	0.03	0.06	0.28	1.53	0.77	0.77	0.03	0.02	0.00	0.45	0.45	0.05	0.01	0.06	0.004
Nd	2.31	6.24	0.11	8.30	0.48	0.17	9.14	1.57	0.14	0.33	1.13	1.96	0.13	0.21	1.13	5.21	2.63	2.56	0.11	0.09	0.01	1.72	1.72	0.15	0.01	0.27	0.02
Sm	0.46	1.00	0.03	1.27	0.09	0.08	1.66	0.32	0.08	0.08	0.18	0.32	0.04	0.04	0.41	0.86	0.38	0.43	0.03	0.02	0.00	0.56	0.56	0.04	0.01	0.06	0.01
Eu	0.21	0.31	0.01	0.35	0.05	0.06	0.50	0.12	0.05	0.03	0.06	0.09	0.01	0.01	0.22	0.31	0.11	0.15	0.01	0.01	0.00	0.26	0.26	0.04	0.00	0.03	0.005
Gd	0.62	0.84	0.03	0.90	0.14	0.13	0.99	0.37	0.16	0.09	0.14	0.26	0.07	0.04	0.70	1.18	0.31	0.49	0.04	0.03	0.01	0.77	0.77	0.08	0.01	0.05	0.01
Tb	0.12	0.12	0.01	0.10	0.03	0.02	0.10	0.07	0.03	0.02	0.02	0.04	0.01	0.01	0.13	0.25	0.05	0.09	0.01	0.00	0.00	0.11	0.11	0.01	0.00	0.00	0.002
Dy	1.00	0.89	0.06	0.66	0.26	0.20	0.61	0.58	0.25	0.13	0.14	0.31	0.11	0.06	1.15	2.08	0.45	0.68	0.06	0.03	0.02	0.83	0.83	0.11	0.01	0.02	0.01
Ho	0.23	0.20	0.01	0.14	0.06	0.04	0.12	0.13	0.06	0.03	0.03	0.07	0.03	0.01	0.28	0.46	0.10	0.15	0.01	0.01	0.00	0.19	0.19	0.02	0.003	0.004	0.00
Y	7.00	6.28	0.38	4.24	1.88	1.24	3.35	3.85	1.69	0.97	0.93	2.12	0.93	0.41	8.97	13.60	3.08	4.81	0.39	0.23	0.14	5.73	5.73	0.75	0.12	0.07	0.12
Er	0.74	0.61	0.05	0.39	0.21	0.13	0.35	0.41	0.20	0.10	0.09	0.23	0.09	0.04	0.99	1.39	0.31	0.43	0.04	0.02	0.02	0.60	0.60	0.08	0.01	0.01	0.01
Tm	0.12	0.09	0.01	0.06	0.04	0.02	0.05	0.06	0.03	0.02	0.01	0.04	0.02	0.01	0.17	0.20	0.05	0.06	0.01	0.00	0.00	0.09	0.09	0.01	0.00	0.001	0.00
Yb	0.96	0.61	0.07	0.40	0.25	0.15	0.37	0.45	0.26	0.13	0.11	0.26	0.11	0.05	1.32	1.39	0.33	0.41	0.04	0.02	0.02	0.69	0.69	0.09	0.01	0.004	0.01
Lu	0.14	0.09	0.01	0.06	0.04	0.02	0.05	0.07	0.04	0.02	0.02	0.04	0.01	0.01	0.21	0.21	0.05	0.06	0.01	0.00	0.00	0.10	0.10	0.01	0.00	0.001	0.00
∑HFSE	56.83	26.83	4.79	20.06	16.89	10.80	31.00	11.02	15.54	7.14	8.04	15.01	6.71	2.42	114.18	83.46	15.79	17.22	2.27	1.57	1.47	49.58	49.58	6.45	0.05	0.03	0.09
∑LILE	7804.99	1950.96	464.76	2896.46	904.44	12932.97	49015.59	1971.57	13179.04	1197.82	3119.43	2608.13	1353.80	638.92	17440.52	2454.13	3388.59	2819.21	1117.01	319.81	275.72	10793.69	10793.69	18349.26	16.55	17.60	17.06
Cr/Th	176.9	190.9	60.0	57.5	92.0	9797.8	96.3	46.8	4249.6	375.0	348.0	150.9	1115.0	640.4	126.1	40.0	102.3	57.0	903.4	544.3	473.3	374.8	374.8	682.5	52160.4	144.5	843.8
Th/Sc	0.4	0.3	0.1	0.6	0.1	0.005	1.2	0.4	0.02	0.2	0.2	0.3	0.1	0.1	0.4	1.2	0.7	0.9	0.1	0.05	0.03	0.2	0.2	0.2	0.001	0.006	0.002
Y/Ho	30.8	32.0	27.5	30.6	32.4	28.1	28.9	30.3	28.6	30.0	29.3	29.8	30.9	29.7	31.9	29.8	30.3	32.7	30.8	30.1	31.1	30.3	30.3	31.8	40.6	18.7	41.3
Eu/Eu*	1.6	1.4	1.5	1.4	1.7	2.4	1.6	1.4	1.6	1.5	1.5	1.3	1.1	1.7	1.6	1.2	1.3	1.4	1.8	1.7	1.3	1.8	1.8	3.0	2.1	2.2	2.2
Yb/PrSN	3.6	1.0	6.4	0.5	5.0	10.7	0.4	2.8	23.7	3.7	0.9	1.3	8.5	2.0	12.2	2.4	1.1	1.4	3.8	2.9	21.3	4.0	4.0	5.2	5.6	0.2	6.9

3.3. The conglomerate matrix

The clasts of the Puddingstone conglomerates are hosted in a fine grained, silicified matrix (Figs. 2e-h). Al content of of the matrix is generally low, with much of the matrix material having Al concentrations <1,100 ppm (Fig. 5). This indicates that silt, clay or volcanic detritus were unlikely to be the primary precursor matrix material as the immobile nature of Al would allow this to still be reflected in the geochemistry of the matrix, had it originally been an Al-rich material (Pearce & McCann, 1973). Candidates for the precursor-matrix material include carbonate cement or a primary silica cement - as would be possible in an Archean Ocean of near-saturation level of amorphous silica (Siever, 1992). As many of the major elements which are found in carbonates (eg. Na, Ca) are extremely fluid mobile, the original matrix material of the Puddingstone conglomerates is difficult to ascertain. This is reflected in the trace element geochemistry of the matrix material, with CaO rarely exceeding 500 ppm for all samples. However, as both carbonate and silica allow the fluid from which they were precipitated to be inferred, analysis of the Puddingstone matrix nonetheless allows a possible fluid composition to be reconstructed.

Detrital signatures were excluded using the methods as mentioned in *Section 3.1*. The only exception to this is sample TSA, in which Ti is found elevated in all analyses, indicative of detrital particles being entrained prior to matrix cementation.

Many of the trace and rare earth elements in the matrix are below detection limits. Extremely low REE concentrations are further indication that the matrix material was likely directly precipitated from a fluid. However, such analyses provided spikey REE+Y patterns and such results could not be evaluated. The graphed matrix material of MMT, MSA15-CQ-10 and MSA15-CQ-1 can be taken to represent a fluid composition, with the sum of Al, Zr and Ti not exceeding 86 ppm, 271 ppm and 280 ppm for the graphed values respectively. As mentioned, detrital input was unavoidable for the TSA simple matrix, with Al, Zr and Ti summing 5,821 ppm. As such, caution was taken when interpreting this result.

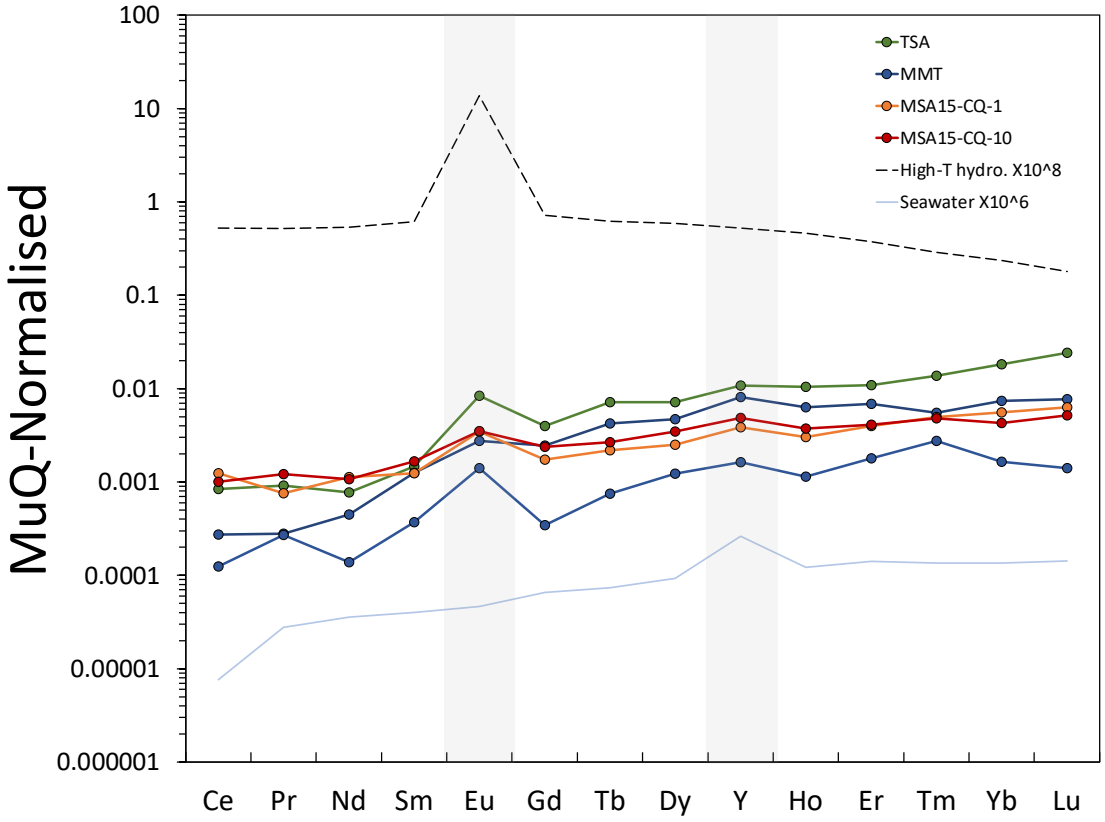

Figure 11: REE+Y patterns of the Puddingstone conglomerate matrix. LREE>HREE inherited from seawater and Eu/Eu*>1 inherited from a hydrothermal component.

The discussed matrix components show distinctly seawater-like REE+Y patterns. The samples are enriched in HREEs when compared to LREEs (HREE>LREE), express positive Eu anomalies (Eu/Eu*), and contain super-chondritic Y/Ho ratios (excluding TSA which contains detrital material). As Y/Ho ratios can only be fractionated in aqueous solution, the super-chondritic Y/Ho ratio of 33-37.5 which are observed in the matrix component of samples MMT, MSA15-CQ-10 and MSA15-CQ-1, lends evidence that the conglomerates were silicified in an aqueous environment (Bau, 1999; 2000; Shields & Webb, 2004).

The positive REE slope indicates that this aqueous solution had a marine component, whereas the observed positive Eu anomalies indicate that the fluid was charged with some degree of hydrothermal solution. These features are highlighted Fig. 11, where comparisons have been made with modern, shallow seawater (Alibo & Nozaki, 1999) and modern high-temperature hydrothermal black smoker fluid (Bau & Dulski, 1999). This illustrates that the positively sloped REE pattern and positive Y/Ho values likely came

from a seawater contribution, whilst the positive Eu anomalies originated from a hydrothermal component.

As MSA15-CQ-1 and MSA15-CQ-10 show consistently low detrital elements, they offer the best means to constrain a silicifying fluid. In MSA15-CQ-1 Eu/Eu* = 2.2 and in MSA15-CQ-10 Eu/Eu* = 1.8. These Eu anomaly values are close the range expected for Archean seawater (Eu/Eu* 1-2). Therefore, the positive Eu anomalies within the matrix material are likely a product of being precipitated from silica-saturated Archean seawater rather than being strongly influenced by local hydrothermal effluent.

As mentioned in the methods, the internal standard values (SiO_2) were arbitrarily chosen. In order to more accurately constrain the trace element values of the matrix material, future work may focus on determining the internal standard value through precise methods such as microprobe. However, as the observed REE+Y patterns are ratio-based the discussed patterns are valid, nonetheless.

Table 6:

Major and trace element composition of the Puddingstone conglomerate matrix described in the text. Empty fields represent measurements which were below the detection limit. ΣHFSE: sum of Zr, Hf, Nb, Ta and Y; ΣLILE: sum of Cs, Rb and Ba. Calculation of Eu/Eu* is given in *Section 3.4.2*. Note: SiO_2 values were arbitrarily chosen.

Sample	TSA	MMT	MMT	MSA15-CQ-1	MSA15-CQ-10
Element (wt%)					
SiO2	95.000	95.000	95.000	95.000	95.000
Al2O3	1.085	0.007	0.016	0.051	0.042
MnO	0.000	0.063	0.010	0.171	0.000
CaO	0.083	0.054	0.066	0.047	0.035
(ppm)					
Cs	0.375	0.063	0.052	0.048	0.060
Ba	1606.030	13.570	33.360	74.830	125.090
Rb	10.450	0.057	0.196	0.359	0.308
Th	0.064	0.002	0.001	0.008	0.016
U	0.119	0.044	0.025	0.005	0.028
Nb	0.087	0.007	0.005	0.006	0.031
Ta	0.009	-	-	0.0002	0.005
Pb	0.300	0.059	0.050	0.136	0.068
Sr	2.850	1.170	1.261	1.092	1.232
Zr	2.290	0.035	0.044	0.128	0.252
Hf	0.098	0.003	0.001	0.003	0.009
Ti	72.500	2.910	3.410	2.840	21.280
Sc	1.640	0.560	1.096	0.952	0.866
V	5.990	0.203	0.104	0.412	0.416
Cr	34.490	1.143	0.984	1.143	1.484
Co	1.439	0.174	0.229	0.619	0.871
Ni	6.060	1.830	3.330	5.330	6.930
As	7.780	0.930	4.800	5.250	10.810
La	36.840	5.050	8.230	2.840	0.279
Ce	0.060	0.019	0.009	0.088	0.072
Pr	0.008	0.002	0.002	0.006	0.010
Nd	0.025	0.015	0.005	0.037	0.035
Sm	0.010	0.009	0.003	0.009	0.012
Eu	0.013	0.004	0.002	0.005	0.006
Gd	0.025	0.016	0.002	0.011	0.015
Tb	0.007	0.004	0.001	0.002	0.003
Dy	0.042	0.028	0.007	0.015	0.021
Ho	0.013	0.008	0.001	0.004	0.005
Y	0.345	0.258	0.052	0.123	0.154
Er	0.037	0.023	0.006	0.013	0.014
Tm	0.007	0.003	0.001	0.003	0.002
Yb	0.059	0.024	0.005	0.018	0.014
Lu	0.012	0.004	0.001	0.003	0.003
∑HFSE	2.83	0.30	0.10	0.26	0.45
∑LILE	1616.86	13.69	33.61	75.24	125.46
Y/Ho	27.17	33.46	37.48	33.33	33.77
Eu/Eu*	2.50	1.22	2.85	2.25	1.76
Yb/PrSN	19.95	26.25	6.07	7.33	3.53

3.4. Silica veins and chert

In this section of the thesis, silica veins and chert from the Barite Valley, Puddingstone Hill and the Masenjane Barite Workings are discussed in order to further constrain the possible mechanisms for silicification in the southern Fig Tree Group.

Although no published data exists on the Puddingstone Hill and Masenjane Barite Working sites, recently Lowe and colleagues (2019) have conducted extensively detailed field-based work on Fig Tree chert dykes and barite deposits in the Barite Valley. The study follows from the earlier interpretations by Lowe (2013) to conclude that chert dykes in the area represent fractures in the upper crust which allowed the downwards flow of volcaniclastic sediment and Member 4 dacitic tuff (Galić, 2015) of the Mapepe Basin which was later silicified to form pale green chert.

If the conclusions of Lowe et al. (2019) are correct, then the chert 'dykes' in the Eastern Barite Valley have no relation to barite deposition and barite geochemistry carries little information on the composition of Archean sea water. Instead, the studies concludes that sulphate was sourced from meteoric water. Such a conclusion would hold implications to conflicting studies which have used barite from the EBV to make conclusions on the composition of Paleoarchean seawater (eg. Roerdink et al., 2022).

3.4.2. Immobile element ratios of chert

Immobile element ratios (Cr/Th vs Th/Sc) were used to make preliminary assumptions on the origin of the silica veins and chert (Fig. 12). Due to heterogeneities in many of the samples, individual ablation points were graphed rather than averages of analyses. The geochemical data were compared to silicified Mendon komatiites which underlie the Barite Valley (M5v, M3v2; Decker et al., 2015), banded black-and-white Mendon cherts which were collected from the Puddingstone Hill and Masenjane Barite Workings sites (PMC, MMC; from the unpublished MSc thesis of Esmee Wardenburg, 2019), ~3.226 Ga plagioclase-phyric dacitic rocks of the Schoongezicht Formation (SG; Kohler & Annhaeuser, 2002) and the average composition of Fig Tree south facies shale (FTSF; Hofmann, 2005).

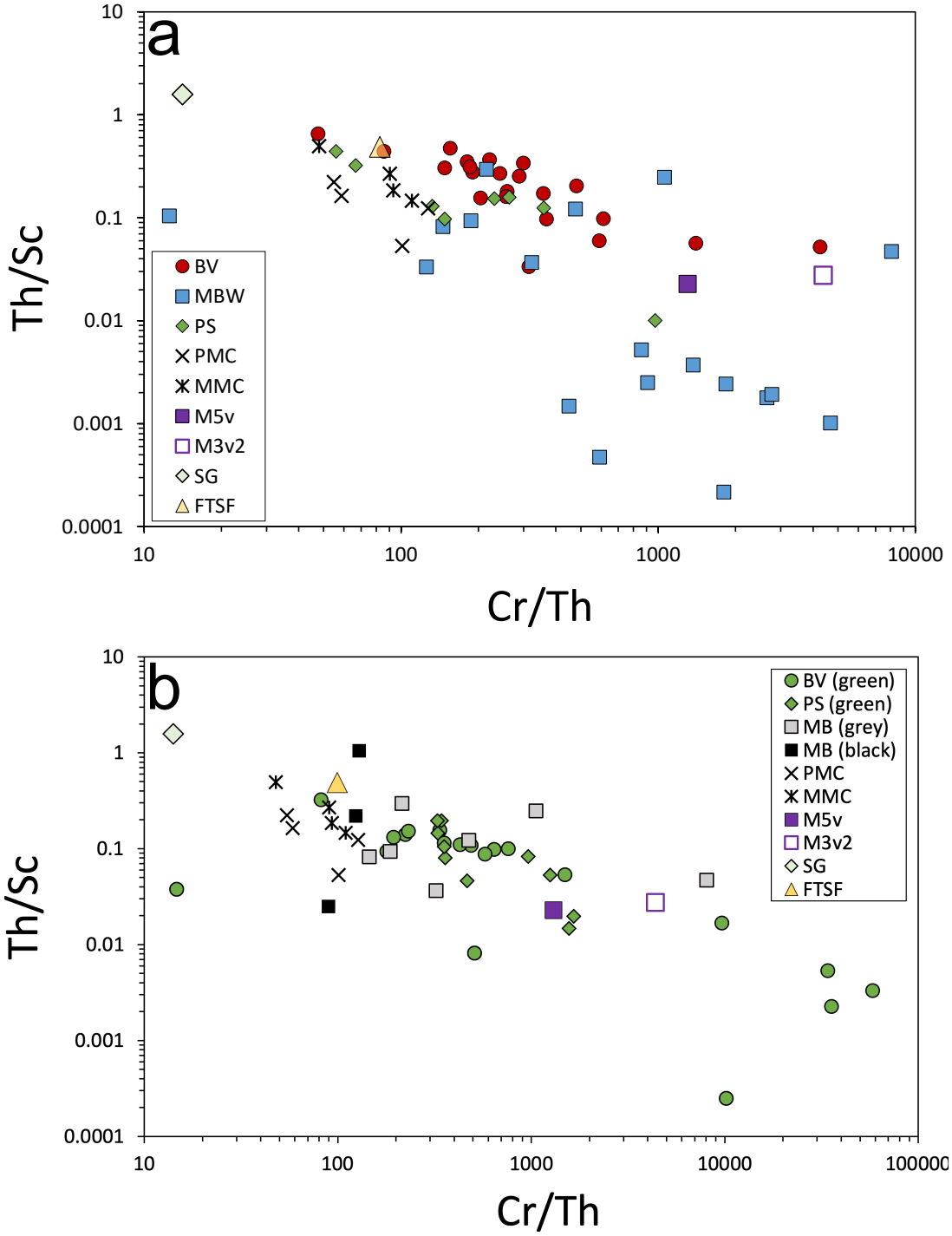

Figure 12: Immobile trace element plots of the Barite Valley silica vein (*BV*); 2 grey chert silica veins from the Masenjane Barite Workings (*MBW*); a white chert silica vein from the Masenjane Barite Workings (19-MB-01); and 2 Puddingstone Hill (*PS*) black chert silica veins compared to the average south facies Fig Tree shale (FTSF: Hofmann, 2005); silicified Mendon komatiites (M5v, M3v2: Decker, 2015); ~3.28 Ga dacite of the Schoongezicht Formation (SG: Kohler & Annhaeusser 2002). Black and white Mendon chert from the Puddingstone Hill site (*PMC*) and the Masenjane site (MMC) **A)** Th/Sc vs Cr/Th for the Barite Valley (BV), Masenjane Barite Workings (MBW); **B)** Ti/Zr vs Cr/Th. Note: All axes are in log form.

For the silica veins, wide variations in the immobile element ratios indicate that the sampled material is heterogeneous. This is expected from the material being a combination of volcanic and/or sedimentary detritus, silicifying fluid and assimilated wall rock. For both the silica veins and chert, the relatively high Cr/Th ratios (consistently >100), and relatively low Th/Sc ratios (consistantly <1) suggest that the material does not represent silicified felsic material. Instead, the green cherts in Barite Valley which have been suggested to represent silicified felsic ash (Lowe et al., 2019) have immobile element ratios indicative of a mafic-ultramafic signature. However, as this is controlled by elevated Cr concentrations (81-446 ppm) such signatures may be a result of Cr-rich inclusions (discussed below).

Although dissimilar, none of the locations show evidence that the chert or silica veins represent silicified felsic material that was erupting at the time. None of the trace element patterns for any of the locations exhibit elevated Zr values, which would be expected if the primary influence on their composition was felsic volcanic detritus (Thurston et al., 2012). Furthermore, none of the chert samples from any of the locations show characteristic felsic REE+Y patterns characteristic of felsic ash or volcaniclastics (LREE>HREE) (Figs. 14, 16, 18).

3.4.3. The Eastern Barite Valley (EBV)

Trace element patterns of the Barite Valley silica veins are similar to that of sericite shales which have been found in the EBV (Ledevin et al., 2015). Similarities include Cr and Ni enrichment, (relatively) flat REE+Y patterns, and Ba-enrichment (which is to be expected for most of the rocks found in the Barite Valley). These similarities can be used to conclude that the majority of the material that is entrained in the chert veins is derived from the surrounding shale. Further to this, the trace element profiles of the chert are similar to the silica veins. This can be used to infer that venting from the silica veins (or chert dykes) may have also led to chert deposition, or that chert in the EBV represents silicified host-rock. An apparent deviation from all of the EBV chert samples to the surrounding shales is the significant depletion in Co. However, as Co can be leached during the Si-metasomatism of volcanic rocks and shales this is likely a result of post-depositional fluid-rock interactions (e.g. Hofmann, 2005).

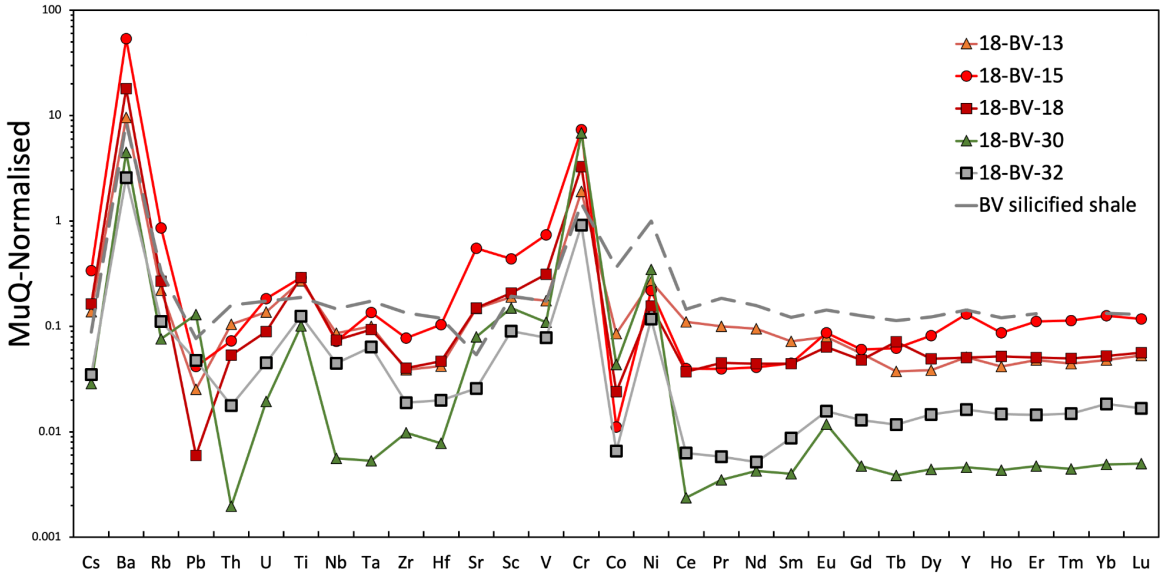

Figure 13: Shale-normalised trace element diagram of chert from Barite Valley. 18-BV-13: the upper portion of the main silica vein; 18-BV-15: the middle of the silica vein; 18-BV-18: the lower portion of the silica vein; 18-BV-30: green chert; 18-BV-32: grey chert. Results were plotted with silicified sericite shale found in the barite Valley which has been interpreted to be dyke host rock (Ledevin, 2015).

Elevated Cr levels in all of the EBV samples likely indicate the presence of chromite ($FeCr_2O_4$) or fuchsite $K(Al, Cr)_2(OH)_2$. Cr concentrations are most enriched in the green chert (18-BV-30). Although some green Cr-rich cherts found in the BGB have been found to represent silicified komatiitic ash (Hofmann, 2013), Cr-enrichment in the green chert found in the EBV is unlikely to have such an origin as no basaltic or komatiitic volcanism has been documented during the Mapepe time. Although immobile, Cr nucleation within hydrothermal solutions has been documented in cases where there is a significant concentration of Cr at the fluid source (Arai et al., 2014). Fluid in the EBV may have circulated through the underlying Overwacht unit, mobilising significant amounts of Cr. This would allow the silica veins and green chert in the Barite Valley to be elevated in Cr when compared to the surrounding shales. Chromite particles may then have acted as a nucleation site for Si to form Cr-rich green chert. Such an interpretation would agree with the stratigraphy of the EBV, in which silica veins are seen to cut the underlying altered komatiitic rocks (Lowe et al. 2019).

The middle portion of the silica vein collected from the EBV (18-BV-15) shows a REE+Y pattern with Y/Ho = 39; HREE>LREE; and Eu/Eu* = 1.7 (Fig. 14). The interpretation of

this result can be met as a result of a seawater-bearing fluid being charged through the host-rock. Sufficient concentrations of such a fluid could overwhelmed the flat REE+Y pattern that would be expected from the surrounding shale host-rock (Migdisov et al. 2016). Sample 18-BV-15 is also enriched by almost a magnitude higher in Ba than the surrounding shales (Ledevin, 2015). This may be used as evidence that the seawater-derived fluid which formed the silica vein also cause Ba mobilisation in the EBV.

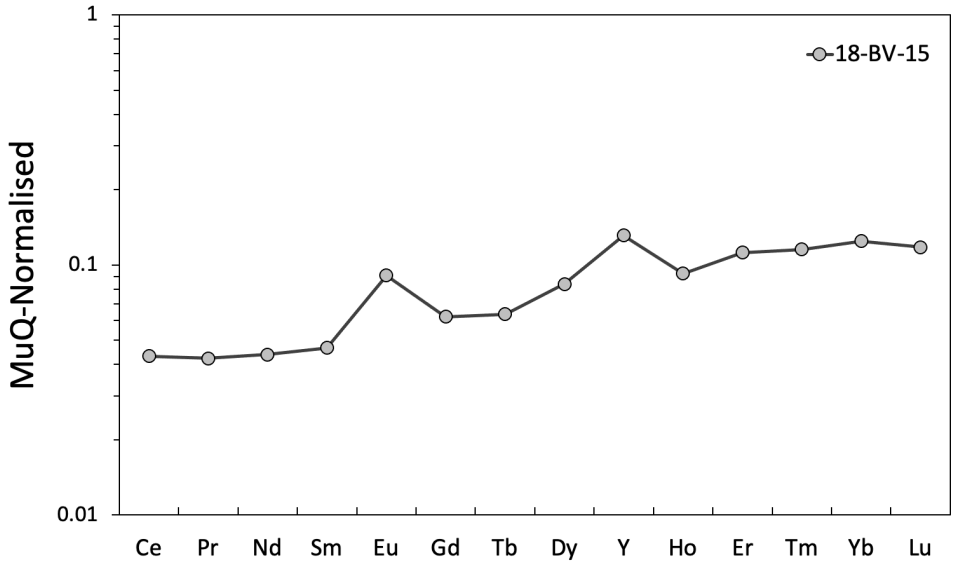

Figure 14: REE+Y pattern of the middle section of the middle of the Barite Valley silica vein (18-BV-15).

Table 7:

Major and trace element composition of Barite Valley chert and silica veins. ΣHFSE: sum of Zr, Hf, Nb, Ta and Y; ΣLILE: sum of Cs, Rb and Ba. *n* = number of ablation points averaged to give presented values. SiO_2 values obtained from unpublished MSc thesis of Jeroen Postema

Sample	**18-BV-13**	**18-BV-15**	**18-BV-18**	**18-BV-30**	**18-BV-32**
n	4	3	1	3	3
Description	*Upper portion chert dyke*	*Middle portion chert dyke*	*Lower portion chert dyke*	*Green chert*	*Grey chert*
Element (wt%)					
SiO2	94.97	94.97	94.97	94.97	94.97
Al2O3	2.76	12.52	3.92	0.64	1.04
MnO	0.0001	0.0003	0.0001	0.0004	0.0001
CaO	0.11	0.19	0.12	0.08	0.08
(ppm)					
Cs	0.74	1.82	0.88	0.15	0.19
Ba	3805.11	21315.77	7132.92	1770.85	1022.50
Rb	17.52	68.17	21.39	6.06	8.88
Th	1.17	0.81	0.59	0.02	0.20
U	0.39	0.52	0.25	0.05	0.13
Nb	1.33	1.11	1.13	0.09	0.69
Ta	0.11	0.15	0.10	0.01	0.07
Pb	0.52	0.85	0.12	2.65	0.97
Sr	21.01	78.01	21.16	11.35	3.65
Zr	7.71	15.42	8.03	1.95	3.76
Hf	0.22	0.55	0.25	0.04	0.11
Sc	3.12	7.23	3.43	2.47	1.48
V	20.99	88.47	37.48	13.14	9.41
Cr	123.67	473.86	211.79	440.24	59.02
Co	1.91	0.25	0.54	0.98	0.15
Ni	8.38	6.94	4.92	10.98	3.72
As	4.71	2.00	7.28	78.82	1.59
La	4.43	2.03	2.10	1.52	0.33
Ce	7.87	2.85	2.63	0.17	0.45
Pr	0.85	0.33	0.38	0.03	0.05
Nd	3.12	1.34	1.46	0.14	0.17
Sm	0.50	0.31	0.31	0.03	0.06
Eu	0.13	0.14	0.10	0.02	0.02
Gd	0.35	0.39	0.31	0.03	0.08
Tb	0.04	0.06	0.07	0.004	0.01
Dy	0.23	0.48	0.29	0.03	0.09
Ho	0.05	0.11	0.06	0.01	0.02
Y	1.63	4.15	1.62	0.15	0.52
Er	0.16	0.38	0.17	0.02	0.05
Tm	0.02	0.06	0.03	0.00	0.01
Yb	0.16	0.41	0.17	0.02	0.06
Lu	0.03	0.06	0.03	0.002	0.01
∑HFSE	11.00	21.38	11.14	2.23	5.14
∑LILE	3823.37	21385.76	7155.19	1777.06	1031.57
Cr/Th	105.8	584.5	357.2	20142.0	299.1
Th/Sc	0.4	0.1	0.2	0.01	0.1
Y/Ho	32.0	39.1	25.5	27.7	28.7

3.4.4. Masenjane Barite Workings (MBW)

Trace element patterns of the MBW samples are variable and erratic. This may represent highly variable compositions. However, as many of the samples were found to be highly weathered, caution must be taken when interpreting the results as such patterns may be an effect of post-depositional element mobilisation.

The 'grey feeder silica vein' (19-MB-24) and black chert (19-MB-22) sampled from MBW display large Ba enrichments (320 and 66 times higher than MuQ respectively). As these samples were found between a barite block and above domal barite, such a large Ba-enrichment may be due to post-depositional Ba remobilisation. Similar to as is seen in the EBV green cherts, a grey silica vein sampled from the MBW (19-MB-24) is enriched in Cr (and to a lesser amount Ni) which indicates that the silicifying fluid which led to its formation may have circulated through the underlying Onverwacht strata.

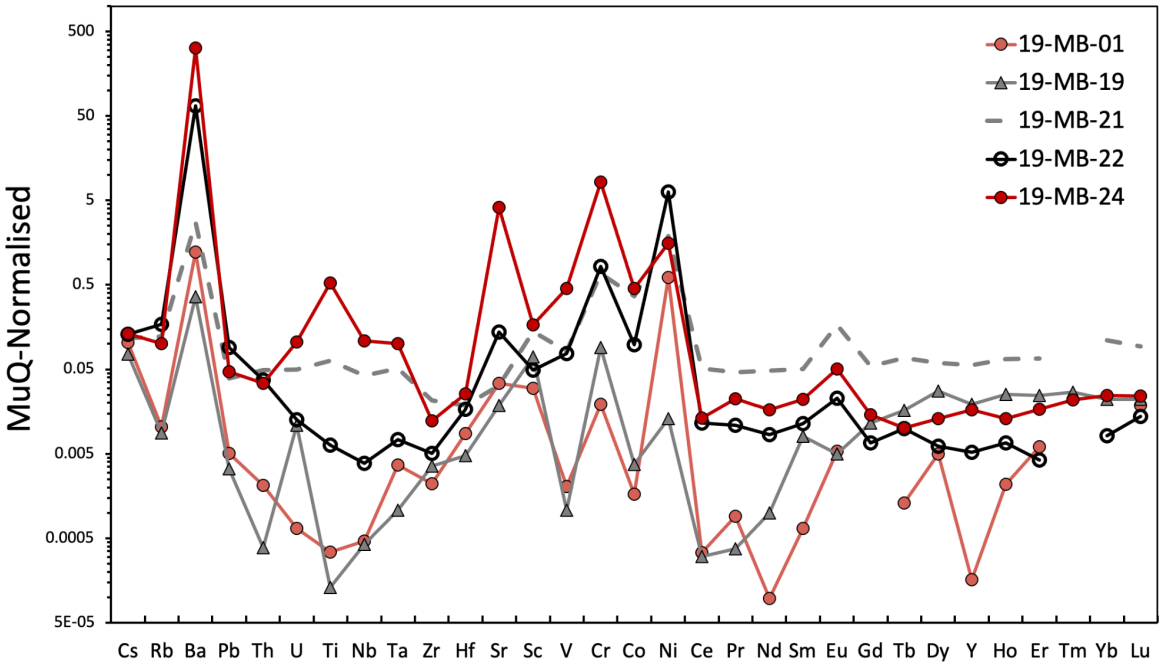

Figure 15: MuQ-normalised distribution of selected elements of the Masenjane chert samples. 19-MB-01: White weathered silica vein; 19-MB-19: grey chert; 19-MB-22: black massive chert; 19-MB-24: grey silica vein which crosses barite. Black and white banded Mendon chert (19-MB-21) was added for comparison. Ti-values are PAAS values. Tm was not measured for 19-MB-01, 190MB-21 and 19-MB-22.

In the field it was interpreted that sample 19-MB-19 may represent a silica vein. The extremely low Al content of 19-MB-19 (average 569 ppm) indicates that this grey chert sample likely does not have its origin as igneous or sedimentary material that was silicified (Hickman-Lewis et al., 2018). When compared to the clasts of TSA which were deemed to be Mapepe Basin precipitates, 19-MB-19 shows similar REE+Y patterns (Fig. 16). The REE+Y profile is heavily enriched in HREEs, and a positive Eu anomaly of 1.6 and a super-chondritic Y/Ho ratio of 37 is observed. This indicates that silica veining in the MBW was produced as a result of seawater-derived silica precipitating within fractures. Interestingly, the Eu anomaly is lower than those seen in the majority of the hydrogenous Puddingstone clasts, and below those considered associated with increased Archean hydrothermal activity. If fluid circulation which caused silica veining as seen in sample 19-MB-19 was indeed induced due to diffuse hydrothermal activity, the low Eu anomalies suggest that the vein formed either in a distal position to a diffuse hydrothermal vent site, or it formed during waning stages in hydrothermal activity. As Cr is enriched when compared to the rest of the trace elements, such an interpretation may again be reconciled with fluid circulation through the underlying Onverwacht strata.

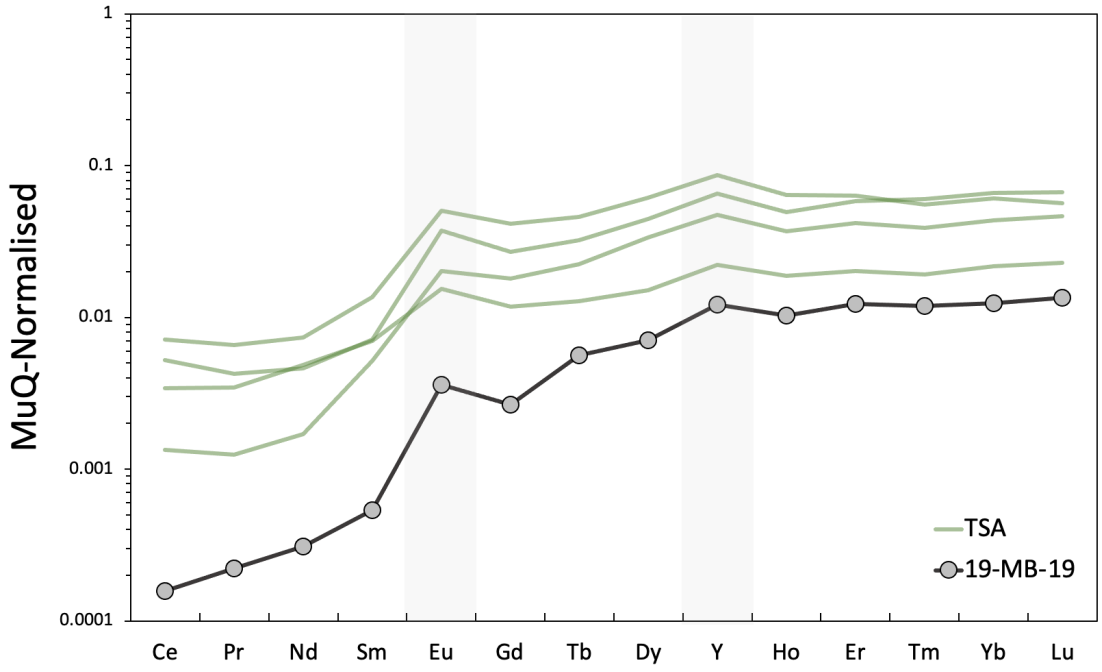

Figure 16: Comparison of Puddingstone conglomerate chert clasts (PSCC) which show a MuQ-normalised seawater REE+Y signature to chert sample 19-MB-19 from the Masenjane Barite Workings.

Table 8:

Major and trace element composition of Masejane chert and silica veins. ΣHFSE: sum of Zr, Hf, Nb, Ta and Y; ΣLILE: sum of Cs, Rb and Ba. *n* = number of ablation points averaged. SiO_2 values and 19-MB-01, 19-MB-21 and 19-MB-22 data obtained from unpublished MSc thesis of Esmee Waardenburg (2020). Blank values represent unmeasured elements. "-" values represent values below the detection limit. 19-MB-19 was measured by LA-ICP-MS in the University of Bergen.

Sample	**19-MB-01**	**19-MB-19**	**19-MB-21**	**19-MB-22**	**19-MB-24**
n	2	1	4	3	3
Description	*White weathered silica vein*	*Grey silica vein*	*Black/white banded Mendon chert*	*Black chert*	*Grey feeder chert crossing barite*
Element (wt%)					
SiO2	99.895	99.891	91.157	99.585	99.226
Al2O3		1.098			1.600
MnO	0.0001	0.011	0.237	0.002	0.003
CaO	0.023	0.018	0.082	0.033	0.202
(ppm)					
Cs	0.55	0.41	0.63	0.70	0.72
Ba	511.18	144.19	1085.79	26079.87	126965.46
Rb	0.89	0.70	9.80	13.51	8.06
Th	0.03	0.00	0.55	0.42	0.38
U	0.00	0.03	0.14	0.04	0.30
Nb	0.00	0.01	0.65	0.06	1.66
Ta	0.00	0.00	0.06	0.01	0.11
Pb	0.06	0.07	0.80	1.85	0.95
Sr	4.65	2.64	4.55	19.47	590.96
Zr	0.44	0.71	4.26	1.00	2.43
Hf	0.07	0.03	0.10	0.09	0.14
Ti	1.03	-	189.38	18.94	1577.11
Sc	0.49	1.15	2.30	0.80	2.76
V	0.24	0.13	9.79	9.29	54.61
Cr	1.30	5.82	43.57	53.40	531.23
Co	0.04	0.08	8.28	1.47	10.12
Ni	26.94	0.41	59.46	199.77	49.25
As	0.84	0.29	51.18	14.65	31.81
La	62.560	0.009	2.109	64.657	0.589
Ce	0.018	0.017	3.658	0.824	0.939
Pr	0.011	0.003	0.391	0.091	0.190
Nd	0.003	0.012	1.583	0.277	0.542
Sm	0.002	0.007	0.346	0.079	0.152
Eu	0.005	0.013	0.237	0.041	0.315
Gd	-	0.032	0.346	0.043	0.091
Tb	0.001	0.011	0.067	0.010	0.010
Dy	0.015	0.096	0.352	0.024	0.077
Ho	0.001	0.024	0.081	0.008	0.016
Y	0.006	0.876	1.780	0.165	0.528
Er	0.016	0.085	0.226	0.014	0.056
Tm		0.012			0.011
Yb	-	0.087	0.359	0.026	0.080
Lu	0.013	0.011	0.046	0.007	0.012
∑HFSE	0.5	1.6	6.8	1.3	4.9
∑LILE	512.6	145.3	1096.2	26094.1	126974.2
Cr/Th	37.6	1366.6	79.5	127.9	1393.1
Th/Sc	0.1	0.0	0.2	0.5	0.1
Y/Ho	4.4	37.1	21.9	20.2	33.0
Yb/PrSN		88.1	2.4	0.8	1.1

3.4.5. Puddingstone Hill

Both the trace element patterns and petrography of the grey/green chert and black silica vein samples collected from Puddingstone Hill indicate that different processes were involved in their formation when compared to those of the EBV and MBW sites. The trace element patterns of the Puddingstone Hill samples are similar to those of the Mendon chert which was sampled in the same location (19-PS-02). Commonalities include Cr, Ni and Sc enrichment when compared to the rest of the trace elements. Cr/Th and Th/Sc ratios are also very similar between all of the sampled material from the Puddingstone Hill (101-359 and 0.1-0.2 respectively). This contrasts to the material sampled from the EBV and MBW sites, in which these immobile element ratios are extremely variable. The implications of such a result suggests that all of the sampled material from Puddingstone Hill originated as being similar in composition to that of the Mendon chert.

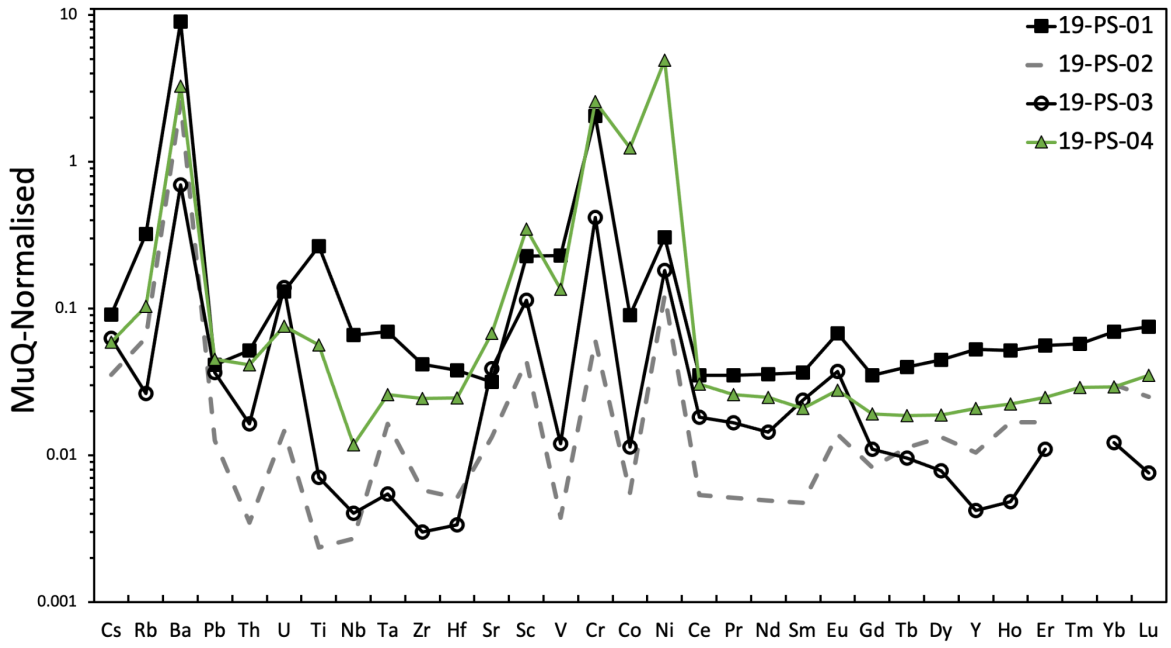

Figure 17: Shale-normalised trace element diagram of chert from the Puddingstone Hill site. 19-PS-01: black silica vein; 19-PS-03: black silica vein found downhill from 19-PS-01; 19-PS-04: grey/green chert which was found in between barite. Black and white banded Mendon chert (19-PS-02) which was found at the site was added for comparison.

Although relatively enriched in Ba, the silica veins and chert sampled from Puddingstone Hill are extremely depleted in Ba when compared to the EBV and MBW samples.

Furthermore, moderate levels of Ba enrichment such as those seen in the Puddingstone Hill samples is a common feature for most Fig Tree sediments (Hofmann, 2005). As such, it is unlikely that the black silica veins sampled from the Puddingstone Hill site represent relict hydrothermal vents which carried a Ba-bearing fluid.

The microscopic observations of the Puddingstone Hill chert show dark, subrounded lithic fragments and irregular carbonaceous 'clots' embedded in a microquartz matrix (Fig. 18). The well-rounded nature of the clasts further argue against a hydrothermal origin for the Puddingstone Hill silica veins; as if this were to be the case brecciated material would be expected. Quartz filled fractures are common features in both 19-PS-01 and 19-PS-03 (Fig. 18d), indicative of post-depositional silicification processes. Further indication of post-depositional silicification is the micro-quartz rim which surrounds lithic fragments in 19-PS-01 (Fig. 18a). In sample 19-PS-03, silicification was so prevalent that the lithic fragments have almost been entirely replaced with micro-quartz (Fig. 18c). This is further reflected in the trace element profiles, in which 19-PS-03 is depleted in all trace elements, likely as a result of element dilution by silica.

As the Puddingstone Hill samples show trace element signatures similar to those of the Mendon chert, and as the microscopic observations show that silicification was a post-depositional process, it is indeed possible that the Puddingstone Hill samples invoke a Neptunian-dyke scenario in which Mendon material migrated into fractures in the crust and was later silicified to form the black chert 'dykes' which were sampled.

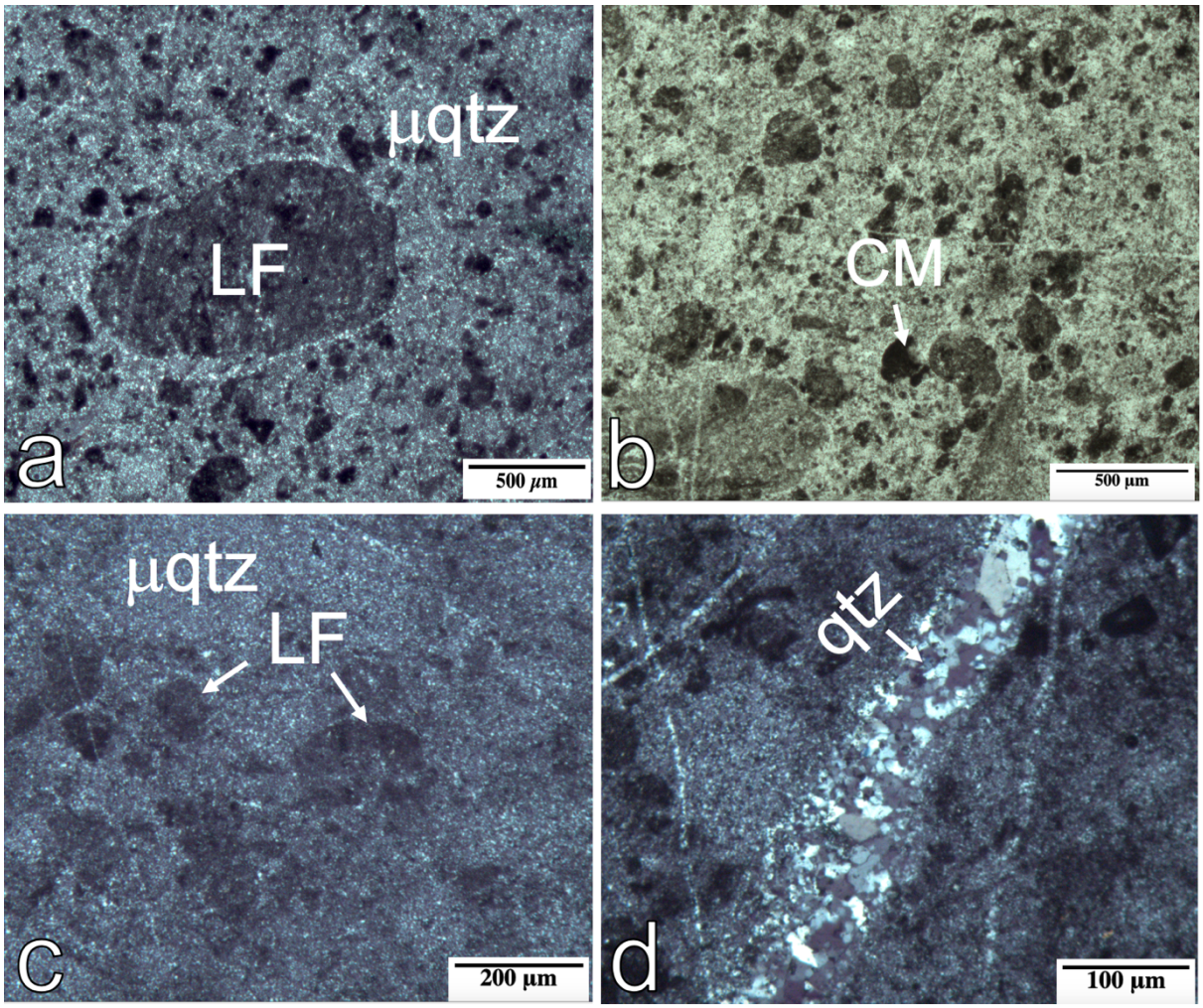

Figure 18: Photomicrographs of the black silica veins from Puddingstone Hill **a)** 19-PS-01 (XPL); **b)** 19-PS-01 (PPL) **c)** 19-PS-03 (XPL) **d)** 19-PS-03 (XPL). *LF* = lithic fragment; *CM* = carbonaceous material; *μQtz* = micro-quartz *Qtz* = quartz.

Table 9:

Major and trace element composition of the Puddingstone Hill chert and silica veins. ΣHFSE: sum of Zr, Hf, Nb, Ta and Y; ΣLILE: sum of Cs, Rb and Ba. *n* = number of ablation points averaged to give presented values. SiO_2 values and 19-PS-02 and 19-PS-03 data obtained from unpublished MSc thesis of Esmee Waardenburg (2020). Blank values represent unmeasured elements.

Sample	**19-PS-01**	**19-PS-02**	**19-PS-03**	**19-PS-04**
n	1	1	1	1
Description	*Black chert dyke*	*Mendon chert*	*Black chert dyke*	*Grey/green chert between barite*
Element				
(wt%)				
SiO2	98.934	95.476	99.895	94.986
Al2O3	3.000			0.989
MnO	0.0003	0.0001	0.001	0.0003
CaO	0.107	0.025	0.077	0.044
(ppm)				
Cs	0.488	0.19	0.336	0.316
Ba	3559.48	1008.62	273.85	1298.26
Rb	25.49	5.01	2.084	8.22
Th	0.575	0.0385	0.1822	0.459
U	0.369	0.0412	0.392	0.214
Nb	1.007	0.0413	0.0615	0.181
Ta	0.0774	0.0183	0.0061	0.0289
Pb	0.846	0.257	0.749	0.916
Sr	4.48	1.89	5.52	9.61
Zr	8.3	1.147	0.598	4.83
Hf	0.201	0.0273	0.0178	0.1311
Ti	792.67	7.04	21.14	168.6
Sc	3.75	0.723	1.87	5.71
V	27.41	0.452	1.439	16.2
Cr	132.47	3.89	26.93	164.82
Co	2.01	0.124	0.255	27.76
Ni	9.6	3.88	5.73	155.09
As	48.26	1.05	71.79	97.44
La	1.72	5.4	37.44	1.94
Ce	2.48	0.379	1.29	2.17
Pr	0.297	0.0433	0.14	0.218
Nd	1.175	0.162	0.47	0.814
Sm	0.2505	0.0326	0.16	0.1325
Eu	0.10575	0.02175	0.05855	0.0434
Gd	0.222	0.0525	0.07	0.122
Tb	0.0394	0.0112	0.01	0.0185
Dy	0.263	0.0781	0.046	0.1107
Ho	0.0629	0.0204	0.006	0.0272
Y	1.68	0.332	0.13	0.664
Er	0.188	0.0566	0.04	0.0837
Tm	0.0293			0.0148
Yb	0.225	0.098	0.04	0.0948
Lu	0.0368	0.0122	0.004	0.0171
∑HFSE	11.3	1.6	0.8	5.8
∑LILE	3585.5	1013.8	276.3	1306.8
Cr/Th	230.4	101.0	147.8	359.1
Th/Sc	0.2	0.1	0.1	0.1
Y/Ho	26.7	16.3	22.7	24.4
Yb/PrSN	2.0	5.9	0.7	1.1

4. Conclusions

This thesis has used trace element concentrations and REE+Y patterns from conglomerates, chert and silica veins from the ~3.26 Ga Fig Tree Group of the Barberton Greenstone Belt in an attempt to constrain the debate as to what controls influenced Paleoarchean silicification processes.

For the conglomerate samples, Al concentrations have been used as a proxy for the entrainment of detrital minerals within the chert which makes up the matrix and many of the clasts. It has been shown that at below approximately 1,100 ppm Al, trace element concentrations and REE+Y patterns vary independent of Al concentration. This has been used to conclude that samples with <1,1000 ppm Al likely represent the composition of a silicifying fluid. The clasts which contain such low concentrations of Al are jaspelites, cherts and ferruginous sediments – chemical sediments which are commonly precipitated directly from hydrous solutions. These clasts consistently exhibit heavy REEs enriched over light REEs (HREE>LREE), variably positive Eu anomalies and often super-chondritic Y/Ho ratios. These patterns are consistent with silica precipitation from fluids derived from Archean seawater. Eu anomalies for samples TSA and MMT are within the range expected for Archean seawater. However, it has been found that some of the clasts in MSA15-CQ-10 and all of the clasts in sample MSA15-CQ-1 display Eu anomalies slightly above those expected for Archean seawater. These moderately elevated Eu anomalies have been used to conclude that low-temperature and/or low concentrations of hydrothermal solutions were venting into the Mapepe Basin whilst silica was precipitating from the water column.

The remaining conglomerate clasts with >1,100 ppm Al have been characterised based on immobile element ratios. Cr/Th and Th/Sc ratios have shown that the majority of the detrital material has an intermediate composition, indicating they are composed of sedimentary detritus. As sedimentation only began after inception of Fig Tree Group, the clasts within the conglomerates are of Fig Tree age. The results have shown that much of these sedimentary conglomerate clasts exhibit REE+Y patterns which deviate from the flat profiles expected from sedimentary material. Instead, many of the silicified sedimentary clasts display moderate positive Eu anomalies, HREE enrichment and super-chondritic Y/Ho ratios: patterns consistent with an Archean marine setting. The matrix

material of the conglomerates display similar seawater-like REE+Y profiles. These results suggest that silicification of these Fig Tree sediments occurred in a marine setting by a seawater-derived fluid.

In the second portion of the thesis, chert and silica veins from the southern Fig Tree Group have been sampled in order to determine whether they may host information regarding Paleoarchean silicification processes. A silica vein from the Masenjane Barite workings, and a portion of a large silica vein from the Eastern Barite Valley exhibit REE+Y patterns consistent with a marine setting. This suggests that a seawater-derived fluid was responsible for silica vein formation in the Eastern Barite Valley and Masenjane sites. Immobile element ratios of samples from the Eastern Barite Valley and Masenjane Barite Workings also exhibit a mafic/ultramafic signature. These results contrast with previous interpretations that chert and silica veins in the Eastern Barite Valley represent silicified felsic material. As no mafic material was erupting during the Mapepe time, the observed mafic/ultramafic signatures can be reconciled by fluid circulation through the underlying Onverwacht strata. As barite is spatially associated with these silica veins, it is likely that barite in the Eastern Barite Valley and Masenjane Barite Workings was also precipitated in a marine environment. The significance of this result is that barite in the Eastern Barite Valley and Masenjane Barite Workings carry information regarding Paleoarchean seawater.

The grey/green chert and black silica veins from the Puddingstone Hill which are discussed in this study show trace element signatures similar to those of the surrounding Mendon chert. Thin section analysis of the Puddingstone silica veins displays rounded lithic fragments which have been silicified in a micro-quartz matrix. The lack of brecciated material nor extreme Ba enrichment in these samples has been used to oppose the idea that the sampled black silica veins represent feeder vents which allowed for barite precipitation. Instead, the similarities with the Mendon chert and evidence for post depositional silicification may agree with a Neptunian-dyke hypothesis in which lithic material migrated into crustal fractures and was later silicified.

5. Acknowledgments

I would like to express my gratitude to Dr. Desiree Roerdink and Dr. Mark van Zuilen whose conversation and input inspired me to more critically assess my thought processes and results. A special thank you to ing. Helen Waard who showed endless patience and support during my time in the LA-ICP-MS lab. As always a huge thank you to my parents for supporting me throughout my education. Most of all I would like to extend my appreciation towards my supervisor Prof. Dr. Paul Mason who kindly shared his knowledge through hours of meetings, discussions and corrections. This time spent has furthered my fascination of geochemistry – and for this I will remain grateful.

This thesis was funded by the Olaf Schuiling Fonds. Conglomerate samples are property of Dr. Kimberly Myers.

6. References

Abbott, A.N., Haley, B.A., McManus, J. and Reimers, C.E., 2015. The sedimentary flux of dissolved rare earth elements to the ocean. *Geochimica et Cosmochimica Acta*, *154*, pp.186-200.

Alibo, D.S. and Nozaki, Y., 1999. Rare earth elements in seawater: particle association, shale-normalization, and Ce oxidation. *Geochimica et cosmochimica acta*, *63*(3-4), pp.363-372.

Anders E. and Grevesse N. (1989) "Abundances of the elements: Meteoritic and solar" *Geochimica et Cosmochimica Acta* **53**, 197-214.

Baldwin, G.J., Thurston, P.C. and Kamber, B.S., 2011. High-precision rare earth element, nickel, and chromium chemistry of chert microbands pre-screened with in-situ analysis. *Chemical Geology*, *285*(1-4), pp.133-143.

Balistrieri, L.S. and Murray, J.W., 1984. Marine scavenging: Trace metal adsorption by interfacial sediment from MANOP Site H. *Geochimica et Cosmochimica Acta*, *48*(5), pp.921-929.

Bau, M., 1991. Rare-earth element mobility during hydrothermal and metamorphic fluid-rock interaction and the significance of the oxidation state of europium. *Chemical geology*, *93*(3-4), pp.219-230.

Bau, M. and Möller, P., 1993. Rare earth element systematics of the chemically precipitated component in Early Precambrian iron formations and the evolution of the terrestrial atmosphere-hydrosphere-lithosphere system. *Geochimica et Cosmochimica Acta*, *57*(10), pp.2239-2249.

Bau, M. and Dulski, P., 1995. Comparative study of yttrium and rare-earth element behaviours in fluorine-rich hydrothermal fluids. *Contributions to Mineralogy and Petrology*, *119*(2), pp.213-223.

Bau, M. and Dulski, P., 1996. Distribution of yttrium and rare-earth elements in the Penge and Kuruman iron-formations, Transvaal Supergroup, South Africa. *Precambrian Research*, *79*(1-2), pp.37-55.

Bau, M., 1999. Scavenging of dissolved yttrium and rare earths by precipitating iron oxyhydroxide: experimental evidence for Ce oxidation, Y-Ho fractionation, and lanthanide tetrad effect. *Geochimica et Cosmochimica Acta*, *63*(1), pp.67-77.

Bolhar, R., Kamber, B.S., Moorbath, S., Fedo, C.M. and Whitehouse, M.J., 2004. Characterisation of early Archaean chemical sediments by trace element signatures. *Earth and Planetary Science Letters*, *222*(1), pp.43-60.

Bolhar, R., Van Kranendonk, M.J. and Kamber, B.S., 2005. A trace element study of siderite–jasper banded iron formation in the 3.45 Ga Warrawoona Group, Pilbara Craton—formation from hydrothermal fluids and shallow seawater. *Precambrian Research*, *137*(1-2), pp.93-114.

Bolhar, R. and Van Kranendonk, M.J., 2007. A non-marine depositional setting for the northern Fortescue Group, Pilbara Craton, inferred from trace element geochemistry of stromatolitic carbonates. *Precambrian Research*, *155*(3-4), pp.229-250.

Bonnand, P., Lalonde, S.V., Boyet, M., Heubeck, C., Homann, M., Nonnotte, P., Foster, I., Konhauser, K.O. and Köhler, I., 2020. Post-depositional REE mobility in a Paleoarchean banded iron formation revealed by La-Ce geochronology: A cautionary tale for signals of ancient oxygenation. *Earth and Planetary Science Letters*, *547*, p.116452.

Buick, R. and Dunlop, J.S.R., 1990. Evaporitic sediments of early Archaean age from the Warrawoona Group, North Pole, Western Australia. *Sedimentology*, *37*(2), pp.247-277.

Byerly, G.R., Kröner, A., Lowe, D.R., Todt, W. and Walsh, M.M., 1996. Prolonged magmatism and time constraints for sediment deposition in the early Archean Barberton greenstone belt: evidence from the Upper Onverwacht and Fig Tree groups. *Precambrian Research*, *78*(1-3), pp.125-138.

Condie, K.C. and Wronkiewicz, D.J., 1990. The Cr/Th ratio in Precambrian pelites from the Kaapvaal Craton as an index of craton evolution. *Earth and Planetary Science Letters*, *97*(3-4), pp.256-267.

Cullers et al. Cullers, R.L., DiMarco, M.J., Lowe, D.R. and Stone, J., 1993. Geochemistry of a silicified, felsic volcaniclastic suite from the early Archaean Panorama Formation, Pilbara Block, Western Australia: an evaluation of depositional and post-depositional processes with special emphasis on the rare-earth elements. *Precambrian Research*, *60*(1-4), pp.99-116.

Curtis, C.D., 1964. Applications of the crystal-field theory to the inclusion of trace transition elements in minerals during magmatic differentiation. *Geochimica et Cosmochimica Acta*, *28*(3), pp.389-403.

Danielson, A., Möller, P. and Dulski, P., 1992. The europium anomalies in banded iron formations and the thermal history of the oceanic crust. *Chemical geology*, *97*(1-2), pp.89-100.

De Baar, H.J., Brewer, P.G. and Bacon, M.P., 1985. Anomalies in rare earth distributions in seawater: Gd and Tb. *Geochimica et Cosmochimica Acta*, *49*(9), pp.1961-1969.

Decker, N.B., Byerly, G.R., Stiegler, M.T., Lowe, D.R. and Stefurak, E., 2015. High resolution tephra and U/Pb chronology of the 3.33–3.26 Ga Mendon Formation, Barberton Greenstone Belt, South Africa. *Precambrian Research*, *261*, pp.54-74.

Derry, L.A. and Jacobsen, S.B., 1990. The chemical evolution of Precambrian seawater: evidence from REEs in banded iron formations. *Geochimica et Cosmochimica Acta*, *54*(11), pp.2965-2977.

de Wit, M.J., Armstrong, R., Hart, R.J. and Wilson, A.H., 1987. Felsic igneous rocks within the 3.3-to 3.5-Ga Barberton greenstone belt: High crustal level equivalents of the surrounding tonalite-trondhjemite terrain, emplaced during thrusting. *Tectonics*, *6*(5), pp.529-549.

de Wit, M.J. and Hart, R.A., 1993. Earth's earliest continental lithosphere, hydrothermal flux and crustal recycling. *Lithos*, *30*(3-4), pp.309-335.

Douville, E., Bienvenu, P., Charlou, J.L., Donval, J.P., Fouquet, Y., Appriou, P. and Gamo, T., 1999. Yttrium and rare earth elements in fluids from various deep-sea hydrothermal systems. *Geochimica et Cosmochimica Acta*, *63*(5), pp.627-643.

Drabon, N., 2018. *Crustal Setting, Provenance and Sedimentation in the Paleoarchean Barberton Greenstone Belt, South Africa*. Stanford University.

Drabon, N., Galić, A., Mason, P.R. and Lowe, D.R., 2019. Provenance and tectonic implications of the 3.28–3.23 Ga Fig Tree Group, central Barberton greenstone belt, South Africa. *Precambrian Research*, *325*, pp.1-19.

Duchac, K.C. and Hanor, J.S., 1987. Origin and timing of the metasomatic silicification of an early Archean komatiite sequence, Barberton Mountain Land, South Africa. *Precambrian Research*, *37*(2), pp.125-146.

Elderfield, H., Wheat, C.G., Mottl, M.J., Monnin, C. and Spiro, B., 1999. Fluid and geochemical transport through oceanic crust: a transect across the eastern flank of the Juan de Fuca Ridge. *Earth and Planetary Science Letters*, *172*(1-2), pp.151-165.

Elderfield, H. and Sholkovitz, E.T., 1987. Rare earth elements in the pore waters of reducing nearshore sediments. *Earth and Planetary Science Letters*, *82*(3-4), pp.280-288.

Galić, A., 2015. *Unravelling atmospheric photolysis and ocean redox chemistry from Paleoarchean pyrite: a multiple sulfur and iron stable isotope study* (Doctoral dissertation, University Utrecht).

Geilert, S., Vroon, P.Z. and van Bergen, M.J., 2014. Silicon isotopes and trace elements in chert record early Archean basin evolution. *Chemical geology*, *386*, pp.133-142.

Graham, S.A., Tolson, R.B., DeCelles, P.G., Ingersoll, R.V., Bargar, E., Caldwell, M., Cavazza, W., Edwards, D.P., Follo, M.F., Handschy, J.F. and Lemke, L., 1986. Provenance modelling as a technique for analysing source terrane evolution and controls on foreland sedimentation. *Foreland basins*, *8*, pp.425-436.

Heinrichs, T.K. and Reimer, T., 1977. A sedimentary barite deposit from the Archean Fig Tree Group of the Barberton Mountain Land (South Africa). *Economic Geology*, *72*(8), pp.1426-1441.

Hessler, A.M. and Lowe, D.R., 2006. Weathering and sediment generation in the Archean: an integrated study of the evolution of siliciclastic sedimentary rocks of the 3.2 Ga Moodies Group, Barberton Greenstone Belt, South Africa. *Precambrian Research*, *151*(3-4), pp.185-210.

Hickman-Lewis, K., Cavalazzi, B., Foucher, F. and Westall, F., 2018. Most ancient evidence for life in the Barberton greenstone belt: Microbial mats and biofabrics of the~ 3.47 Ga Middle Marker horizon. *Precambrian Research*, *312*, pp.45-67.

Hidaka, H., Shimizu, H. and Adachi, M., 2002. U–Pb geochronology and REE geochemistry of zircons from Palaeoproterozoic paragneiss clasts in the Mesozoic Kamiaso conglomerate, central Japan: evidence for an Archean provenance. *Chemical Geology*, *187*(3-4), pp.279-293.

Hirata, T., Shimizu, H., Akagi, T., Sawatari, H. and Masuda, A., 1988. Precise determination of rare earth elements in geological standard rocks by inductively coupled plasma source mass spectrometry. *Analytical sciences*, *4*(6), pp.637-643.

Hofmann, A. and Bolhar, R., 2007. Carbonaceous cherts in the Barberton Greenstone Belt and their significance for the study of early life in the Archean record. *Astrobiology*, *7*(2), pp.355-388.

Hofmann, A. and Harris, C., 2008. Silica alteration zones in the Barberton greenstone belt: A window into subseafloor processes 3.5–3.3 Ga ago. *Chemical Geology*, *257*(3-4), pp.221-239.

Hofmann, A., Bolhar, R., Orberger, B. and Foucher, F., 2013. Cherts of the Barberton Greenstone Belt, South Africa: Petrology and trace-element geochemistry of 3.5 to 3.3 Ga old silicified volcaniclastic sediments. *South African Journal of Geology*, *116*(2), pp.297-322.

Holland, H.D., 2005. Sea level, sediments and the composition of seawater. *American Journal of Science*, *305*(3), pp.220-239.

Homann, M., 2019. Earliest life on earth: evidence from the Barberton Greenstone Belt, South Africa. *Earth-Science Reviews*, *196*, p.102888.

Huston, D.L. and Logan, G.A., 2004. Barite, BIFs and bugs: evidence for the evolution of the Earth's early hydrosphere. *Earth and Planetary Science Letters*, *220*(1-2), pp.41-55.

Jarvis, K.E., Gray, A.L. and McCurdy, E., 1989. Avoidance of spectral interference on europium in inductively coupled plasma mass spectrometry by sensitive measurement of the doubly charged ion. *Journal of Analytical Atomic Spectrometry*, *4*(8), pp.743-747.

Jochum, K.P. and Brueckner, S.M., 2008. Reference materials in geoanalytical and environmental research-review for 2006 and 2007. *Geostandards and Geoanalytical Research*, *32*(4), pp.405-452.

Johannesson, K.H., Hawkins Jr, D.L. and Cortés, A., 2006. Do Archean chemical sediments record ancient seawater rare earth element patterns?. *Geochimica et Cosmochimica Acta*, *70*(4), pp.871-890.

Kamber, B.S. and Webb, G.E., 2001. The geochemistry of late Archaean microbial carbonate: implications for ocean chemistry and continental erosion history. *Geochimica et Cosmochimica Acta*, *65*(15), pp.2509-2525.

Kamber, B.S., Bolhar, R. and Webb, G.E., 2004. Geochemistry of late Archaean stromatolites from Zimbabwe: evidence for microbial life in restricted epicontinental seas. *Precambrian Research*, *132*(4), pp.379-399.

Kamber, B.S., Greig, A. and Collerson, K.D., 2005. A new estimate for the composition of weathered young upper continental crust from alluvial sediments, Queensland, Australia. *Geochimica et Cosmochimica Acta*, *69*(4), pp.1041-1058.

Knauth, L.P., 2005. Temperature and salinity history of the Precambrian ocean: implications for the course of microbial evolution. In *Geobiology: Objectives, concepts, perspectives*(pp. 53-69). Elsevier.

Lawrence, M.G. and Kamber, B.S., 2006. The behaviour of the rare earth elements during estuarine mixing—revisited. *Marine Chemistry*, *100*(1-2), pp.147-161.

Ledevin, M., Arndt, N., Davaille, A., Ledevin, R. and Simionovici, A., 2015. The rheological behaviour of fracture-filling cherts: example of Barite Valley dykes, Barberton Greenstone Belt, South Africa. *Solid Earth*, *6*(1), pp.253-269.

Lee, J.H. and Byrne, R.H., 1993. Complexation of trivalent rare earth elements (Ce, Eu, Gd, Tb, Yb) by carbonate ions. *Geochimica et Cosmochimica Acta*, *57*(2), pp.295-302.

Lowe, D.R. and Byerly, G.R., 1999. Stratigraphy of the west-central part of the Barberton Greenstone Belt, South Africa. *Special Papers-Geological Society of America*, pp.1-36.

Lowe, D.R., Nocita, B.W. and Byerly, G.R., 1999. Foreland basin sedimentation in the Mapepe Formation, southern-facies Fig Tree Group. *Special Papers-Geological Society of America*, pp.233-258.

Lowe, D.R. and Byerly, G.R., 2007. An overview of the geology of the Barberton Greenstone Belt and vicinity: implications for early crustal development. *Developments in Precambrian geology*, *15*, pp.481-526.

Lowe, D.R., Drabon, N. and Byerly, G.R., 2019. Crustal fracturing, unconformities, and barite deposition, 3.26–3.23 Ga, Barberton Greenstone Belt, South Africa. *Precambrian Research*, *327*, pp.34-46.

Migdisov, A., Williams-Jones, A.E., Brugger, J. and Caporuscio, F.A., 2016. Hydrothermal transport, deposition, and fractionation of the REE: Experimental data and thermodynamic calculations. *Chemical Geology*, *439*, pp.13-42.

Muller, É., Philippot, P., Rollion-Bard, C., Cartigny, P., Assayag, N., Marin-Carbonne, J., Mohan, M.R. and Sarma, D.S., 2017. Primary sulfur isotope signatures preserved in high-grade Archean barite deposits of the Sargur Group, Dharwar Craton, India. *Precambrian Research*, *295*, pp.38-47.

Nijman, W. and Valkering, M.E., 1998. Growth fault control of Early Archaean cherts, barite mounds and chert-barite veins, North Pole Dome, Eastern Pilbara, Western Australia. *Precambrian Research*, *88*(1-4), pp.25-52.

Nocita, B.W. and Lowe, D.R., 1990. Fan-delta sequence in the Archean Fig Tree Group, Barberton Greenstone Belt, South Africa. *Precambrian Research*, *48*(4), pp.375-393.

Nothdurft, L.D., Webb, G.E. and Kamber, B.S., 2004. Rare earth element geochemistry of Late Devonian reefal carbonates, Canning Basin, Western Australia: confirmation of a seawater REE proxy in ancient limestones. *Geochimica et Cosmochimica Acta*, *68*(2), pp.263-283.

Nozaki, Y., Zhang, J. and Amakawa, H., 1997. The fractionation between Y and Ho in the marine environment. *Earth and Planetary Science Letters*, *148*(1-2), pp.329-340.

Pack, A., Russell, S.S., Shelley, J.M.G. and Van Zuilen, M., 2007. Geo-and cosmochemistry of the twin elements yttrium and holmium. *Geochimica et Cosmochimica Acta*, *71*(18), pp.4592-4608.
Pearce, J.A. and Norry, M.J., 1979. Petrogenetic implications of Ti, Zr, Y, and Nb variations in volcanic rocks. *Contributions to mineralogy and petrology*, *69*(1), pp.33-47.

Pinti, D.L., Mineau, R. and Clement, V., 2009. Hydrothermal alteration and microfossil artefacts of the 3,465-million-year-old Apex chert. *Nature Geoscience*, *2*(9), pp.640-643.

Planavsky, N., Bekker, A., Rouxel, O.J., Kamber, B., Hofmann, A., Knudsen, A. and Lyons, T.W., 2010. Rare earth element and yttrium compositions of Archean and Paleoproterozoic Fe formations revisited: new perspectives on the significance and mechanisms of deposition. *Geochimica et Cosmochimica Acta*, *74*(22), pp.6387-6405.

Roerdink, D.L., Mason, P.R., Farquhar, J. and Reimer, T., 2012. Multiple sulfur isotopes in Paleoarchean barites identify an important role for microbial sulfate reduction in the early marine environment. *Earth and Planetary Science Letters*, *331*, pp.177-186.

Roerdink, D.L., Ronen, Y., Strauss, H. and Mason, P.R., 2022. Emergence of felsic crust and subaerial weathering recorded in Palaeoarchaean barite. *Nature Geoscience*, *15*(3), pp.227-232.

Schopf, J.W., 1993. Microfossils of the Early Archean Apex chert: new evidence of the antiquity of life. *Science*, *260*(5108), pp.640-646.

Shields, G.A. and Webb, G.E., 2004. Has the REE composition of seawater changed over geological time?

Sholkovitz, E.R., Landing, W.M. and Lewis, B.L., 1994. Ocean particle chemistry: the fractionation of rare earth elements between suspended particles and seawater. *Geochimica et Cosmochimica Acta*, *58*(6), pp.1567-1579.

Shields, G. and Webb, G., 2004. Has the REE composition of seawater changed over geological time?. *Chemical Geology*, *204*(1-2), pp.103-107.

Siever, R., 1992. The silica cycle in the Precambrian. *Geochimica et Cosmochimica Acta*, *56*(8), pp.3265-3272.

Sleep, N.H. and Windley, B.F., 1982. Archean plate tectonics: constraints and inferences. *The Journal of Geology*, *90*(4), pp.363-379.

Smirnova, E.V., Mysovskaya, I.N., Lozhkin, V.I., Sandimirova, G.P., Pakhomova, N.N. and Smagunova, A.A., 2006. Spectral interferences from polyatomic barium ions in inductively coupled plasma mass spectrometry. *Journal of Applied Spectroscopy*, *73*(6), pp.911-917.

Sugitani, K., 1992. Geochemical characteristics of Archean cherts and other sedimentary rocks in the Pilbara Block, Western Australia: evidence for Archean seawater enriched in hydrothermally-derived iron and silica. *Precambrian Research*, *57*(1-2), pp.21-47.

Stiegler, M.T., 2009. *Bridging the gap between deep-mantle and surface processes: The sedimentology and petrology of komatiitic tuffs of the 3.5–3.2 Ga Onverwacht Group, Barberton greenstone belt, South Africa*. Stanford University.

Stoll, E., Drabon, N. and Lowe, D.R., 2021. Provenance and paleogeography of Archean Fig Tree siliciclastic rocks in the East-Central Barberton Greenstone Belt, South Africa. *Precambrian Research*, *354*, p.106041.

Sugahara, H., Sugitani, K., Mimura, K., Yamashita, F. and Yamamoto, K., 2010. A systematic rare-earth elements and yttrium study of Archean cherts at the Mount Goldsworthy greenstone belt in the Pilbara Craton: Implications for the origin of microfossil-bearing black cherts. *Precambrian Research*, *177*(1-2), pp.73-87.

Sugitani, K. and Mimura, K., 1998. Redox change in sedimentary environments of Triassic bedded cherts, central Japan: possible reflection of sea-level change. *Geological Magazine*, *135*(6), pp.735-753.

Sun, S.S., 1984. Geochemical characteristics of Archaean ultramafic and mafic volcanic rocks: implications for mantle composition and evolution. In *Archaean Geochemistry* (pp. 25-46). Springer, Berlin, Heidelberg.

Tice, M.M. and Lowe, D.R., 2006a. The origin of carbonaceous matter in pre-3.0 Ga greenstone terrains: A review and new evidence from the 3.42 Ga Buck Reef Chert. *Earth-Science Reviews*, *76*(3-4), pp.259-300.

Tice, M.M. and Lowe, D.R., 2006b. Hydrogen-based carbon fixation in the earliest known photosynthetic organisms. *Geology*, *34*(1), pp.37-40.

Vennemann, T.W. and Smith, H.S., 1999. Geochemistry of mafic and ultramafic rocks in the type section of the Kromberg Formation, Barberton greenstone belt, South Africa. *Geologic Evolution of the Barberton Greenstone Belt, South Africa. Geological Society of America, Special Papers*, *329*, pp.133-150.

Taylor, S.R. and McLennan, S.M., 1985. The continental crust: its composition and evolution.

Taylor, S.R. and McLennan, S.M., 1995. The geochemical evolution of the continental crust. *Reviews of geophysics*, *33*(2), pp.241-265.

Thurston, P.C., Kamber, B.S. and Whitehouse, M., 2012. Archean cherts in banded iron formation: insight into Neoarchean ocean chemistry and depositional processes. *Precambrian Research*, *214*, pp.227-257.

Van Baalen, M.R., 1993. Titanium mobility in metamorphic systems: a review. *Chemical Geology*, *110*(1-3), pp.233-249.

van den Boorn, S.H., van Bergen, M.J., Nijman, W. and Vroon, P.Z., 2007. Dual role of seawater and hydrothermal fluids in Early Archean chert formation: evidence from silicon isotopes. *Geology*, *35*(10), pp.939-942.

Van Kranendonk, M.J., Webb, G.E. and Kamber, B.S., 2003. Geological and trace element evidence for a marine sedimentary environment of deposition and biogenicity of 3.45 Ga stromatolitic carbonates in the Pilbara Craton, and support for a reducing Archaean ocean. *Geobiology*, *1*(2), pp.91-108.

Viehmann, S., Bau, M., Hoffmann, J.E. and Münker, C., 2015. Geochemistry of the Krivoy Rog Banded Iron Formation, Ukraine, and the impact of peak episodes of increased global magmatic activity on the trace element composition of Precambrian seawater. *Precambrian Research*, *270*, pp.165-180.

Viljoen, M.J., 1969. An introduction to the geology of the Barberton granite-greenstone terrain. *Spec. Publ. Geol. Soc. S. Afr.*, *2*, pp.9-28.

Wandres, A.M., Bradshaw, J.D., Weaver, S., Maas, R., Ireland, T. and Eby, N., 2004. Provenance analysis using conglomerate clast lithologies: a case study from the Pahau terrane of New Zealand. *Sedimentary Geology*, *167*(1-2), pp.57-89.

Webb, G.E. and Kamber, B.S., 2000. Rare earth elements in Holocene reefal microbialites: a new shallow seawater proxy. *Geochimica et Cosmochimica Acta*, *64*(9), pp.1557-1565.

Zhang P C, Brady P V, Arthur S E, Zhou W Q, Sawyer D, et Hesterberg D A. 2001. Adsorption of barium(II) on montmorillonite : an EXAFS study. *Colloids and Surfaces - A : Physicochemical and Engineering Aspects*, 190(3) : 239–249. (Cité pages 196 et 197.)

APPENDIX A

Labelled Puddingstone conglomerate clasts

Geochemical data obtained by handheld XRF.

Courtousey of Kimberly Myers

TSA

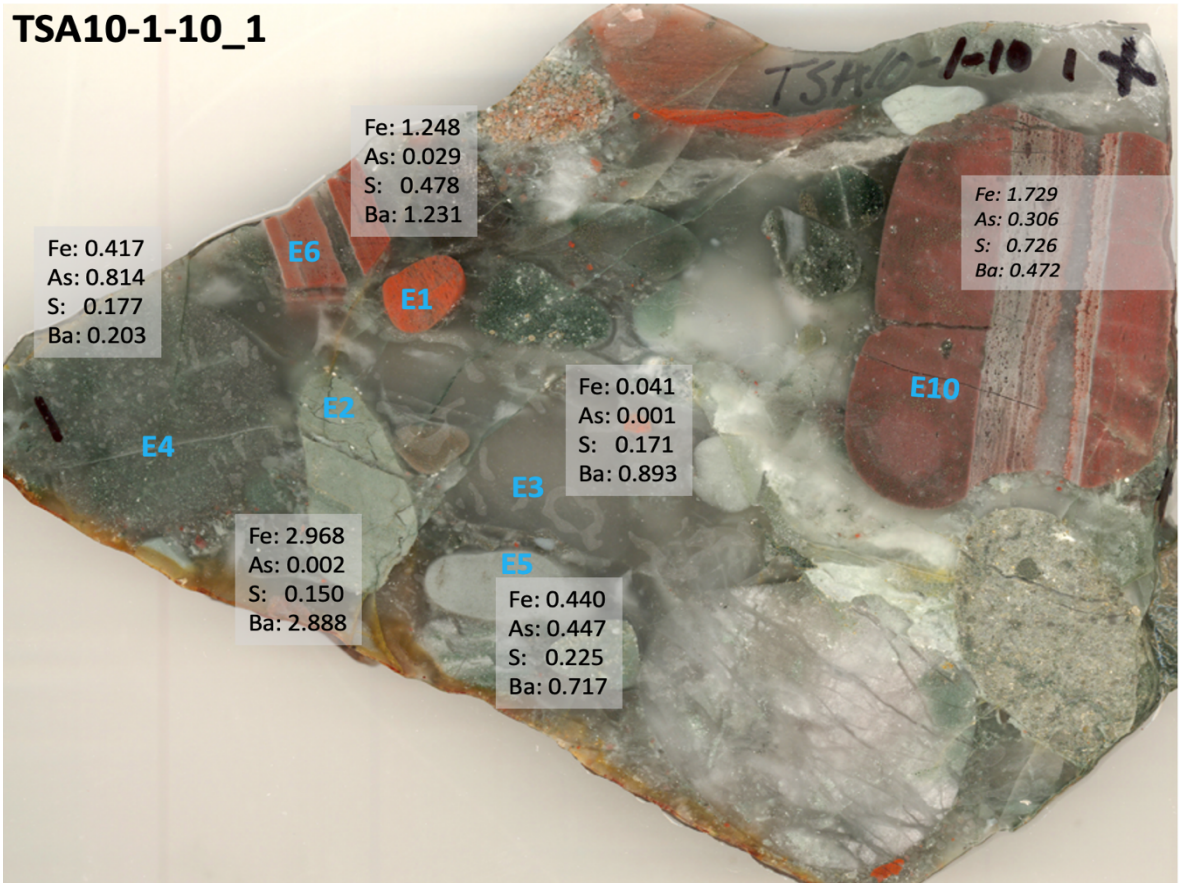
TSA10-1-10_1
Fe: 1.248
As: 0.029
S: 0.478
Ba: 1.231
Fe: 0.417
As: 0.814
S: 0.177
Ba: 0.203
E6
E1
Fe: 1.729
As: 0.306
S: 0.726
Ba: 0.472
E10
E2
E4
Fe: 0.041
As: 0.001
S: 0.171
Ba: 0.893
E3
Fe: 2.968
As: 0.002
S: 0.150
Ba: 2.888
E5
Fe: 0.440
As: 0.447
S: 0.225
Ba: 0.717

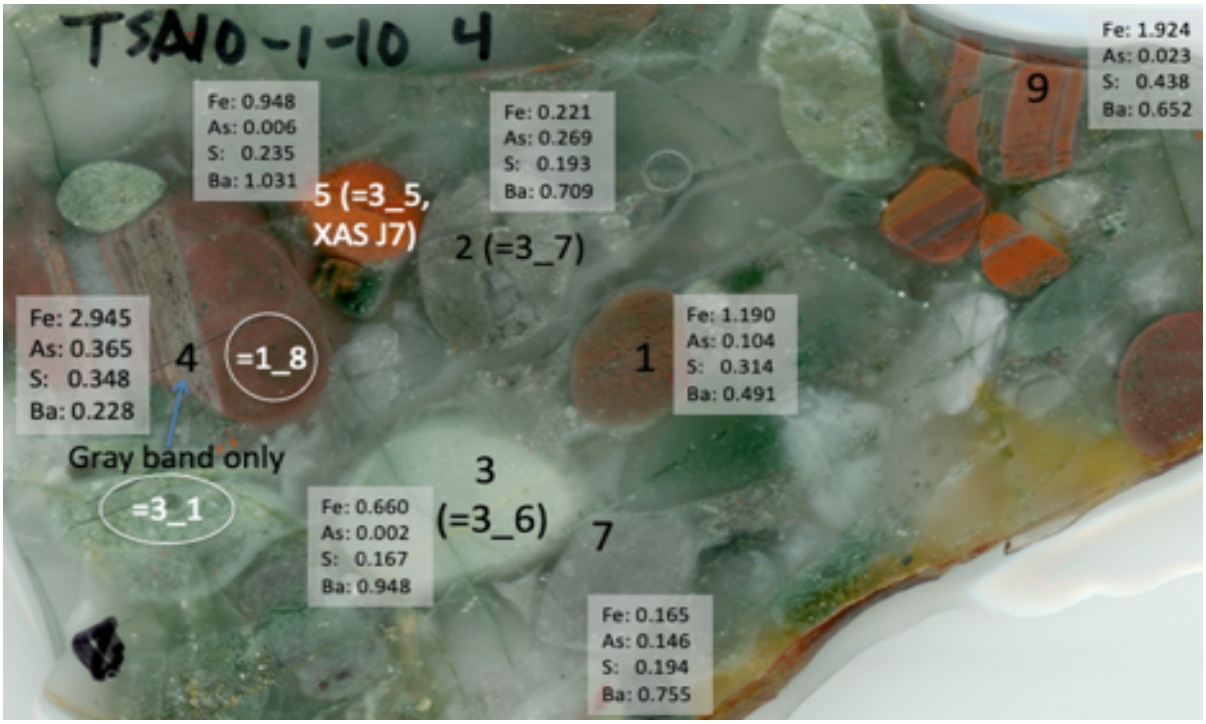
TSA10-1-10 4
Fe: 0.948
As: 0.006
S: 0.235
Ba: 1.031
Fe: 0.221
As: 0.269
S: 0.193
Ba: 0.709
Fe: 1.924
As: 0.023
S: 0.438
Ba: 0.652
9
5 (=3_5, XAS J7)
2 (=3_7)
Fe: 2.945
As: 0.365
S: 0.348
Ba: 0.228
4
=1_8
1
Fe: 1.190
As: 0.104
S: 0.314
Ba: 0.491
Gray band only
=3_1
3
(=3_6)
7
Fe: 0.660
As: 0.002
S: 0.167
Ba: 0.948
Fe: 0.165
As: 0.146
S: 0.194
Ba: 0.755

MMT

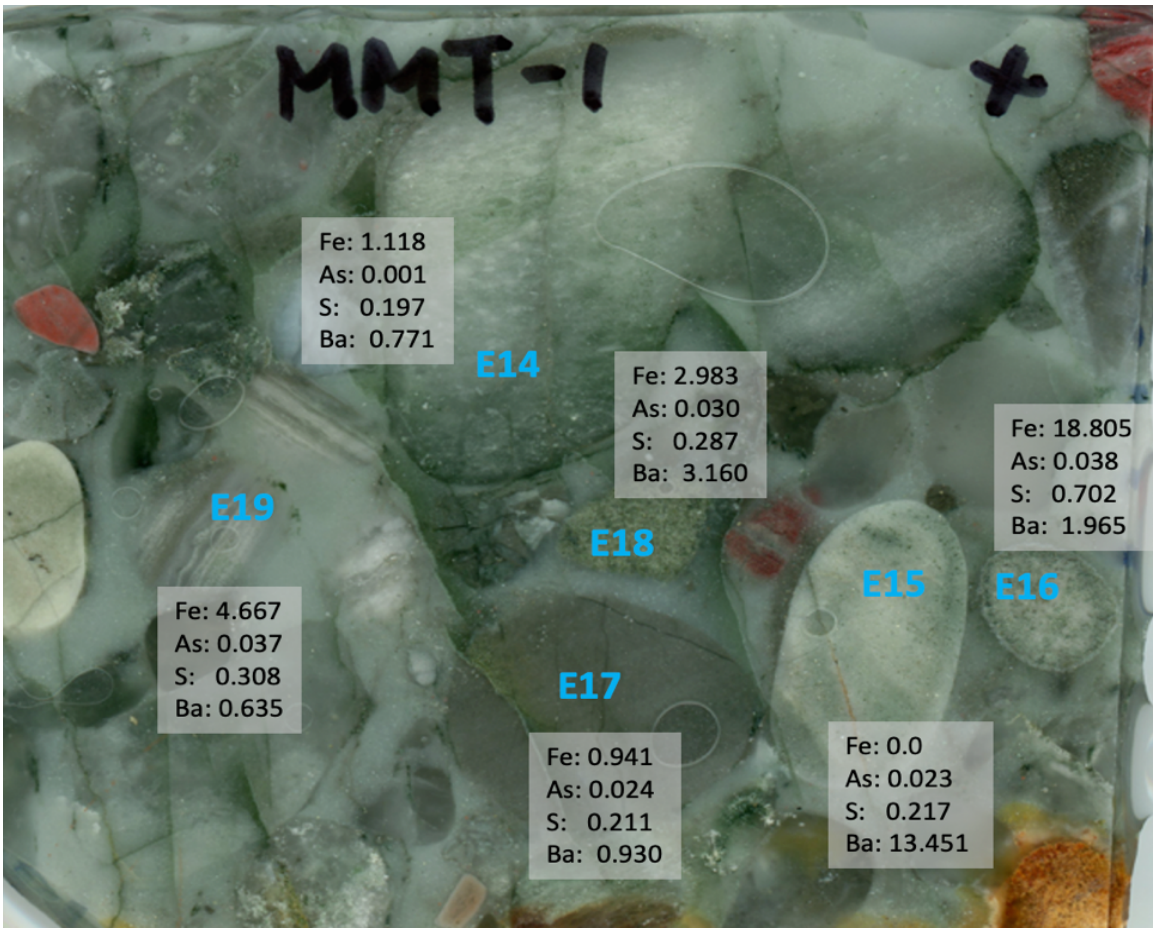
MMT-1
Fe: 1.118
As: 0.001
S: 0.197
Ba: 0.771
E14
Fe: 2.983
As: 0.030
S: 0.287
Ba: 3.160
Fe: 18.805
As: 0.038
S: 0.702
Ba: 1.965
E19
E18
E15
E16
Fe: 4.667
As: 0.037
S: 0.308
Ba: 0.635
E17
Fe: 0.941
As: 0.024
S: 0.211
Ba: 0.930
Fe: 0.0
As: 0.023
S: 0.217
Ba: 13.451

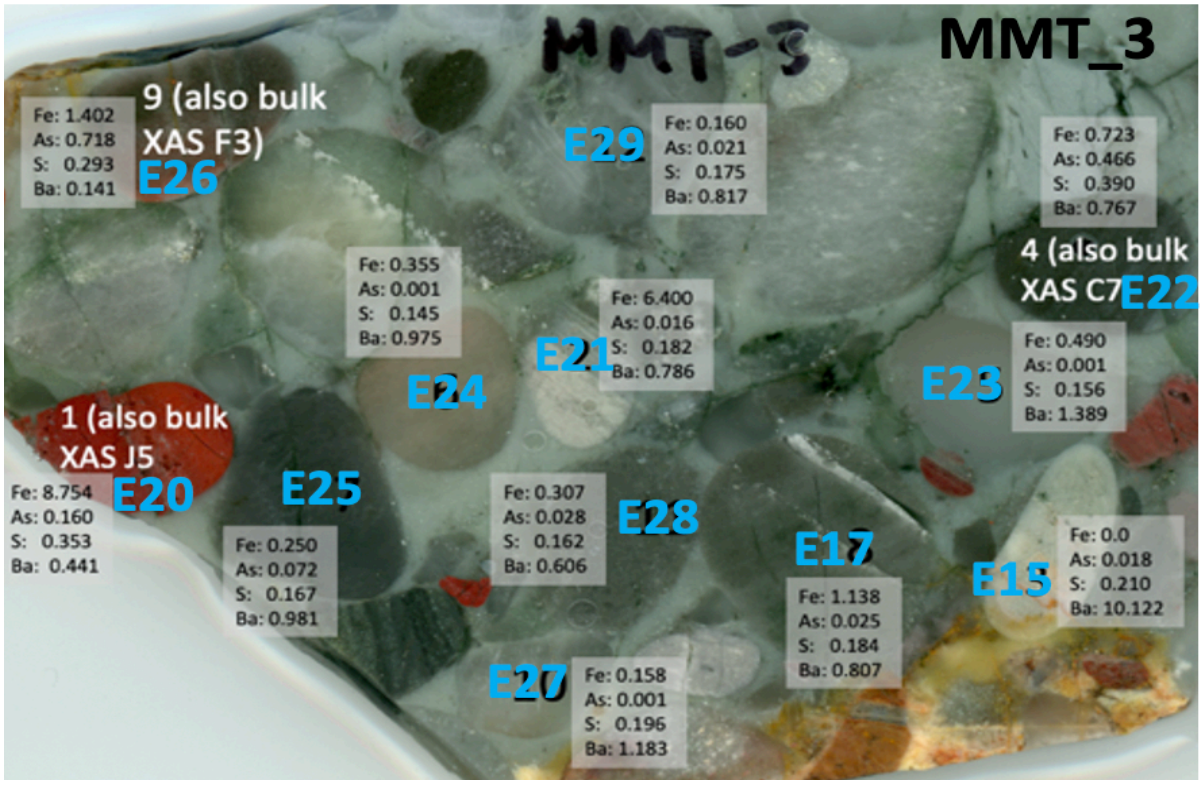
MMT-3
MMT_3
Fe: 1.402
As: 0.718
S: 0.293
Ba: 0.141
9 (also bulk
XAS F3)
E26
E29
Fe: 0.160
As: 0.021
S: 0.175
Ba: 0.817
Fe: 0.723
As: 0.466
S: 0.390
Ba: 0.767
4 (also bulk
XAS C7
E22
Fe: 0.355
As: 0.001
S: 0.145
Ba: 0.975
Fe: 6.400
As: 0.016
S: 0.182
Ba: 0.786
E21
E24
E23
Fe: 0.490
As: 0.001
S: 0.156
Ba: 1.389
1 (also bulk
XAS J5
Fe: 8.754
As: 0.160
S: 0.353
Ba: 0.441
E20
E25
Fe: 0.307
As: 0.028
S: 0.162
Ba: 0.606
E28
E17
E15
Fe: 0.0
As: 0.018
S: 0.210
Ba: 10.122
Fe: 0.250
As: 0.072
S: 0.167
Ba: 0.981
Fe: 1.138
As: 0.025
S: 0.184
Ba: 0.807
E27
Fe: 0.158
As: 0.001
S: 0.196
Ba: 1.183

MSA15-CQ-1

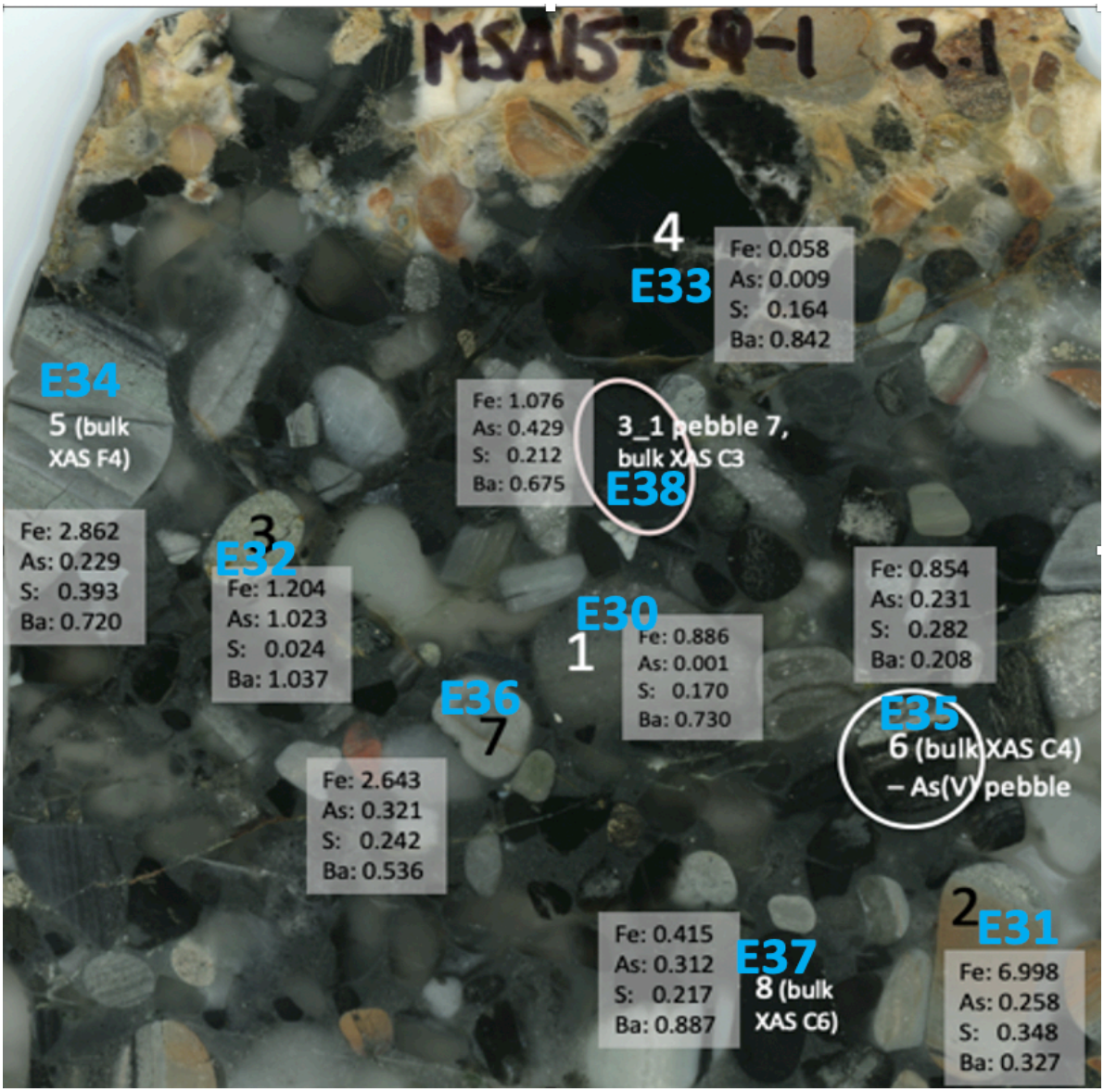
MSA15-CQ-1 2.1
4
E33
Fe: 0.058
As: 0.009
S: 0.164
Ba: 0.842
E34
5 (bulk XAS F4)
Fe: 1.076
As: 0.429
S: 0.212
Ba: 0.675
3_1 pebble 7, bulk XAS C3
E38
Fe: 2.862
As: 0.229
S: 0.393
Ba: 0.720
3
E32
Fe: 1.204
As: 1.023
S: 0.024
Ba: 1.037
E30
1
Fe: 0.886
As: 0.001
S: 0.170
Ba: 0.730
Fe: 0.854
As: 0.231
S: 0.282
Ba: 0.208
E36
7
E35
6 (bulk XAS C4) – As(V) pebble
Fe: 2.643
As: 0.321
S: 0.242
Ba: 0.536
Fe: 0.415
As: 0.312
S: 0.217
Ba: 0.887
E37
8 (bulk XAS C6)
2
E31
Fe: 6.998
As: 0.258
S: 0.348
Ba: 0.327

MSA15-CQ-10

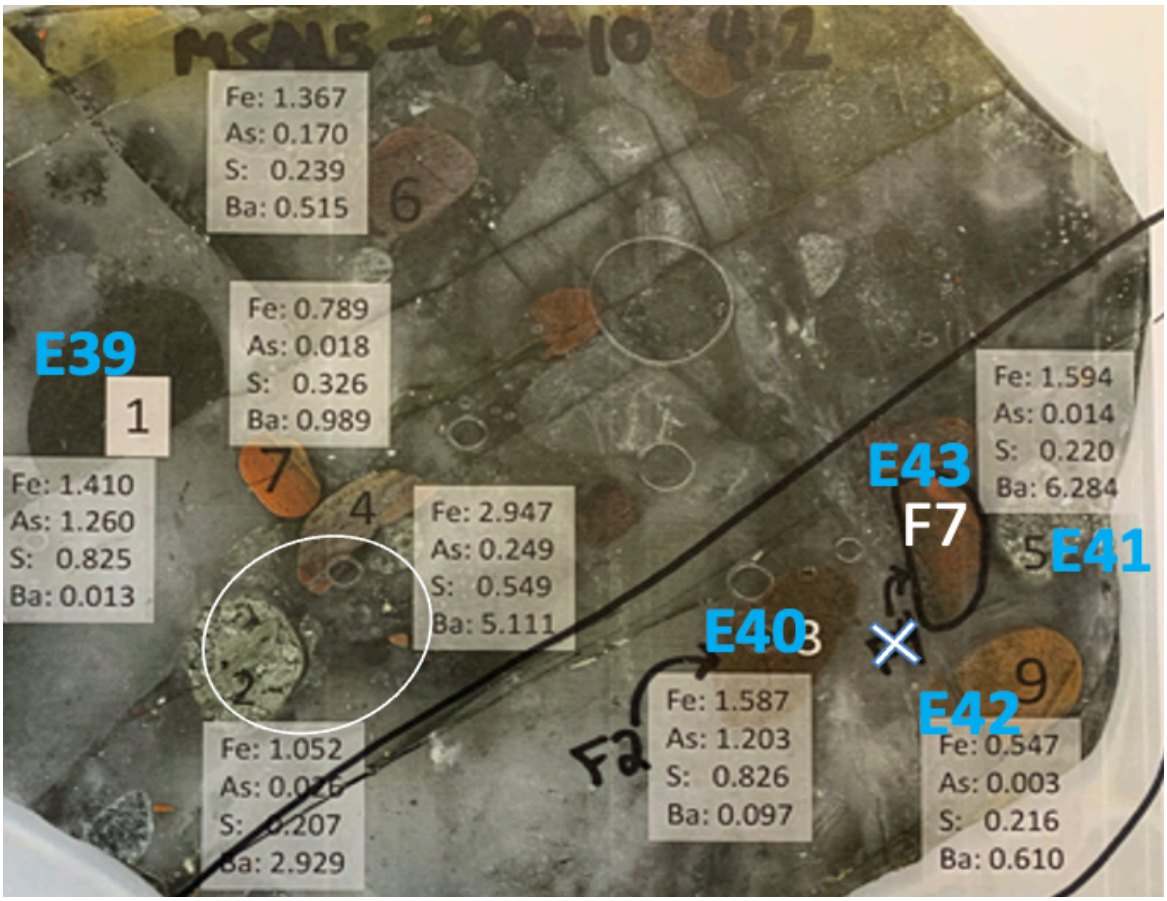
MSA15-CQ-10 4.2
Fe: 1.367
As: 0.170
S: 0.239
Ba: 0.515
E39
1
Fe: 0.789
As: 0.018
S: 0.326
Ba: 0.989
Fe: 1.410
As: 1.260
S: 0.825
Ba: 0.013
Fe: 2.947
As: 0.249
S: 0.549
Ba: 5.111
E43
F7
Fe: 1.594
As: 0.014
S: 0.220
Ba: 6.284
E41
E40
Fe: 1.587
As: 1.203
S: 0.826
Ba: 0.097
E42
Fe: 0.547
As: 0.003
S: 0.216
Ba: 0.610
Fe: 1.052
As: 0.026
S: 0.207
Ba: 2.929

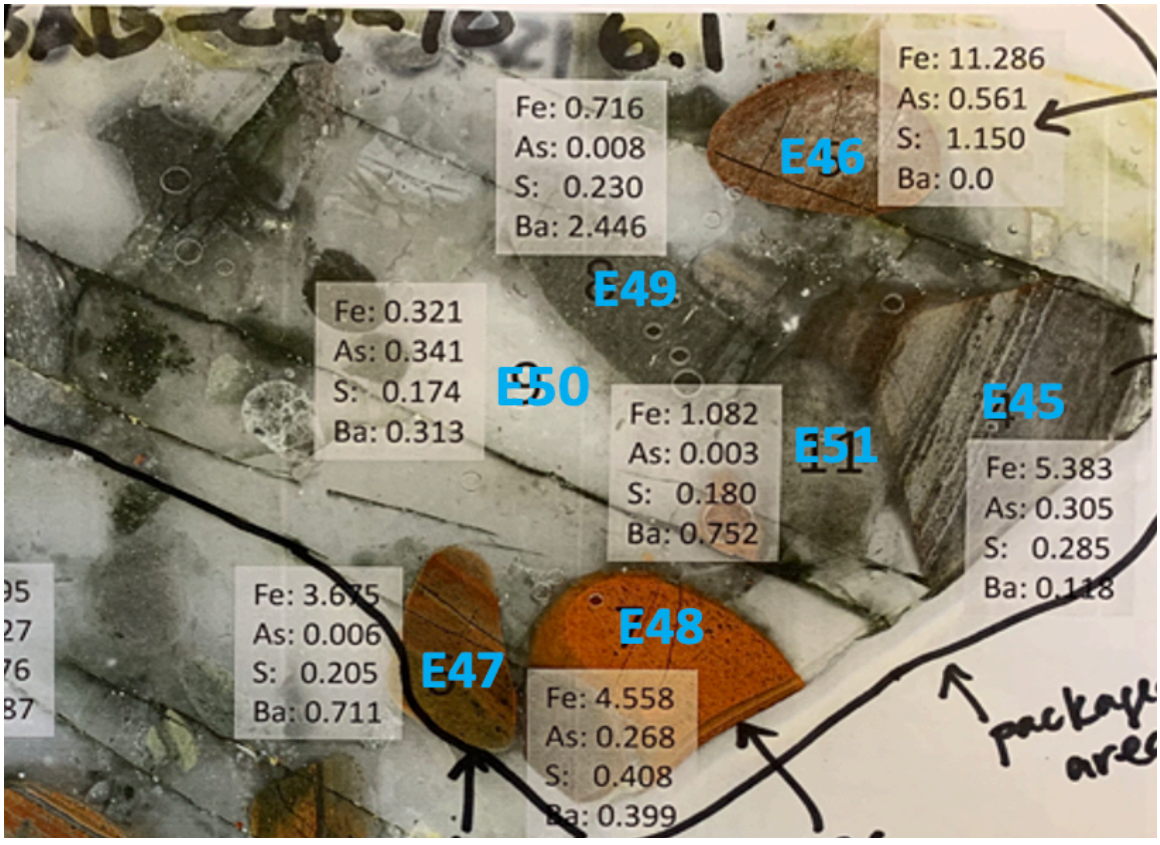
Fe: 0.716
As: 0.008
S: 0.230
Ba: 2.446
Fe: 11.286
As: 0.561
S: 1.150
Ba: 0.0
E46
E49
Fe: 0.321
As: 0.341
S: 0.174
Ba: 0.313
E50
Fe: 1.082
As: 0.003
S: 0.180
Ba: 0.752
E51
E45
Fe: 5.383
As: 0.305
S: 0.285
Ba: 0.118
Fe: 3.675
As: 0.006
S: 0.205
Ba: 0.711
E47
E48
Fe: 4.558
As: 0.268
S: 0.408
Ba: 0.399

APPENDIX B

Individual LA-ICP-MS analyses for the Puddingstone conglomerate clasts

BDL = below detection limit

* = measurements used for REE+Y and trace element profiles in the main text

Slab ref.	TSA10-1-10_1					
Sample code	**E1-1**	**E1-2**	**E1-3**	**E1-4**	**E1-5**	**E1-6**
Description	*Jaspelite*					
Element (ppm)						
Al	190.910	528.420	1254.290	78.450	690.900	1670.290
Si	401063.030	401063.030	401063.030	401063.060	401063.000	401063.030
Ca	391.800	239.530	398.970	217.120	339.030	393.680
Sc	1.529	1.408	1.247	0.997	1.139	1.068
Ti	5.740	7.640	18.120	9.120	BDL	13.110
V	0.157	0.264	0.610	0.105	0.736	0.742
Cr	1.065	0.899	0.859	0.569	0.429	0.973
Mn	11.340	11.440	11.430	9.520	40.470	14.770
Co	0.431	1.222	0.698	18.340	3.550	1.530
Ni	2.120	8.350	3.530	102.540	18.320	9.520
As	24.330	90.560	32.290	1045.210	215.990	87.100
Rb	0.041	0.055	0.131	0.023	BDL	0.090
Sr	6.940	6.380	13.170	7.200	19.290	8.980
Y	0.090	0.060	0.240	0.060	0.267	0.095
Zr	0.019	BDL	0.040	0.070	BDL	0.040
Nb	0.024	0.007	0.024	0.010	0.083	0.042
Cs	0.062	0.061	0.080	0.050	0.145	0.086
Ba	31.350	BDL	93.790	34.770	70.080	43.440
Hf	0.001	BDL	0.002	0.001	BDL	BDL
Ta	0.001	BDL	0.002	0.001	BDL	0.001
Pb	0.384	BDL	0.522	8.340	1.700	0.754
Th	0.002	BDL	0.002	0.002	0.002	BDL
U	0.004	BDL	0.012	0.003	0.007	0.001
La	0.1877	BDL	0.0748	0.4640	0.7400	0.3920
Ce	0.1228	BDL	0.1434	0.0364	0.2950	0.0965
Pr	0.0135	BDL	0.0172	0.0043	0.0423	0.0088
Nd	0.0516	BDL	0.0671	0.0166	0.1970	0.0465
Sm	0.0186	BDL	0.0248	0.0062	0.0739	0.0131
Eu	0.0120	0.0031	0.0166	0.0084	0.0382	0.0141
Gd	0.0230	BDL	0.0460	0.0099	0.0731	0.0257
Tb	0.0034	BDL	0.0061	0.0015	0.0102	0.0028
Dy	0.0167	BDL	0.0334	0.0108	0.0511	0.0163
Ho	0.0027	BDL	0.0067	0.0020	0.0092	0.0035
Er	0.0068	BDL	0.0150	0.0052	0.0260	0.0063
Tm	0.0007	BDL	0.0014	0.0008	0.0030	0.0013
Yb	0.0040	BDL	0.0085	0.0046	0.0110	0.0052
Lu	0.0005	BDL	0.0010	0.0006	0.0014	0.0006
Y/Ho	32.93		35.71	30.05	29.02	27.49
Eu/Eu*	2.60		2.37	4.87	2.30	4.10

Slab ref.	TSA10-1-10_1								
Sample code	**E2-1**	***E2-2**	**E2-3**	**E2-4**	**E2-5**	**E2-6**	**E2-7**	**E2-8**	**E2-9**
Description	*Carbonaceous clastic material*								
Element (ppm)									
Al	72275.390	41429.110	43237.280	1095.670	3825.890	40311.140	38964.070	37011.640	35888.940
Si	254287.060	383478.470	383478.440	383478.470	383478.470	383478.470	383473.690	383473.690	383473.690
Ca	49575.390	807.000	800.930	287.540	425.520	805.130	523.850	530.710	514.840
Sc	32.910	7.570	7.200	0.712	1.180	8.850	8.450	6.450	9.310
Ti	16382.550	1601.660	1123.190	4.660	2095.340	1797.580	1713.830	937.080	1036.950
V	441.190	100.010	96.340	0.562	8.390	104.020	94.280	92.210	91.170
Cr	16.870	511.330	491.660	2.450	42.500	512.780	468.390	568.060	436.830
Mn	1535.000	40.130	57.040	0.388	4.700	32.040	34.160	29.350	22.220
Co	37.820	1.500	0.989	2.780	3.500	2.950	1.536	1.153	0.913
Ni	11.970	108.940	158.470	3.200	13.940	88.850	100.910	89.070	61.940
As	1.250	5.180	3.110	1.660	6.640	11.560	3.930	3.060	3.240
Rb	47.160	62.410	55.550	1.710	4.790	67.790	63.900	61.160	62.930
Sr	329.430	19.230	16.190	14.030	72.090	12.150	11.070	7.680	9.780
Y	31.560	7.000	15.820	0.186	1.004	6.690	7.880	3.480	14.520
Zr	163.440	45.400	28.810	0.949	5.860	41.340	45.070	21.940	81.140
Nb	11.470	2.950	1.790	0.010	5.200	4.010	4.110	1.480	1.620
Cs	1.080	1.650	1.490	0.095	0.171	1.920	1.710	1.520	1.680
Ba	651.530	7740.930	7125.730	1944.600	9743.870	8671.290	7022.910	7232.480	7373.910
Hf	4.300	1.140	0.770	0.027	0.154	1.090	1.260	0.603	2.310
Ta	0.710	0.336	0.211	0.001	0.508	0.430	0.526	0.178	0.198
Pb	10.070	0.720	1.890	0.260	0.800	0.840	1.061	0.432	0.864
Th	5.320	2.890	12.050	0.078	1.160	4.350	BDL	BDL	BDL
U	1.580	1.690	2.630	0.029	0.340	2.100	BDL	BDL	BDL
La	23.8700	4.4200	347.6800	0.3460	4.8100	9.2400	13.4100	4.3200	11.0800
Ce	51.1800	7.6200	568.8500	0.0251	3.0100	15.9600	22.5200	8.1000	19.3200
Pr	6.1800	0.7010	47.6700	0.0026	0.2800	1.4100	2.0500	0.7150	1.7400
Nd	26.9200	2.3100	135.4300	0.0066	1.0530	4.4200	6.5900	2.3500	5.5700
Sm	6.1350	0.4570	10.2250	0.0057	0.3120	0.6065	0.8735	0.3275	0.9300
Eu	1.7800	0.2135	3.7100	0.0102	0.1370	0.2765	0.3335	0.1340	0.4225
Gd	6.1000	0.6170	4.6000	0.0147	0.2070	0.6830	0.7980	0.3460	1.2600
Tb	0.9100	0.1170	0.6050	0.0029	0.0248	0.1270	0.1530	0.0612	0.2620
Dy	5.8500	1.0010	3.5100	0.0265	0.1660	1.0200	1.2000	0.5250	2.1900
Ho	1.1700	0.2270	0.5780	0.0059	0.0349	0.2200	0.2660	0.1130	0.5040
Er	3.3800	0.7410	1.3000	0.0203	0.1190	0.7430	0.9100	0.3810	1.5900
Tm	0.4820	0.1210	0.1480	0.0028	0.0181	0.1180	0.1490	0.0580	0.2660
Yb	3.1600	0.9570	0.8640	0.0189	0.1280	0.8780	1.0500	0.4540	1.9000
Lu	0.4520	0.1420	0.1130	0.0032	0.0213	0.1350	0.1640	0.0700	0.3040
Y/Ho	26.97	30.84	27.37	31.53	28.77	30.41	29.62	30.80	28.81
Eu/Eu*	1.26	1.63	1.97	4.26	2.26	1.74	1.56	1.63	1.51

Slab ref.	TSA10-1-10_1			TSA10-1-10_1			TSA10-1-10_1		
Sample code	**E3-1**	**E3-2**	**E3-3**	**E4-4**	**E4-5**	**E4-6**	***E5-7**	***E5-8**	***E5-9**
Description	*Translucent chert*			*Translucent chert*			*Clastic material*		
Element (ppm)									
Al	84.500	937.650	19229.330	213.180	2206.030	182.600	8701.120	6237.060	8468.940
Si	397323.470	397323.470	397323.470	400583.220	400583.220	400583.190	400374.060	400374.130	400374.090
Ca	220.840	358.380	305.170	220.650	359.330	339.500	548.270	571.770	658.790
Sc	1.033	1.260	3.670	1.064	1.565	1.019	3.240	2.710	3.230
Ti	5.150	1.700	517.900	7.820	13.470	7.230	1249.420	1071.240	1417.030
V	0.092	0.216	43.120	0.037	2.940	0.190	21.340	14.270	23.580
Cr	0.707	1.681	255.410	0.731	3.800	0.959	220.720	158.730	231.500
Mn	0.262	2.005	9.880	0.318	17.360	1.890	BDL	0.659	1.596
Co	0.013	0.266	3.350	0.016	0.065	0.010	68.680	28.760	31.480
Ni	BDL	1.610	38.660	0.321	8.090	0.739	253.570	132.490	168.210
As	1.700	14.400	4.090	1.730	2.890	1.590	527.790	259.280	286.260
Rb	0.104	0.109	33.980	0.247	0.031	0.029	15.340	11.870	15.360
Sr	1.030	40.510	3.980	1.181	1.369	0.838	10.530	4.050	6.240
Y	0.003	0.009	1.370	0.001	0.025	0.001	7.590	7.290	3.950
Zr	0.040	0.221	8.000	0.018	0.033	0.024	13.500	22.530	18.720
Nb	0.011	0.004	0.850	0.004	0.007	0.003	1.755	1.434	2.000
Cs	0.048	0.073	0.873	0.046	0.034	0.036	0.430	0.374	0.464
Ba	28.940	9257.250	4246.600	117.420	6.640	6.580	2064.430	1547.010	2197.600
Hf	0.002	0.006	0.250	0.001	0.001	0.000	0.374	0.431	0.472
Ta	BDL	0.002	0.095	0.001	0.001	0.001	0.148	0.120	0.166
Pb	0.085	0.410	0.885	0.245	0.053	0.040	1.770	0.912	1.327
Th	BDL	BDL	BDL	0.000	0.001	0.000	1.218	0.624	1.359
U	BDL	BDL	BDL	0.001	0.004	0.011	0.658	0.545	0.772
La	23.5000	26.5100	15.5000	0.0607	1.2330	13.5000	6.4900	5.6200	10.5200
Ce	0.0073	0.2300	4.7500	0.0044	0.0334	0.0117	14.7600	10.1300	20.2600
Pr	0.0008	0.0131	0.4380	0.0002	0.0052	0.0008	1.5340	1.1170	2.2100
Nd	0.0031	0.0415	1.3800	0.0006	0.0074	0.0029	5.8400	4.2900	8.5800
Sm	0.0029	0.0051	0.1875	0.0008	0.0023	0.0010	0.7605	0.8095	1.4240
Eu	BDL	0.0205	0.0821	0.0005	0.0014	0.0005	0.2795	0.2555	0.4030
Gd	BDL	BDL	0.1560	0.0007	0.0026	0.0007	0.8720	0.8890	0.7730
Tb	BDL	0.0014	0.0291	BDL	0.0006	BDL	0.1297	0.1419	0.0980
Dy	0.0024	0.0034	0.1960	0.0004	0.0033	0.0003	1.0410	1.0280	0.6050
Ho	BDL	0.0008	0.0456	0.0001	0.0008	0.0001	0.2400	0.2160	0.1317
Er	BDL	BDL	0.1330	BDL	0.0020	0.0002	0.7340	0.6630	0.4300
Tm	0.0008	0.0008	0.0274	0.0001	0.0004	BDL	0.1184	0.0875	0.0659
Yb	BDL	0.0023	0.1780	0.0004	0.0018	0.0010	0.7450	0.6000	0.4840
Lu	BDL	BDL	0.0297	BDL	0.0002	BDL	0.1117	0.0718	0.0739
Y/Ho		11.54	30.04	16.44	30.00	12.60	31.63	33.75	29.99
Eu/Eu*		13.51	1.87	4.68	2.12	3.27	1.52	1.29	1.50

Slab ref.	TSA10-1-10_1								
Sample code	***E6-1**	**E6-2**	**E6-3**	**E6-7**	**E6-4**	**E6-5**	**E6-6**	***E6-8**	**E6-9**
Description	*Jaspelitic lam.*	*Jaspelitic lam.*	*Jaspelitic lam.*	*Jaspelitic lam.*	*Chert lam.*	*Chert lam.*	*Chert lam.*	*Chert lam.*	*Chert lam.*
Element (ppm)									
Al	182.730	525.380	467.730	641.990	4068.900	2205.880	1820.680	1336.860	1343.410
Si	400993.410	400993.440	400993.440	400992.910	400993.440	400993.440	400993.410	400992.910	400992.910
Ca	293.840	238.990	236.210	167.980	221.530	226.860	171.480	329.910	327.020
Sc	0.827	0.653	0.679	1.300	1.480	1.104	0.873	1.750	1.570
Ti	7.890	4.300	4.610	2.820	13.490	18.190	5.470	7.100	3.980
V	0.229	0.243	0.306	0.102	5.290	2.710	1.410	0.866	0.668
Cr	0.660	0.816	0.848	0.619	6.990	5.480	2.030	1.451	1.140
Mn	69.950	29.820	58.480	6.600	17.010	6.520	5.230	158.700	32.470
Co	0.850	0.687	0.845	1.031	9.310	5.770	0.103	4.650	2.190
Ni	5.020	5.060	11.610	32.410	170.540	27.150	8.490	21.350	14.860
As	20.530	15.020	8.250	3.960	3077.840	586.650	1.350	128.410	11.550
Rb	0.045	0.054	0.103	0.645	0.011	0.045	0.016	0.064	0.462
Sr	6.570	4.710	15.930	4.820	1.530	2.580	1.124	17.320	11.130
Y	1.500	1.540	0.328	0.478	0.046	0.061	0.037	2.070	1.150
Zr	0.161	0.221	0.106	0.207	0.055	0.078	0.026	0.186	0.474
Nb	0.021	0.026	0.025	0.016	0.008	0.013	0.008	0.057	0.072
Cs	0.145	0.113	0.266	0.125	0.038	0.047	0.048	0.291	0.315
Ba	25.050	21.610	71.430	173.680	194.490	59.520	12.360	57.440	77.700
Hf	0.003	0.005	0.003	0.009	0.003	0.004	0.001	0.004	0.012
Ta	0.002	0.001	0.001	0.002	0.002	0.002	0.001	0.003	0.001
Pb	0.551	0.403	1.100	0.570	18.100	4.970	0.069	2.310	1.560
Th	0.009	0.009	0.003	BDL	0.005	0.014	0.001	BDL	BDL
U	0.024	0.021	0.007	BDL	0.003	0.079	0.002	BDL	BDL
La	0.0446	0.9840	0.2390	4.8800	0.0281	2.3100	5.0200	2.4500	2.3900
Ce	0.0952	0.1279	0.4210	0.0835	0.0633	0.0610	0.0179	0.3700	1.5500
Pr	0.0105	0.0139	0.0358	0.0084	0.0062	0.0078	0.0024	0.0360	0.1700
Nd	0.0557	0.0608	0.1620	0.0411	0.0308	0.0364	0.0091	0.1520	0.6650
Sm	0.0354	0.0327	0.0466	0.0136	0.0084	0.0177	0.0051	0.0493	0.1180
Eu	0.0318	0.0309	0.0257	0.0109	0.0054	0.0060	0.0034	0.0586	0.0530
Gd	0.1150	0.1210	0.0743	0.0331	0.0074	0.0123	0.0076	0.1710	0.1320
Tb	0.0222	0.0224	0.0093	0.0050	0.0008	0.0017	0.0011	0.0319	0.0209
Dy	0.1970	0.1760	0.0488	0.0618	0.0060	0.0101	0.0064	0.2620	0.1400
Ho	0.0452	0.0390	0.0100	0.0158	0.0009	0.0013	0.0018	0.0599	0.0352
Er	0.1410	0.1350	0.0287	0.0460	0.0040	0.0046	0.0044	0.1960	0.1040
Tm	0.0198	0.0209	0.0034	0.0077	0.0002	0.0007	0.0005	0.0307	0.0155
Yb	0.1420	0.1350	0.0219	0.0571	0.0036	0.0037	0.0034	0.2150	0.1260
Lu	0.0227	0.0213	0.0032	0.0098	0.0002	0.0006	0.0005	0.0327	0.0180
Y/Ho	33.19	39.49	32.80	30.25	52.87	46.02	21.31	34.56	32.67
Eu/Eu*	1.86	1.84	2.14	2.32	3.18	1.66	2.59	2.42	1.83

Slab ref.	TSA10-1-10_4			TSA10-1-10_4			TSA10-1-10_4		
Sample code	**E7-1**	**E7-2**	**E7-3**	**E8-4**	***E8-5**	**E8-6**	***E9-1**	**E9-2**	**E9-3**
Description	*Ferruginous sed. 1.2wt% Fe*			*Clastic material*			*Clastic material*		
Element (ppm)									
Al	107.540	352.720	217.470	1577.830	1902.240	2674.900	13600.630	9346.800	7564.500
Si	400574.340	400574.310	400574.310	399645.530	399645.560	399645.530	399979.090	399979.060	399979.090
Ca	351.170	293.540	276.430	447.320	421.700	411.110	681.850	630.860	635.030
Sc	1.008	0.998	1.036	1.370	1.343	1.345	3.630	2.740	2.480
Ti	5.350	4.890	11.870	71.950	218.330	169.830	689.830	725.090	310.970
V	0.651	0.423	0.111	1.755	2.130	2.760	25.740	15.240	11.820
Cr	0.912	1.054	0.762	8.490	12.050	12.670	132.190	78.870	67.500
Mn	4.080	8.480	9.500	0.490	18.970	0.687	3.930	1.110	2.400
Co	1.235	13.070	0.734	12.230	4.400	9.250	1.267	4.780	3.570
Ni	4.640	44.830	3.990	77.670	25.110	57.130	39.050	29.480	31.390
As	26.340	419.240	9.280	228.470	83.930	158.510	4.560	38.870	17.190
Rb	0.050	0.027	0.173	2.730	3.280	4.760	21.840	16.620	12.890
Sr	2.940	4.320	2.710	2.260	3.080	2.250	41.130	6.930	11.760
Y	0.106	0.153	0.049	1.597	0.382	0.500	4.240	2.950	4.820
Zr	0.094	0.039	0.036	2.410	3.550	2.740	13.580	12.780	9.780
Nb	0.009	0.004	0.007	0.200	0.686	0.496	1.711	1.375	0.756
Cs	0.042	0.042	0.053	0.142	0.175	0.185	0.547	0.465	0.352
Ba	12.070	15.100	30.040	398.070	461.310	626.130	2874.070	2033.020	1635.450
Hf	BDL	0.002	0.002	0.072	0.102	0.079	0.328	0.373	0.278
Ta	BDL	0.000	0.001	0.021	0.066	0.062	0.203	0.153	0.081
Pb	BDL	5.150	0.203	0.705	0.870	0.638	0.129	0.430	0.501
Th	BDL	0.002	0.001	0.145	0.201	0.236	2.300	2.260	1.350
U	0.002	0.004	0.002	0.102	0.128	0.119	0.762	0.708	0.506
La	2.0700	3.2300	9.7800	4.3100	2.6700	5.3000	14.5000	10.5100	8.1300
Ce	0.1521	0.1636	0.0586	0.1215	0.3050	0.3490	23.5300	20.4700	9.5300
Pr	0.0154	0.0195	0.0069	0.0146	0.0296	0.0409	2.3100	2.2100	0.9500
Nd	0.0793	0.0905	0.0339	0.0520	0.1068	0.1630	8.3000	8.3600	3.4200
Sm	0.0171	0.0228	0.0240	0.0299	0.0257	0.0425	1.2715	1.3675	0.5890
Eu	0.0098	0.0132	0.0079	0.0191	0.0113	0.0139	0.3545	0.3060	0.1630
Gd	0.0219	0.0289	0.0105	0.1016	0.0297	0.0444	0.8980	0.7290	0.5570
Tb	0.0028	0.0037	0.0018	0.0232	0.0067	0.0077	0.1023	0.0709	0.0935
Dy	0.0147	0.0217	0.0102	0.2060	0.0615	0.0733	0.6570	0.4520	0.6920
Ho	0.0024	0.0050	0.0020	0.0460	0.0139	0.0165	0.1386	0.0999	0.1605
Er	0.0038	0.0105	0.0055	0.1302	0.0525	0.0558	0.3910	0.3140	0.4820
Tm	BDL	0.0015	0.0004	0.0193	0.0083	0.0100	0.0595	0.0430	0.0701
Yb	0.0030	0.0072	0.0038	0.1201	0.0729	0.0711	0.4010	0.4560	0.4980
Lu	BDL	0.0010	0.0003	0.0173	0.0117	0.0116	0.0606	0.0523	0.0700
Y/Ho	43.72	30.56	24.29	34.72	27.46	30.30	30.59	29.53	30.03
Eu/Eu*	2.39	2.44	1.71	1.14	1.52	1.32	1.43	1.24	1.17

Slab ref.	TSA10-1-10_4								
Sample code	**E10-1**	**E10-2**	**E10-3**	***E10-4**	**E10-5**	**E10-6**	**E10-7**	**E10-8**	**E10-9**
Description	*Jasper lam.*	*Jasper lam.*	*Jasper lam.*	*Grey lamination*	*Grey lamination*	*Grey lamination*	*Chert lamination*	*Chert lamination*	*Chert lamination*
Element (ppm)									
Al	528.660	374.360	1242.020	433.360	312.870	1664.870	113.200	606.760	536.060
Si	400756.250	400756.250	400756.280	400756.250	400756.220	400756.250	400756.310	400756.310	400756.310
Ca	687.950	534.550	444.950	543.120	424.030	487.430	626.420	560.440	491.380
Sc	1.938	1.845	1.643	1.799	1.590	1.766	1.507	1.518	1.457
Ti	4.320	3.700	4.130	14.780	13.110	20.990	5.150	25.640	38.210
V	0.753	0.223	0.668	1.467	1.079	2.730	0.143	0.151	0.267
Cr	1.573	1.245	1.131	2.790	1.828	2.800	1.074	1.890	2.240
Mn	23.990	25.020	25.030	133.470	99.990	126.760	57.790	0.699	5.410
Co	3.560	2.800	15.230	17.270	9.960	7.830	0.166	0.065	0.177
Ni	30.820	18.800	91.400	91.680	57.300	67.150	2.340	1.800	5.450
As	69.310	152.600	1179.130	1356.860	928.870	618.400	4.320	3.580	6.190
Rb	0.068	0.052	0.047	0.151	0.070	0.084	0.159	0.335	0.298
Sr	9.120	10.020	6.290	24.810	20.140	21.560	2.217	2.540	3.380
Y	0.331	0.298	0.126	2.750	0.845	4.220	20.840	0.019	0.016
Zr	0.155	0.065	0.071	0.329	0.251	0.370	0.374	0.197	0.753
Nb	0.023	0.009	0.008	0.085	0.078	0.065	0.006	0.012	0.011
Cs	0.110	0.095	0.071	0.219	0.182	0.180	0.046	0.095	0.125
Ba	54.430	47.850	31.420	106.080	69.340	117.300	34.810	104.340	798.340
Hf	0.004	0.002	0.001	0.006	0.004	0.009	0.007	0.010	0.021
Ta	0.000	BDL	0.001	0.005	0.004	0.004	0.002	0.002	0.001
Pb	2.430	2.690	12.610	9.750	6.340	5.740	0.168	0.193	0.469
Th	0.003	0.001	0.001	0.020	0.010	0.018	0.033	0.001	0.004
U	0.008	0.007	0.005	0.032	0.011	0.045	0.072	0.002	0.006
La	26.6300	21.0500	15.3100	0.3420	2.8100	1.1630	66.7800	84.8300	252.1100
Ce	0.2660	0.2064	0.0812	0.5050	0.3760	0.5570	14.8000	0.0495	0.1058
Pr	0.0266	0.0241	0.0105	0.0557	0.0418	0.0652	1.6580	0.0013	0.0109
Nd	0.1227	0.1130	0.0585	0.2430	0.1790	0.3160	7.0100	0.0246	0.0221
Sm	0.0309	0.0311	0.0155	0.0932	0.0499	0.1206	1.3515	0.0035	0.0120
Eu	0.0253	0.0194	0.0120	0.0791	0.0377	0.0931	0.7040	BDL	0.0100
Gd	0.0444	0.0448	0.0166	0.2630	0.0940	0.3500	1.7300	0.0094	0.0081
Tb	0.0047	0.0046	0.0024	0.0455	0.0179	0.0613	0.2780	0.0004	0.0006
Dy	0.0290	0.0319	0.0195	0.3610	0.1049	0.4800	2.1400	0.0075	0.0056
Ho	0.0068	0.0104	0.0042	0.0778	0.0260	0.1108	0.5080	0.0002	0.0002
Er	0.0182	0.0239	0.0110	0.2140	0.0690	0.3160	1.4600	0.0016	0.0018
Tm	0.0023	0.0021	0.0016	0.0282	0.0096	0.0428	0.2050	0.0005	BDL
Yb	0.0151	0.0123	0.0052	0.1970	0.0577	0.2690	1.2410	0.0022	0.0031
Lu	0.0021	0.0016	0.0007	0.0278	0.0100	0.0390	0.1790	0.0010	0.0005
Y/Ho	48.39	28.65	29.69	35.35	32.50	38.09	41.02	106.67	73.64
Eu/Eu*	3.52	2.71	3.29	2.08	2.22	1.84	2.00	0.00	4.62

Slab ref.	TSA10-1-10_4					TSA10-1-10_4			
Sample code	**E11-1**	**E11-2**	**E11-3**	***E11-4**	**E11-5**	**E12-1**	**E12-2**	***E12-3**	**E12-4**
Description	*Jaspelite*					*Clastic material*			
Element (ppm)									
Al	98.300	437.390	235.400	37.000	44.990	2014.890	3400.830	3744.920	1822.470
Si	399361.000	399361.000	399360.970	399333.470	399333.470	400931.840	400931.840	400931.840	400931.630
Ca	571.610	329.580	567.140	BDL	238.650	453.280	464.330	526.140	266.640
Sc	1.370	1.181	1.224	1.131	1.008	1.648	2.290	2.400	1.290
Ti	8.570	24.870	70.710	BDL	19.130	50.840	269.710	316.310	143.150
V	0.131	0.762	0.184	0.157	0.429	5.080	7.250	9.080	4.420
Cr	0.947	5.740	1.118	BDL	0.773	18.800	20.230	31.270	14.000
Mn	21.250	6.610	11.650	31.260	6.740	1.663	0.534	0.527	0.307
Co	0.432	1.189	0.191	0.580	0.362	5.000	110.530	11.120	9.020
Ni	2.680	6.130	5.050	2.560	0.970	55.390	896.410	74.760	70.360
As	25.510	9.310	12.930	25.970	8.210	84.100	1569.240	131.100	154.770
Rb	0.057	0.161	0.065	BDL	0.023	3.270	5.520	6.390	3.570
Sr	9.980	2.280	10.090	9.400	5.140	2.318	9.000	4.240	2.160
Y	0.268	0.160	2.730	0.706	0.161	0.195	1.030	1.880	0.466
Zr	0.249	0.503	0.549	BDL	0.040	1.565	7.930	14.040	3.360
Nb	0.012	0.039	0.026	BDL	0.008	0.078	0.671	0.527	0.323
Cs	0.122	0.079	0.088	0.093	0.068	0.145	0.195	0.243	0.129
Ba	41.330	341.870	63.470	6.600	21.810	482.100	800.120	897.810	452.120
Hf	0.005	0.016	0.012	BDL	0.002	0.047	0.147	0.387	0.097
Ta	0.002	0.003	0.002	BDL	0.001	0.006	0.060	0.051	0.034
Pb	1.270	0.282	1.430	0.608	0.299	0.167	BDL	0.248	0.141
Th	0.006	0.023	0.005	BDL	0.001	0.045	0.186	0.340	BDL
U	0.005	0.039	0.033	0.007	0.005	0.063	0.295	0.571	BDL
La	0.3910	61.4000	4.9500	BDL	0.0384	23.6100	89.6300	20.5500	10.8500
Ce	0.2600	0.0762	0.4280	0.2430	0.0774	0.1785	0.7220	1.1910	0.1088
Pr	0.0320	0.0092	0.0456	0.0293	0.0078	0.0170	0.0947	0.1283	0.0145
Nd	0.1027	0.0552	0.1920	0.1600	0.0288	0.0626	0.2920	0.4780	0.0591
Sm	0.0274	0.0164	0.0544	0.0481	0.0101	0.0159	0.0424	0.0935	0.0194
Eu	0.0223	0.0092	0.0417	0.0242	0.0101	0.0063	0.0260	0.0508	0.0125
Gd	0.0305	0.0253	0.1600	0.0749	0.0202	0.0143	0.0674	0.1400	0.0323
Tb	0.0058	0.0028	0.0330	0.0126	0.0032	0.0030	0.0133	0.0307	0.0085
Dy	0.0326	0.0174	0.2930	0.0886	0.0198	0.0284	0.1330	0.2610	0.0606
Ho	0.0096	0.0050	0.0720	0.0228	0.0057	0.0074	0.0331	0.0581	0.0174
Er	0.0251	0.0200	0.2410	0.0680	0.0174	0.0173	0.1100	0.2110	0.0507
Tm	0.0031	0.0020	0.0358	0.0098	0.0021	0.0031	0.0167	0.0364	0.0083
Yb	0.0229	0.0213	0.2370	0.0702	0.0164	0.0278	0.1360	0.2460	0.0676
Lu	0.0043	0.0028	0.0378	0.0112	0.0025	0.0055	0.0223	0.0436	0.0115
Y/Ho	27.92	32.13	37.92	30.96	28.50	26.24	31.12	32.36	26.78
Eu/Eu*	3.09	2.32	1.63	1.73	3.16	1.58	1.93	1.67	1.69

Slab ref.	TSA10-1-10_4		TSA10-1-10_4			TSA10-1-10_4		
Sample code	**E12-5**	**E12-6**	***E13-1**	***E13-2**	***E13-3**	***MATRIX-1**	**MATRIX-2**	**MATRIX-3**
Description	*Clastic material*		*Clastic material with chert filled fracture*					
Element (ppm)								
Al	2208.430	2501.820	65036.710	63476.900	78097.980	5746.360	1535.060	804.380
Si	400931.660	400931.630	387611.530	387611.500	387611.500	430044.220	430044.220	430044.220
Ca	306.990	169.850	1360.740	1286.110	1367.670	589.800	440.040	423.690
Sc	1.450	1.460	13.740	13.390	13.770	1.640	1.303	1.324
Ti	105.360	201.240	2147.910	2584.590	2198.320	72.500	72.410	6.350
V	7.910	7.000	188.440	180.900	208.070	5.990	1.648	0.440
Cr	24.730	21.400	609.780	590.140	769.430	34.490	14.210	2.490
Mn	0.288	0.297	71.790	64.740	128.380	2.540	BDL	0.619
Co	14.960	15.170	1.049	0.978	1.742	1.439	1.427	0.062
Ni	103.740	132.400	131.780	116.140	232.870	6.060	1.050	1.880
As	213.970	249.720	1.630	1.590	2.090	7.780	14.970	1.130
Rb	4.020	4.450	98.780	98.400	92.200	10.450	2.100	0.884
Sr	3.380	2.440	6.810	4.990	6.750	2.850	0.871	2.280
Y	0.669	0.730	1.540	0.944	1.231	0.345	BDL	0.013
Zr	4.120	5.080	8.580	7.960	7.370	2.290	BDL	0.187
Nb	0.251	0.394	1.154	1.422	1.066	0.087	0.076	0.007
Cs	0.160	0.156	2.440	2.530	2.258	0.375	0.120	0.135
Ba	481.760	573.720	12893.150	13157.160	12452.000	1606.030	453.710	864.980
Hf	0.117	0.147	0.276	0.248	0.304	0.098	BDL	0.009
Ta	0.022	0.042	0.105	0.106	0.105	0.009	0.012	BDL
Pb	0.271	0.154	0.139	0.151	0.171	0.300	BDL	0.117
Th	BDL	BDL	0.078	0.056	0.067	0.064	0.012	0.015
U	BDL	BDL	0.293	0.286	0.308	0.119	0.040	0.006
La	4.3900	4.8100	0.0484	0.0367	0.1106	36.8400	14.9800	111.5900
Ce	6.2000	0.9090	0.2940	0.1265	0.2990	0.0596	BDL	0.1860
Pr	0.5860	0.0930	0.0477	0.0186	0.0407	0.0077	BDL	0.0288
Nd	2.0700	0.3410	0.2420	0.0726	0.1980	0.0254	BDL	0.1210
Sm	0.2915	0.0644	0.1104	0.0331	0.0873	0.0101	BDL	0.0176
Eu	0.0730	0.0225	0.0704	0.0469	0.0599	0.0132	BDL	0.0130
Gd	0.1380	0.0521	0.1840	0.0778	0.1420	0.0253	BDL	0.0073
Tb	0.0160	0.0126	0.0324	0.0151	0.0266	0.0071	BDL	0.0009
Dy	0.1070	0.1070	0.2670	0.1240	0.2080	0.0421	BDL	0.0004
Ho	0.0196	0.0262	0.0546	0.0333	0.0441	0.0127	0.0022	0.0005
Er	0.0770	0.0710	0.1670	0.1100	0.1260	0.0369	0.0052	0.0019
Tm	0.0133	0.0124	0.0260	0.0171	0.0204	0.0070	BDL	0.0002
Yb	0.0870	0.1080	0.1740	0.1300	0.1370	0.0590	0.0085	0.0048
Lu	0.0131	0.0157	0.0284	0.0205	0.0225	0.0119	0.0020	0.0006
Y/Ho	34.13	27.86	28.21	28.35	27.91	27.17		27.14
Eu/Eu*	1.38	1.37	2.08	3.62	2.20	2.50		4.11

Slab ref.	MMT-1						MMT-1		
Sample code	**E14-1**	**E14-2**	**E14-3**	**E14-4**	***E14-5**	**E14-6**	**E15-1**	***E15-2**	**E15-3**
Description	*Translucent chert*						*Clastic material*		
Element (ppm)									
Al	26.330	7641.990	28.920	29.180	31.650	19.100	30233.960	79897.750	29090.840
Si	394185.500	394185.500	394185.500	394192.440	394192.410	394192.440	381134.190	381134.220	381134.190
Ca	404.310	576.190	289.260	130.910	274.440	209.970	814.070	1415.020	806.660
Sc	0.660	1.085	0.553	0.610	0.712	0.732	2.620	4.100	1.870
Ti	3.260	10.210	2.890	4.190	1.590	0.493	1564.270	1361.440	1176.770
V	0.368	3.960	0.055	0.070	0.137	0.184	30.180	115.320	27.190
Cr	0.853	1.437	0.845	0.508	0.917	0.671	95.450	462.020	101.180
Mn	727.270	1596.860	77.520	74.250	307.710	674.270	22.230	183.430	9.630
Co	0.421	0.804	0.040	0.046	0.239	0.232	3.100	4.230	2.900
Ni	2.410	19.470	0.312	0.639	1.870	1.930	32.840	87.290	46.690
As	2.020	0.613	0.484	0.405	1.490	0.394	18.960	11.030	29.210
Rb	0.032	0.061	0.029	0.046	0.038	0.028	32.580	70.500	17.770
Sr	1.950	1.860	1.380	0.854	1.360	1.230	12.200	28.300	9.600
Y	0.434	0.263	0.263	0.019	0.210	0.045	6.760	3.350	3.450
Zr	0.031	0.082	0.081	0.004	0.011	0.004	59.070	22.490	30.080
Nb	0.004	0.014	0.001	0.002	0.006	0.003	4.990	3.760	3.700
Cs	0.056	0.065	0.046	0.042	0.042	0.049	0.798	2.180	0.529
Ba	11.120	33.310	9.570	12.610	13.220	8.390	21838.730	48942.910	32523.280
Hf	0.001	0.002	0.002	0.001	BDL	0.000	1.730	0.738	0.985
Ta	0.001	0.001	0.000	BDL	BDL	BDL	0.746	0.662	0.489
Pb	0.055	0.100	0.041	0.027	0.011	0.061	1.690	1.230	1.036
Th	0.002	0.003	0.003	0.001	BDL	0.000	9.130	4.800	4.770
U	0.015	0.075	0.011	0.038	0.025	0.012	1.820	1.210	1.030
La	0.0277	3.0600	3.8700	0.0928	2.8600	6.1500	34.4800	13.0800	11.7000
Ce	0.0670	0.0192	0.0169	0.0106	0.0204	0.0146	63.9700	24.1300	24.4200
Pr	0.0073	0.0052	0.0034	0.0018	0.0030	0.0015	6.3200	2.5100	2.5800
Nd	0.0409	0.0193	0.0113	0.0029	0.0139	0.0113	21.8000	9.1400	9.3400
Sm	0.0146	0.0047	0.0063	0.0036	0.0046	0.0027	3.1250	1.6550	1.3595
Eu	0.0088	0.0039	0.0028	0.0007	0.0040	0.0014	0.7520	0.4970	0.3930
Gd	0.0362	0.0087	0.0242	0.0014	0.0125	0.0023	1.5630	0.9910	0.7450
Tb	0.0067	0.0027	0.0049	0.0002	0.0028	0.0008	0.1710	0.1027	0.0928
Dy	0.0655	0.0302	0.0347	0.0028	0.0281	0.0076	1.1260	0.6060	0.5900
Ho	0.0136	0.0075	0.0078	0.0007	0.0077	0.0013	0.2280	0.1160	0.1242
Er	0.0460	0.0329	0.0255	0.0014	0.0193	0.0058	0.6690	0.3450	0.3820
Tm	0.0066	0.0057	0.0033	0.0003	0.0028	0.0012	0.0997	0.0520	0.0583
Yb	0.0563	0.0468	0.0221	0.0023	0.0245	0.0093	0.7060	0.3650	0.4090
Lu	0.0078	0.0082	0.0039	0.0006	0.0040	0.0016	0.1040	0.0533	0.0598
Y/Ho	31.91	35.11	33.76	26.71	27.34	34.77	29.65	28.88	27.78
Eu/Eu*	1.54	1.81	0.79	1.06	1.83	1.62	1.33	1.62	1.53

Slab ref.	MMT-1			MMT-1			MMT-1	
Sample code	***E17-1**	**E17-2**	**E17-3**	***E18-1**	***E18-2**	***E18-3**	**E19-1**	***E19-2**
Description	*Clastic material*			*Clastic material*			*Clastic material*	
Element (ppm)								
Al	6797.940	2565.170	7174.740	22669.990	39950.150	31868.780	10306.320	6371.780
Si	396391.340	396391.310	396391.280	397086.440	397086.440	397086.440	397170.560	397170.560
Ca	574.630	408.540	845.500	671.990	735.230	740.660	413.030	425.350
Sc	1.730	1.870	1.146	3.770	7.100	6.800	1.058	0.885
Ti	434.550	205.050	277.490	2448.190	3009.870	3476.440	411.780	367.890
V	7.800	3.100	7.610	74.500	165.530	140.500	19.900	9.930
Cr	30.400	16.310	51.860	310.570	712.590	642.680	194.960	80.630
Mn	707.960	36.490	40.450	71.120	200.360	103.300	215.410	89.300
Co	5.200	1.023	2.940	17.480	10.810	7.880	4.990	4.020
Ni	33.560	7.710	30.570	77.540	113.540	73.460	40.250	11.930
As	15.150	7.810	22.840	79.140	31.290	35.400	9.470	12.870
Rb	6.030	3.470	4.610	11.980	21.810	24.430	11.470	11.240
Sr	10.310	2.870	17.600	12.250	9.510	8.890	2.790	2.870
Y	3.850	78.750	3.010	1.520	2.220	1.320	0.786	0.966
Zr	5.660	232.820	6.570	10.030	14.430	9.420	4.470	5.500
Nb	1.260	0.434	0.719	1.700	1.990	2.520	0.519	0.473
Cs	0.187	0.127	0.188	0.403	0.630	0.685	0.288	0.310
Ba	1965.350	557.100	575.280	13620.970	12252.320	13603.890	1408.550	1186.270
Hf	0.131	5.160	0.157	0.277	0.426	0.283	0.132	0.166
Ta	0.122	0.057	0.066	0.132	0.170	0.195	0.043	0.038
Pb	0.930	0.298	1.950	0.317	0.439	0.388	0.460	0.321
Th	0.650	0.950	1.650	0.120	0.137	0.135	0.469	0.215
U	0.280	2.060	0.422	0.367	0.424	0.317	0.165	0.191
La	4.0500	2.9000	20.0100	0.0227	0.8410	0.0285	4.8500	2.6400
Ce	4.0900	0.9300	33.6100	0.1320	0.2520	0.2020	2.7500	0.8760
Pr	0.4220	0.1160	3.4000	0.0185	0.0426	0.0261	0.2740	0.0888
Nd	1.5700	0.7540	12.6300	0.0791	0.2370	0.1100	0.9360	0.3290
Sm	0.3150	1.1100	2.1650	0.0425	0.1245	0.0583	0.1350	0.0773
Eu	0.1195	0.7285	0.6090	0.0378	0.0573	0.0410	0.0416	0.0308
Gd	0.3670	4.7800	1.7500	0.1180	0.2270	0.1230	0.0988	0.0890
Tb	0.0713	1.2800	0.1470	0.0259	0.0433	0.0248	0.0158	0.0173
Dy	0.5780	11.1300	0.6360	0.2170	0.3310	0.1970	0.1123	0.1330
Ho	0.1270	2.4600	0.1120	0.0504	0.0794	0.0472	0.0256	0.0322
Er	0.4050	6.9100	0.3030	0.1820	0.2620	0.1500	0.0844	0.1044
Tm	0.0598	0.9330	0.0447	0.0335	0.0420	0.0263	0.0133	0.0170
Yb	0.4500	5.9700	0.3090	0.2550	0.3400	0.1990	0.1010	0.1270
Lu	0.0693	0.8700	0.0487	0.0392	0.0511	0.0312	0.0158	0.0198
Y/Ho	30.31	32.01	26.88	30.16	27.96	27.97	30.70	30.00
Eu/Eu*	1.40	0.87	1.49	1.88	1.37	1.87	1.44	1.48

Slab ref.	MMT-1	MMT3						MMT3		
Sample code	**E19-3**	***E20-1**	**E20-2**	**E20-3**	**E20-4**	**E20-5**	**E20-6**	**E21-1**	**E21-2**	**E21-3**
Description	*Clastic material*	*Carbonaceous jaspelite 8.75wt%Fe*						*Ferruginous sed. 6.4wt%Fe*		
Element (ppm)										
Al	5082.300	86.600	31.800	60.390	100.580	53.130	120.810	520.090	516.580	477.490
Si	397170.590	399122.500	399122.500	399122.530	399122.500	399122.500	399122.530	400945.780	400945.810	400945.780
Ca	348.860	383.850	220.300	427.210	238.920	152.500	150.060	264.520	472.740	249.660
Sc	0.869	1.192	1.072	1.156	1.326	0.886	0.873	1.154	1.048	0.973
Ti	492.100	7.380	3.550	3.200	2.780	1.700	2.540	2.680	4.220	1.180
V	7.090	0.385	0.178	0.380	0.319	0.017	0.067	0.322	0.671	0.957
Cr	56.440	1.181	0.927	1.339	2.720	0.735	22.150	1.218	1.558	1.710
Mn	1.680	1132.980	97.920	4213.990	456.710	9.460	103.330	506.410	963.420	343.200
Co	1.850	3.390	2.030	2.720	3.280	0.016	0.355	1.117	1.740	3.330
Ni	6.880	16.650	52.170	28.260	20.020	0.858	2.320	11.030	13.670	30.100
As	10.160	283.520	608.110	404.730	518.780	1.580	4.840	14.370	43.540	71.830
Rb	8.870	0.034	0.033	0.024	0.040	0.025	0.053	0.641	0.089	0.241
Sr	4.160	4.360	2.210	4.860	5.660	0.428	0.997	3.700	4.550	3.210
Y	1.450	1.416	0.101	0.321	0.266	0.003	0.167	0.155	0.148	0.094
Zr	9.810	0.085	0.042	0.058	0.056	0.040	0.099	0.222	0.071	0.061
Nb	0.595	0.017	0.009	0.009	0.013	0.003	0.004	0.020	0.020	0.009
Cs	0.272	0.076	0.042	0.065	0.101	0.031	0.031	0.084	0.068	0.070
Ba	1030.350	18.030	11.250	17.190	24.460	13.120	18.380	121.160	31.110	54.230
Hf	0.234	0.001	0.001	0.001	0.001	0.001	0.004	0.004	0.002	0.001
Ta	0.042	0.001	BDL	BDL	0.000	BDL	0.000	0.000	0.000	0.000
Pb	0.241	3.490	8.770	5.780	3.850	BDL	0.246	0.273	0.283	0.245
Th	0.203	0.002	0.003	0.001	0.003	BDL	0.004	0.002	0.004	BDL
U	0.290	0.014	0.011	0.005	0.004	BDL	0.007	0.004	0.004	BDL
La	1.1390	1.2420	0.2070	0.8910	0.0437	10.2500	1.6080	0.7760	1.6430	2.5600
Ce	0.4290	0.0672	0.1150	0.1930	0.1104	0.0036	0.0995	0.0430	0.1310	0.0227
Pr	0.0441	0.0101	0.0271	0.0239	0.0135	0.0009	0.0144	0.0054	0.0145	0.0028
Nd	0.1980	0.0515	0.0609	0.0997	0.0585	0.0023	0.0496	0.0231	0.0759	0.0123
Sm	0.0607	0.0267	0.0121	0.0276	0.0190	0.0006	0.0160	0.0068	0.0201	0.0046
Eu	0.0287	0.0209	0.0072	0.0146	0.0108	BDL	0.0099	0.0106	0.0244	0.0058
Gd	0.1171	0.0663	0.0161	0.0380	0.0329	0.0017	0.0156	0.0116	0.0300	0.0069
Tb	0.0259	0.0157	0.0024	0.0069	0.0050	BDL	0.0040	0.0025	0.0040	0.0017
Dy	0.2440	0.1361	0.0164	0.0482	0.0410	0.0016	0.0217	0.0173	0.0176	0.0088
Ho	0.0506	0.0418	0.0033	0.0112	0.0095	0.0002	0.0056	0.0044	0.0047	0.0021
Er	0.1730	0.1035	0.0097	0.0347	0.0292	BDL	0.0184	0.0137	0.0139	0.0082
Tm	0.0276	0.0150	0.0015	0.0068	0.0048	0.0001	0.0025	0.0018	0.0024	0.0009
Yb	0.1920	0.1282	0.0099	0.0574	0.0361	0.0005	0.0236	0.0143	0.0142	0.0112
Lu	0.0314	0.0190	0.0015	0.0082	0.0042	BDL	0.0039	0.0026	0.0025	0.0014
Y/Ho	28.66	33.88	30.48	28.64	28.03	18.89	29.63	35.64	31.76	44.07
Eu/Eu*	1.26	1.70	2.33	1.86	1.96		2.17	4.52	4.72	3.66

Slab ref.	MMT3			MMT3					
Sample code	**E22-1**	***E22-2**	**E22-3**	**E23-1**	**E23-2**	**E23-3**	**E23-4**	**E23-5**	**E23-6**
Description	*Clastic material*			*Translucent chert*					
Element (ppm)									
Al	14003.840	15372.970	11577.890	198.850	784.650	234.450	160.580	157.560	575.610
Si	393498.000	393497.970	393498.000	402545.280	402545.310	402545.310	402552.250	402552.250	402552.250
Ca	971.170	670.490	662.920	443.700	423.940	319.720	230.920	150.060	185.800
Sc	2.500	2.390	2.260	0.821	0.667	0.725	0.766	0.684	0.646
Ti	345.230	890.220	463.790	1.470	4.030	9.250	5.940	2.010	3.220
V	27.030	34.060	19.590	0.018	0.594	0.063	0.014	0.016	0.058
Cr	149.160	198.350	112.580	7.480	1.910	1.156	0.480	1.313	0.890
Mn	25.360	3.880	5.500	0.305	4.390	0.769	0.276	0.293	0.374
Co	55.100	48.340	45.820	0.144	0.037	0.152	0.030	0.013	0.009
Ni	202.820	207.090	185.210	3.490	2.840	7.910	10.040	2.370	2.160
As	727.450	424.570	630.590	2.000	1.730	4.700	1.460	1.730	1.500
Rb	22.960	25.000	19.700	0.300	0.344	0.323	0.250	0.219	0.864
Sr	11.540	4.100	3.690	1.640	1.780	1.860	1.640	1.760	1.650
Y	1.561	0.927	2.120	0.039	0.002	0.021	0.001	0.001	BDL
Zr	7.630	5.610	11.750	0.217	0.047	0.327	0.049	0.040	0.038
Nb	0.470	1.253	0.756	0.004	0.003	0.008	0.002	0.004	0.003
Cs	0.537	0.523	0.474	0.083	0.067	0.067	0.058	0.065	0.087
Ba	3027.900	3093.910	2587.960	68.330	73.110	72.800	54.780	53.840	179.610
Hf	0.231	0.170	0.324	0.007	0.002	0.006	BDL	0.001	0.001
Ta	0.038	0.079	0.059	0.000	0.001	0.001	BDL	0.000	0.000
Pb	20.200	16.150	12.640	0.097	0.049	0.169	BDL	0.043	0.058
Th	1.420	0.570	0.746	0.008	0.001	0.001	BDL	0.000	0.001
U	0.456	0.262	0.571	0.084	0.002	0.002	BDL	0.001	0.001
La	7.9100	1.3600	5.6500	0.0057	1.7200	6.1600	2.0000	0.1256	0.4590
Ce	13.1100	2.8100	4.9400	0.0141	0.0017	0.0185	0.0324	0.0038	0.0062
Pr	1.4020	0.3050	0.5310	0.0021	0.0003	0.0014	BDL	0.0004	0.0005
Nd	5.5700	1.1320	1.9600	0.0128	0.0017	0.0024	0.0011	0.0006	0.0012
Sm	0.9465	0.1805	0.3240	0.0042	0.0003	0.0010	0.0004	0.0002	0.0005
Eu	0.2285	0.0560	0.0921	0.0017	BDL	BDL	BDL	BDL	0.0006
Gd	0.5650	0.1392	0.2630	0.0043	0.0013	BDL	BDL	BDL	0.0002
Tb	0.0531	0.0193	0.0422	0.0007	BDL	BDL	BDL	BDL	0.0001
Dy	0.2840	0.1397	0.3130	0.0056	0.0003	0.0004	BDL	BDL	0.0005
Ho	0.0552	0.0316	0.0711	0.0011	BDL	BDL	BDL	BDL	0.0001
Er	0.1700	0.0922	0.2310	0.0041	BDL	0.0005	BDL	BDL	BDL
Tm	0.0283	0.0137	0.0359	0.0007	BDL	0.0002	BDL	BDL	0.0001
Yb	0.1680	0.1061	0.2580	0.0044	BDL	0.0004	BDL	0.0005	BDL
Lu	0.0248	0.0153	0.0381	0.0006	0.0001	0.0001	BDL	0.0000	0.0000
Y/Ho	28.28	29.34	29.82	34.86					
Eu/Eu*	1.32	1.48	1.29	1.73					6.02

Slab ref.	MMT3							
Sample code	**E24-1**	**E24-2**	**E24-3**	**E24-4**	**E24-5**	***E24-6**	**E24-7**	**E24-8**
Description	*Translucent chert*							
Element (ppm)								
Al	143.690	379.260	198.860	188.950	171.530	77.460	184.990	129.320
Si	390839.250	390839.250	390839.250	390846.310	390846.310	390846.280	390846.340	390846.340
Ca	389.690	322.630	272.880	138.420	132.900	116.520	126.900	322.310
Sc	1.346	1.243	1.108	0.857	0.974	0.778	0.775	0.930
Ti	6.330	3.450	5.350	2.400	1.920	3.890	3.240	2.210
V	0.234	0.656	0.130	0.132	0.129	0.059	0.112	0.095
Cr	0.820	0.692	0.630	1.053	0.578	6.730	0.627	0.813
Mn	5.760	11.520	2.400	2.880	5.340	6.340	3.310	3.120
Co	0.185	0.109	0.040	0.082	0.104	0.072	0.428	0.093
Ni	3.480	4.230	1.820	2.010	2.080	8.530	2.010	2.260
As	4.100	7.120	3.800	4.220	2.920	3.290	4.330	3.620
Rb	0.117	0.589	0.283	0.254	0.224	0.045	0.254	0.172
Sr	2.520	2.110	1.430	2.650	2.110	2.000	2.060	2.530
Y	0.023	0.384	1.014	0.137	0.313	0.030	0.013	0.014
Zr	0.056	0.049	0.173	0.063	0.050	0.068	0.050	0.115
Nb	0.005	0.002	0.004	0.002	0.002	0.001	0.001	0.004
Cs	0.067	0.058	0.049	0.061	0.057	0.046	0.060	0.060
Ba	36.490	114.310	75.100	64.230	62.770	20.130	62.300	52.220
Hf	0.001	0.002	0.003	0.001	BDL	0.001	0.002	0.003
Ta	0.000	BDL	0.001	0.001	BDL	0.000	0.000	BDL
Pb	0.160	0.180	0.084	0.230	BDL	0.073	0.155	0.134
Th	0.001	0.001	0.004	0.001	BDL	0.005	0.000	0.000
U	0.002	0.003	0.009	0.002	BDL	0.001	0.001	0.001
La	0.7390	4.0100	4.6600	0.7540	1.4900	1.8300	5.8400	0.4280
Ce	0.0182	0.0123	0.0167	0.0117	0.0045	0.0101	0.0069	0.0152
Pr	0.0030	0.0017	0.0010	0.0041	0.0010	0.0009	0.0004	0.0050
Nd	0.0106	0.0128	0.0092	0.0032	0.0032	0.0040	0.0056	0.0034
Sm	0.0027	0.0076	0.0145	0.0031	0.0043	0.0028	0.0012	0.0019
Eu	0.0029	0.0059	0.0149	0.0032	0.0065	0.0020	0.0014	0.0026
Gd	0.0061	0.0249	0.0654	0.0104	0.0224	0.0018	0.0011	0.0027
Tb	0.0003	0.0054	0.0171	0.0028	0.0051	0.0006	0.0003	0.0004
Dy	0.0052	0.0528	0.1517	0.0239	0.0415	0.0052	0.0020	0.0021
Ho	0.0009	0.0115	0.0319	0.0049	0.0087	0.0013	0.0004	0.0004
Er	0.0032	0.0376	0.0945	0.0158	0.0270	0.0034	0.0016	0.0014
Tm	0.0009	0.0049	0.0145	0.0025	0.0041	0.0008	0.0003	0.0004
Yb	0.0026	0.0375	0.0864	0.0175	0.0261	0.0041	0.0022	0.0028
Lu	0.0010	0.0053	0.0131	0.0021	0.0048	0.0005	0.0005	0.0002
Y/Ho	26.09	33.36	31.79	27.94	36.02	24.00	30.95	39.43
Eu/Eu*	5.07	1.47	1.33	1.65	1.97	2.67	4.40	5.15

Slab ref.	MMT3			MMT3						
Sample code	**E25-1**	**E25-2**	**E25-3**	**E26-1**	***E26-2**	***E26-3**	**E26-4**	**E26-5**	**E26-6**	**E26-7**
Description	*Grey fractured chert*			*Ferruginous carbonaceous sed. 1.4wt% Fe*						
Element (ppm)										
Al	529.220	526.050	483.940	10.380	8355.050	62.160	1382.030	72.040	751.430	407.590
Si	390213.280	390213.310	390213.310	399297.030	399297.030	399297.030	399304.090	399304.060	399304.090	399304.090
Ca	421.110	358.180	298.210	BDL	688.570	405.930	285.910	368.920	289.230	258.760
Sc	1.005	0.923	0.927	0.240	1.499	0.959	1.679	0.975	1.073	0.966
Ti	15.160	7.510	30.570	BDL	346.370	2.390	7.410	9.130	8.930	13.410
V	0.989	0.257	0.535	BDL	13.850	0.062	2.640	0.030	0.962	0.486
Cr	1.963	0.947	1.362	2.820	112.610	0.578	3.590	0.689	8.980	4.790
Mn	1.143	1.171	0.518	51.500	8.450	139.740	725.100	32.430	85.420	442.030
Co	7.490	1.730	3.390	4.120	1.970	1.112	0.713	3.570	5.520	2.600
Ni	53.520	5.470	24.900	BDL	11.270	2.460	7.780	7.230	19.510	12.280
As	84.260	10.690	39.610	395.180	15.920	22.580	1.730	135.950	72.960	17.480
Rb	0.629	0.662	0.580	BDL	11.530	0.037	0.114	0.032	0.035	0.256
Sr	1.960	1.378	1.528	1.780	3.940	2.590	4.670	2.340	4.130	5.240
Y	1.224	0.010	0.020	0.546	0.934	1.590	0.154	2.030	0.085	0.206
Zr	0.511	0.070	0.131	BDL	5.270	0.078	0.421	0.119	0.088	0.337
Nb	0.027	0.009	0.101	0.011	0.382	0.008	0.007	0.007	0.016	0.012
Cs	0.080	0.072	0.076	BDL	0.240	0.039	0.044	0.043	0.067	0.081
Ba	188.010	177.180	145.820	10.860	1342.030	14.500	125.640	13.700	22.410	263.380
Hf	0.044	BDL	0.008	BDL	0.103	0.001	0.010	0.002	0.002	0.011
Ta	0.003	0.000	0.011	BDL	0.025	BDL	0.001	0.000	0.001	0.001
Pb	0.269	0.112	0.145	2.140	3.440	0.534	0.151	0.761	2.970	2.310
Th	0.030	BDL	0.008	0.001	0.101	0.001	0.004	0.002	0.001	0.008
U	0.039	BDL	0.009	0.007	0.139	0.009	0.011	0.029	0.004	0.010
La	1.1080	2.5500	0.0180	0.0948	0.1221	0.0100	0.4450	0.1696	0.0677	0.2010
Ce	0.0419	0.0172	0.0277	0.0110	0.3040	0.1070	0.0243	0.0210	0.0310	0.0574
Pr	0.0042	0.0011	0.0025	BDL	0.0338	0.0032	0.0037	0.0028	0.0031	0.0079
Nd	0.0198	0.0049	0.0074	BDL	0.1290	0.0247	0.0215	0.0188	0.0151	0.0308
Sm	0.0159	0.0014	0.0015	BDL	0.0398	0.0134	0.0130	0.0230	0.0051	0.0106
Eu	0.0134	0.0013	0.0019	BDL	0.0143	0.0142	0.0072	0.0231	0.0112	0.0106
Gd	0.0767	0.0020	0.0022	0.0430	0.0704	0.0520	0.0270	0.0869	0.0083	0.0142
Tb	0.0182	BDL	0.0005	0.0046	0.0139	0.0129	0.0046	0.0208	0.0021	0.0032
Dy	0.1533	0.0007	0.0030	0.0396	0.1130	0.1108	0.0330	0.2130	0.0106	0.0231
Ho	0.0349	0.0031	0.0006	0.0127	0.0302	0.0294	0.0056	0.0572	0.0025	0.0061
Er	0.1033	BDL	0.0022	0.0473	0.0875	0.0963	0.0173	0.1930	0.0078	0.0217
Tm	0.0128	BDL	0.0004	0.0073	0.0155	0.0140	0.0027	0.0284	0.0014	0.0036
Yb	0.0810	BDL	0.0021	0.0324	0.1100	0.0973	0.0231	0.1980	0.0087	0.0272
Lu	0.0130	BDL	0.0006	0.0060	0.0139	0.0136	0.0040	0.0276	0.0017	0.0039
Y/Ho	35.07	3.28	31.43	42.99	30.93	54.08	27.42	35.49	33.64	33.99
Eu/Eu*	1.12	6.18	3.66	0.00	1.07	1.62	1.65	1.60	6.01	3.25

Slab ref.	MMT3							
Sample code	**E27-1**	**E27-2**	**E27-3**	**E27-4**	**E27-5**	**E27-6**	**E27-7**	***E27-8**
Description	*Translucent chert*							
Element (ppm)								
Al	65.500	69.540	90.690	94.570	400.390	53.670	68.580	48.670
Si	390812.560	390812.530	390812.530	390812.530	390824.030	390824.030	390824.030	390824.030
Ca	272.280	456.910	324.670	307.910	201.840	156.730	133.250	114.360
Sc	0.870	1.310	1.408	1.124	0.754	0.702	0.706	0.732
Ti	2.120	3.530	4.950	3.330	3.730	3.830	2.050	5.050
V	0.014	0.341	0.265	0.269	0.047	0.009	0.011	0.017
Cr	0.776	1.870	0.779	0.666	2.170	0.640	0.613	0.743
Mn	0.239	2262.180	736.460	1398.880	0.801	0.125	0.171	0.555
Co	0.012	4.750	1.580	4.230	0.026	0.017	0.011	0.023
Ni	42.220	26.670	11.600	57.840	0.912	5.730	3.870	0.781
As	1.850	949.510	74.190	1484.630	1.890	1.090	1.180	1.610
Rb	0.073	0.040	0.050	0.033	0.542	0.074	0.100	0.071
Sr	1.930	6.630	6.340	4.710	2.230	1.400	0.907	2.030
Y	BDL	0.321	2.130	0.318	0.006	0.024	0.359	0.822
Zr	0.032	0.235	0.080	0.060	0.030	0.011	0.052	0.048
Nb	0.002	0.010	0.011	0.010	0.013	0.002	0.003	0.005
Cs	0.060	0.081	0.099	0.081	0.078	0.053	0.047	0.068
Ba	25.740	20.420	23.570	19.660	108.700	25.640	24.780	26.400
Hf	0.000	0.003	0.001	0.001	0.001	BDL	0.001	BDL
Ta	0.000	0.001	BDL	0.000	0.001	BDL	BDL	BDL
Pb	0.062	5.600	0.849	7.230	0.227	0.051	0.036	BDL
Th	0.000	0.009	0.003	0.002	0.000	0.001	0.001	BDL
U	0.005	0.017	0.007	0.004	0.003	0.001	0.011	0.019
La	3.0400	0.2750	0.1880	0.2880	0.2170	0.2030	1.6540	4.9000
Ce	0.0071	0.6100	0.3930	0.6170	0.0039	0.0051	0.0031	0.0039
Pr	0.0007	0.0716	0.0445	0.0688	0.0010	0.0001	BDL	0.0010
Nd	0.0024	0.2970	0.2120	0.2860	0.0012	0.0196	0.0020	0.0050
Sm	0.0007	0.0588	0.0667	0.0579	BDL	0.0007	0.0049	0.0085
Eu	0.0016	0.0204	0.0417	0.0218	0.0010	0.0006	0.0049	0.0078
Gd	BDL	0.0573	0.1560	0.0580	0.0010	BDL	0.0198	0.0380
Tb	BDL	0.0082	0.0324	0.0068	0.0005	0.0004	0.0040	0.0082
Dy	0.0004	0.0505	0.2630	0.0521	0.0006	0.0029	0.0355	0.0732
Ho	BDL	0.0106	0.0624	0.0092	0.0006	0.0007	0.0103	0.0217
Er	BDL	0.0305	0.2140	0.0357	0.0019	0.0023	0.0342	0.0619
Tm	BDL	0.0050	0.0333	0.0052	0.0003	0.0005	0.0041	0.0104
Yb	BDL	0.0401	0.2380	0.0426	BDL	0.0035	0.0380	0.0729
Lu	0.0001	0.0051	0.0352	0.0064	0.0003	0.0003	0.0051	0.0114
Y/Ho	#VALUE!	30.25	34.13	34.42	9.78	36.52	34.72	37.88
Eu/Eu*	15.58	1.53	1.54	1.76	3.90	1.71	1.72	1.39

Slab ref.	MMT3			MMT3			MMT-1			MMT3		
Sample code	**E28-1**	***E28-2**	**E28-3**	**E29-1**	**E29-2**	**E29-3**	**MATRIX-1**	***MATRIX-2**	**MATRIX-3**	***MATRIX-4**	**MATRIX-5**	**MATRIX-6**
Description	*Grey clastic material*			*Translucent chert*								
Element (ppm)												
Al	2352.290	2594.460	174.560	552.970	19.740	1834.850	15594.200	35.060	824.470	82.570	11853.120	5296.780
Si	390773.340	390773.340	390773.340	397181.470	397181.470	397181.470	444067.280	444067.280	444067.280	444067.470	444067.470	444067.440
Ca	501.840	504.020	395.130	226.290	209.950	291.930	479.500	388.290	362.010	468.280	958.800	601.580
Sc	1.210	1.626	0.884	1.712	1.525	1.410	1.555	0.560	0.531	1.096	2.230	2.230
Ti	85.190	141.980	5.030	16.690	3.430	15.590	287.780	2.910	11.260	3.410	5277.560	11.650
V	3.870	6.980	0.027	0.245	0.025	0.314	24.160	0.203	0.399	0.104	24.430	15.270
Cr	15.550	64.680	0.674	2.120	3.210	3.560	165.340	1.143	0.822	0.984	200.050	16.310
Mn	0.517	1.684	0.320	0.455	0.499	0.634	6.330	487.130	55.090	81.280	28.790	178.390
Co	4.500	3.230	0.010	2.120	0.024	1.035	1.150	0.174	0.103	0.229	2.950	1.074
Ni	26.110	14.110	1.434	14.190	1.700	19.180	10.850	1.830	2.590	3.330	16.700	16.810
As	52.410	22.610	2.840	16.230	1.960	27.900	6.220	0.930	3.400	4.800	24.530	5.060
Rb	3.530	4.150	0.224	0.189	0.018	0.525	28.050	0.057	0.097	0.196	21.360	0.023
Sr	3.320	4.810	1.990	1.628	1.164	2.490	5.350	1.170	5.200	1.261	13.370	1.144
Y	0.100	0.408	0.001	0.341	0.006	0.123	2.140	0.258	0.075	0.052	2.100	0.025
Zr	0.768	1.783	0.044	1.148	0.083	0.321	11.380	0.035	0.231	0.044	10.770	0.106
Nb	0.099	0.160	0.005	0.043	0.003	0.017	0.297	0.007	0.030	0.005	6.480	0.004
Cs	0.194	0.211	0.067	0.050	0.046	0.074	0.613	0.063	0.057	0.052	0.494	0.053
Ba	618.060	634.560	57.130	392.370	10.690	2899.520	3624.010	13.570	25.080	33.360	3507.730	11.840
Hf	0.021	0.055	0.001	0.030	0.001	0.008	0.324	0.003	0.006	0.001	0.298	0.007
Ta	0.009	0.014	BDL	0.005	0.000	0.003	0.023	BDL	0.002	BDL	0.457	0.001
Pb	0.202	0.538	0.057	0.151	0.050	4.680	0.481	0.059	0.093	0.050	1.042	0.615
Th	0.105	0.101	0.000	0.020	0.001	0.013	0.274	0.002	0.004	0.001	0.638	0.007
U	0.027	0.050	0.003				0.368	0.044	0.016	0.025	0.638	0.006
La	2.4300	1.1430	1.1040	5.4200	7.6200	1.6760	1.2900	5.0500	3.0000	8.2300	6.1200	0.2210
Ce	0.4790	0.5890	0.0019	0.0354	0.0487	0.0501	0.7420	0.0194	0.0576	0.0089	2.3600	0.0133
Pr	0.0889	0.0601	0.1274	0.0039	0.0008	0.0059	0.0840	0.0024	0.0119	0.0023	0.2380	0.0017
Nd	0.1930	0.2100	BDL	0.0148	BDL	0.0199	0.3270	0.0148	0.0270	0.0046	0.8990	0.0049
Sm	0.0308	0.0363	0.0005	0.0066	0.0010	0.0056	0.0908	0.0087	0.0109	0.0025	0.2155	0.0026
Eu	0.0111	0.0143	BDL	0.0067	0.0014	0.0194	0.0434	0.0043	0.0081	0.0022	0.0902	0.0011
Gd	0.0190	0.0372	BDL	0.0279	BDL	0.0106	0.1390	0.0156	0.0106	0.0022	0.2470	0.0051
Tb	0.0020	0.0058	0.0035	0.0056	BDL	0.0025	0.0344	0.0042	0.0020	0.0007	0.0464	0.0010
Dy	0.0156	0.0621	0.0005	0.0493	BDL	0.0214	0.8310	0.0278	0.0137	0.0072	0.3590	0.0035
Ho	0.0038	0.0137	BDL	0.0108	BDL	0.0041	0.0687	0.0077	0.0027	0.0014	0.0869	0.0009
Er	0.0106	0.0413	BDL	0.0345	0.0016	0.0120	0.2390	0.0232	0.0076	0.0060	0.2440	0.0027
Tm	0.0022	0.0068	BDL	0.0050	BDL	0.0019	0.0385	0.0028	0.0008	0.0014	0.0407	0.0007
Yb	0.0111	0.0467	BDL	0.0342	0.0009	0.0140	0.2830	0.0239	0.0056	0.0053	0.2800	0.0055
Lu	0.0017	0.0081	BDL	0.0052	0.0003	0.0021	0.0451	0.0038	0.0009	0.0007	0.0427	0.0007
Y/Ho	26.03	29.69	#VALUE!	31.52	#VALUE!	29.76	31.15	33.46	27.81	37.48	24.17	28.20
Eu/Eu*	1.93	1.67	0.00	1.69	9.67	9.06	1.36	1.22	3.01	2.85	1.58	1.20

Slab ref.	MSA15-CQ-1_2.1						MSA15-CQ-1_2.1		
Sample code	**E30-1**	**E30-2**	**E30-3**	**E30-4**	**E30-5**	**E30-6**	**E31-1**	**E31-2**	***E31-3**
Description	*Grey chert*						*Ferruginous sed. 6.998wt% Fe*		
Element (ppm)									
Al	92.650	229.440	191.710	200.200	113.170	146.210	151.410	139.910	114.340
Si	399362.940	399362.940	399362.940	399370.090	399370.090	399370.090	400789.630	400789.590	400789.590
Ca	316.050	228.410	200.510	312.050	226.980	226.270	577.030	367.880	255.170
Sc	0.922	0.809	0.738	0.887	0.735	0.684	0.903	0.842	0.823
Ti	4.910	6.180	2.370	8.060	1.300	6.510	2.320	2.850	1.690
V	0.287	0.215	0.117	0.245	0.114	0.095	0.623	0.361	0.208
Cr	2.100	2.350	0.779	0.914	2.380	0.804	1.643	1.526	2.620
Mn	176.380	0.961	105.740	34.760	115.090	82.420	1275.870	847.460	258.640
Co	0.118	0.112	0.085	0.072	0.051	0.071	12.810	135.470	16.910
Ni	1.550	1.810	0.956	0.925	0.850	0.719	38.010	623.540	107.340
As	3.060	3.600	2.710	1.990	1.380	1.410	1116.400	12.590	12.670
Rb	0.142	0.341	0.271	0.201	0.152	0.182	0.035	0.033	0.027
Sr	1.150	1.101	0.820	0.974	1.730	1.417	4.820	3.230	2.950
Y	0.047	0.019	0.023	0.014	0.006	0.017	0.358	0.229	0.163
Zr	0.297	0.208	0.350	0.066	0.043	0.122	1.650	0.095	0.052
Nb	0.009	0.011	0.004	0.009	0.003	0.005	0.013	0.034	0.020
Cs	0.050	0.050	0.064	0.069	0.054	0.047	0.093	0.109	0.097
Ba	30.660	64.150	56.330	37.420	35.490	44.290	7.820	8.160	6.700
Hf	BDL	0.008	0.003	0.009	0.001	0.003	0.003	0.003	0.001
Ta	BDL	0.001	0.001	0.001	0.001	0.000	0.001	0.001	0.001
Pb	BDL	0.066	0.062	0.036	0.042	BDL	2.110	1.810	0.507
Th	BDL	0.007	0.006	0.011	0.002	BDL	0.009	0.006	0.003
U	BDL	0.008	0.002	0.003	0.002	BDL	0.011	0.007	0.007
La	0.2700	1.1780	2.7500	1.2440	2.4400	1.4370	0.0422	0.0316	0.0170
Ce	0.0112	0.0310	0.1488	0.0230	0.0128	0.0189	0.0951	0.0653	0.0467
Pr	0.0010	0.0010	0.0010	0.0017	0.0011	0.0017	0.0113	0.0083	0.0059
Nd	0.0050	0.0051	0.0029	0.0055	0.0058	0.0200	0.0563	0.0360	0.0239
Sm	0.0019	0.0022	0.0016	0.0015	0.0009	0.0065	0.0168	0.0113	0.0076
Eu	0.0010	0.0014	0.0011	0.0010	BDL	0.0029	0.0163	0.0101	0.0092
Gd	0.0029	0.0029	0.0024	BDL	BDL	0.0040	0.0338	0.0194	0.0147
Tb	0.0008	0.0003	0.0007	BDL	BDL	0.0003	0.0055	0.0036	0.0032
Dy	0.0068	0.0048	0.0040	0.0020	0.0007	0.0021	0.0479	0.0337	0.0217
Ho	0.0012	0.0011	0.0009	0.0004	0.0002	BDL	0.0108	0.0077	0.0058
Er	0.0049	0.0023	0.0024	0.0027	0.0007	0.0007	0.0376	0.0285	0.0187
Tm	0.0010	0.0006	0.0004	0.0005	0.0001	0.0002	0.0068	0.0047	0.0036
Yb	BDL	0.0019	0.0022	0.0018	0.0018	0.0012	0.0554	0.0368	0.0256
Lu	0.0009	0.0005	0.0004	0.0003	0.0002	BDL	0.0093	0.0065	0.0045
Y/Ho	39.41	17.55	26.25	36.32	25.35		33.15	29.59	28.06
Eu/Eu*	1.51	2.76	1.76			2.58	3.00	2.78	3.27

Slab ref.	MSA15-CQ-1_2.1			MSA15-CQ-1_2.1			
Sample code	**E32-1**	**E32-2**	***E32-3**	**E33-1**	**E33-2**	**E33-3**	**E33-4**
Description	*Clastic material 1.2wt% Fe*			*Fractured black translucent chert*			
Element (ppm)							
Al	259627.030	70713.550	88700.140	551.470	843.040	591.100	941.070
Si	322257.750	322257.780	322257.750	402090.060	402090.060	402090.030	402090.030
Ca	2752.170	1089.710	1474.120	294.750	222.710	189.890	634.640
Sc	15.480	3.370	5.480	0.853	0.691	0.681	0.698
Ti	79705.800	1015.910	2919.710	0.749	4.340	2.850	34.160
V	369.130	77.400	100.860	0.114	0.367	0.259	0.315
Cr	894.580	203.030	258.480	0.701	0.863	0.577	6.470
Mn	112.400	26.710	35.650	0.481	0.265	0.204	8.150
Co	3.310	4.650	8.820	0.091	0.639	0.604	0.134
Ni	55.220	47.340	42.770	1.720	7.240	7.110	4.850
As	19.660	75.590	67.620	2.860	12.150	11.710	18.310
Rb	420.280	112.990	140.690	0.712	0.980	0.643	0.783
Sr	39.310	7.820	9.780	2.630	3.570	2.780	3.750
Y	47.900	0.827	8.970	0.126	0.390	0.092	0.246
Zr	472.070	8.180	107.110	1.740	3.230	1.040	3.070
Nb	192.490	0.738	4.040	0.019	0.029	0.020	0.042
Cs	12.560	4.260	4.740	0.182	0.192	0.183	0.146
Ba	49337.200	13440.080	17295.090	154.590	199.040	157.460	229.970
Hf	12.590	0.169	2.680	0.013	0.028	0.011	0.052
Ta	14.770	0.072	0.348	0.000	0.002	0.001	0.003
Pb	11.960	BDL	0.962	0.071	0.117	0.158	0.740
Th	27.760	BDL	2.050	0.001	0.009	0.003	0.169
U	11.840	0.132	1.760	0.128	0.201	0.074	0.090
La	3.6100	0.4070	1.3050	1.7400	0.0022	3.8500	4.3300
Ce	7.4500	0.2580	2.5300	0.0042	0.0088	0.0033	0.8620
Pr	0.9400	0.0283	0.2810	0.0007	0.0014	0.0004	0.0349
Nd	4.4700	0.0947	1.1250	0.0026	0.0079	0.0013	0.1490
Sm	2.8600	0.0328	0.4095	0.0036	0.0101	0.0033	0.0302
Eu	1.1630	0.0297	0.2190	0.0027	0.0081	0.0021	0.0070
Gd	4.8600	0.0549	0.6960	0.0074	0.0346	0.0055	0.0312
Tb	0.8920	0.0080	0.1345	0.0014	0.0068	0.0016	0.0048
Dy	6.9800	0.0715	1.1530	0.0178	0.0562	0.0103	0.0353
Ho	1.6710	0.0176	0.2810	0.0041	0.0121	0.0029	0.0073
Er	5.5700	0.0729	0.9940	0.0134	0.0346	0.0099	0.0188
Tm	0.9080	0.0137	0.1680	0.0018	0.0051	0.0014	0.0030
Yb	6.6900	0.0781	1.3150	0.0153	0.0361	0.0097	0.0197
Lu	1.0310	0.0134	0.2090	0.0017	0.0051	0.0010	0.0036
Y/Ho	28.67	46.99	31.92	30.43	32.23	31.12	33.88
Eu/Eu*	1.29	3.23	1.65	2.06	1.59	1.55	0.98

Slab ref.	MSA15-CQ-1_2.1			MSA15-CQ-1_2.	MSA15-CQ-1_2.1							
Sample code	***E34-1**	**E34-2**	**E34-3**	**E35-1**	**E36-1**	**E36-2**	**E36-3**	**E36-4**	**E36-5**	***E36-6**	**E36-7**	**E36-8**
Description	*Carbonaceous ferruginous sed. 2.86 wt% Fe*			*Ferruginous sed.*	*Ferruginous sed. 2.6wt% Fe*							
Element (ppm)												
Al	50.500	831.730	98.230	260.920	202.210	236.900	167.450	439.950	98.340	140.320	466.910	378.990
Si	399366.220	399366.220	399366.220	399846.750	397813.410	397813.380	397813.380	397820.250	397820.250	397820.250	397820.250	397820.280
Ca	214.290	410.090	165.210	207.900	498.600	542.920	381.600	428.450	457.480	442.090	545.440	426.820
Sc	0.831	0.938	0.834	0.575	1.061	1.083	0.995	0.737	0.863	0.907	0.979	0.935
Ti	3.300	1.860	1.210	2.200	4.290	4.000	8.140	9.260	4.930	5.470	3.520	5.100
V	0.112	1.760	0.130	0.033	0.512	0.769	0.384	0.835	0.431	0.394	1.056	1.127
Cr	0.923	9.800	0.612	0.641	2.860	2.250	1.482	1.071	1.007	0.924	2.010	2.700
Mn	86.050	1750.950	87.810	0.343	1447.210	2607.540	1331.010	1285.400	2133.830	1977.810	1957.610	1843.310
Co	6.050	0.627	7.020	0.012	2.970	1.840	5.520	1.840	2.640	6.190	8.300	2.960
Ni	40.520	3.090	43.440	1.269	15.670	6.320	12.440	10.030	9.920	40.310	25.620	36.310
As	503.230	14.660	538.890	1.790	139.710	193.710	456.830	418.810	172.100	4650.020	282.140	268.330
Rb	0.025	1.230	0.023	0.326	0.203	0.349	0.097	0.747	0.047	0.024	0.034	0.065
Sr	2.420	8.870	1.850	0.823	3.510	3.860	2.180	7.110	2.450	9.030	4.810	9.840
Y	0.159	0.128	0.117	0.004	0.199	0.245	0.159	0.175	0.228	0.205	0.188	0.174
Zr	0.088	0.071	0.075	0.131	0.167	0.167	0.208	0.102	0.143	0.118	0.241	0.137
Nb	0.004	0.008	0.003	0.002	0.014	0.033	0.013	0.023	0.016	0.019	0.027	0.011
Cs	0.037	0.241	0.035	0.059	0.046	0.061	0.026	0.089	0.026	0.022	0.024	0.024
Ba	7.520	522.690	6.450	80.190	62.260	87.990	28.150	334.080	12.280	2292.100	561.870	1315.490
Hf	0.002	0.002	0.000	0.003	0.003	0.005	0.003	0.002	0.004	0.003	0.006	0.003
Ta	0.000	0.001	BDL	0.000	0.000	0.000	0.000	0.000	0.001	0.001	0.000	0.000
Pb	5.150	0.222	10.630	0.033	2.850	1.630	2.060	1.520	1.700	6.430	1.590	1.780
Th	0.003	0.005	0.002	0.005	0.011	0.010	0.011	0.005	0.004	0.005	0.008	0.011
U	0.004	0.003	0.003	0.001	0.005	0.004	0.004	0.003	0.004	0.003	0.008	0.004
La	0.1507	2.2100	0.0120	0.4550	1.4550	3.3600	1.1960	2.8500	1.3830	1.5900	3.1700	3.6800
Ce	0.0491	0.0640	0.0268	0.0189	0.1341	0.1135	0.0719	0.0673	0.0811	0.0908	0.0837	0.0779
Pr	0.0121	0.0064	0.0033	0.0005	0.0090	0.0107	0.0090	0.0073	0.0103	0.0106	0.0085	0.0079
Nd	0.0230	0.0385	0.0138	0.0092	0.0440	0.0528	0.0355	0.0363	0.0492	0.0394	0.0347	0.0328
Sm	0.0084	0.0103	0.0056	0.0002	0.1300	0.0254	0.0094	0.0113	0.0139	0.0159	0.0123	0.0115
Eu	0.0091	0.0100	0.0076	0.0004	0.0117	0.0128	0.0087	0.0124	0.0118	0.0171	0.0125	0.0101
Gd	0.0131	0.0182	0.0085	BDL	0.0189	0.0265	0.0170	0.0132	0.0207	0.0191	0.0176	0.0187
Tb	0.0026	0.0024	0.0018	BDL	0.0035	0.0043	0.0028	0.0028	0.0038	0.0037	0.0035	0.0037
Dy	0.0201	0.0182	0.0276	0.0006	0.0280	0.0364	0.0219	0.0228	0.0276	0.0273	0.0275	0.0275
Ho	0.0037	0.0044	0.0031	0.0003	0.0063	0.0083	0.0057	0.0060	0.0081	0.0068	0.0068	0.0064
Er	0.0115	0.0111	0.0116	0.0003	0.0226	0.0297	0.0198	0.0165	0.0294	0.0212	0.0261	0.0182
Tm	0.0019	0.0019	0.0019	0.0000	0.0038	0.0055	0.0037	0.0035	0.0049	0.0040	0.0047	0.0041
Yb	0.0147	0.0190	0.0115	0.0015	0.0339	0.0475	0.0270	0.0236	0.0398	0.0318	0.0434	0.0288
Lu	0.0022	0.0033	0.0021	0.0001	0.0054	0.0077	0.0051	0.0104	0.0055	0.0060	0.0066	0.0046
Y/Ho	42.74	29.22	38.33	13.81	31.54	29.63	27.99	29.02	28.25	30.19	27.53	27.06
Eu/Eu*	3.40	3.52	4.27		0.54	2.08	3.02	3.91	2.89	3.91	3.37	2.73

Slab ref.	MSA15-CQ-1_2.1			MSA15-CQ-1_2.1			MSA15-CQ-1_2.1					
Sample code	**E37-1**	***E37-2**	***E37-3**	***E38-1**	***E38-2**	**E38-3**	**MATRIX-1**	***MATRIX-2**	**MATRIX-3**	**MATRIX-4**	**MATRIX-5**	**MATRIX-6**
Description	*Carbonaceous clastic material*			*Carbonaceous clastic material*								
Element (ppm)												
Al	789.350	12176.630	17081.980	14019.660	3831.280	16510.180	120.170	267.960	8606.380	508.250	324.850	129.100
Si	397502.530	397502.560	397502.560	396450.810	396450.810	396450.780	444067.500	444067.530	444067.500	420695.560	420695.560	420695.560
Ca	366.180	514.320	542.720	535.720	374.130	541.440	290.670	333.950	444.740	426.250	267.010	251.150
Sc	0.795	2.370	2.530	2.480	0.854	2.880	0.740	0.952	1.303	0.888	0.898	0.696
Ti	0.299	581.330	802.210	908.310	177.560	871.550	2.380	2.840	308.160	1.350	3.590	3.820
V	0.036	20.240	28.420	23.700	5.150	29.060	0.014	0.412	11.280	0.514	0.025	0.056
Cr	0.759	115.540	178.070	124.860	80.400	178.090	0.838	1.143	239.840	1.253	0.641	0.780
Mn	0.269	4.320	5.700	17.980	2.010	21.800	1.503	1327.120	4.910	4.940	0.229	191.260
Co	0.006	5.260	12.460	12.630	2.890	5.020	0.022	0.619	9.560	0.092	0.012	0.206
Ni	1.143	70.460	211.520	46.230	11.310	23.260	0.367	5.330	123.080	2.430	0.547	2.370
As	3.220	125.130	413.840	103.730	21.140	39.160	2.220	5.250	245.470	2.620	2.110	3.760
Rb	0.931	21.250	30.180	22.940	5.720	22.720	0.139	0.359	13.280	0.099	0.456	0.163
Sr	1.186	5.090	4.750	11.450	2.860	9.880	1.800	1.092	3.230	1.153	1.810	1.052
Y	0.007	13.600	3.080	4.810	0.388	7.100	0.011	0.123	0.483	0.056	0.007	0.021
Zr	0.108	79.620	13.030	14.300	1.960	35.550	0.113	0.128	3.490	0.560	0.095	1.257
Nb	0.001	1.521	2.170	2.280	0.229	2.240	0.002	0.006	0.350	0.002	0.010	0.005
Cs	0.097	0.615	0.960	0.597	0.201	0.582	0.051	0.048	0.388	0.080	0.104	0.045
Ba	306.610	2432.260	3357.450	2795.670	1111.090	3082.880	30.450	74.830	1859.230	18.160	85.620	40.860
Hf	0.004	2.150	0.358	0.357	0.060	0.990	0.002	0.003	0.108	0.017	0.002	0.001
Ta	0.001	0.164	0.230	0.284	0.022	0.252	BDL	0.000	0.036	0.000	0.000	BDL
Pb	0.035	1.260	1.260	1.740	0.424	1.150	0.045	0.136	0.728	0.058	0.026	0.100
Th	0.003	2.890	1.740	2.190	0.089	3.210	0.007	0.008	0.112	0.007	0.001	0.003
U	0.007	1.320	0.578	0.631	0.080	1.120	0.005	0.005	0.096	0.015	0.002	0.002
La	0.8850	8.8700	4.4200	4.6300	0.9380	2.7200	3.5400	2.8400	0.2990	0.2000	0.4040	3.7500
Ce	0.0045	16.2600	8.0400	8.1700	0.2490	4.8500	0.0332	0.0879	0.4160	0.0124	0.0029	0.0353
Pr	0.0016	1.5300	0.7680	0.7720	0.0297	0.4740	0.0013	0.0064	0.0452	0.0016	0.0014	0.0036
Nd	0.0004	5.2100	2.6300	2.5600	0.1094	1.6700	0.0111	0.0372	0.1420	0.0033	0.0048	0.0143
Sm	0.0095	0.8620	0.3780	0.4250	0.0259	0.3535	BDL	0.0086	0.0413	0.0026	BDL	0.0040
Eu	0.0014	0.3110	0.1070	0.1525	0.0131	0.1585	0.0053	0.0055	0.0187	BDL	0.0017	0.0020
Gd	BDL	1.1750	0.3120	0.4900	0.0356	0.6490	BDL	0.0110	0.0411	0.0043	BDL	0.0034
Tb	BDL	0.2450	0.0513	0.0855	0.0064	0.1340	BDL	0.0022	0.0073	0.0010	0.0001	0.0006
Dy	0.0041	2.0800	0.4500	0.6760	0.0606	1.0310	0.0017	0.0148	0.0618	0.0082	0.0005	0.0038
Ho	0.0001	0.4570	0.1017	0.1470	0.0126	0.2320	0.0003	0.0037	0.0155	0.0013	0.0001	0.0007
Er	0.0006	1.3900	0.3090	0.4300	0.0437	0.7080	0.0019	0.0134	0.0557	0.0051	0.0003	0.0022
Tm	0.0002	0.2020	0.0479	0.0606	0.0053	0.1070	BDL	0.0025	0.0082	0.0007	0.0000	0.0004
Yb	0.0003	1.3890	0.3320	0.4130	0.0437	0.7790	0.0016	0.0181	0.0675	0.0069	0.0010	0.0033
Lu	BDL	0.2130	0.0539	0.0608	0.0060	0.1120	0.0006	0.0031	0.0093	0.0010	0.0001	0.0007
Y/Ho	82.33	29.76	30.29	32.72	30.79	30.60	33.53	33.33	31.16	43.31	58.75	31.18
Eu/Eu*		1.20	1.26	1.39	1.79	1.28		2.25	1.85			2.12

Slab ref.	MSA15-CQ-10_4-2			MSA15-CQ-10_4-2					
Sample code	**E39-1**	***E39-2**	**E39-3**	**E40-1**	**E40-2**	***E40-3**	***E40-4**	***E40-5**	**E40-6**
Description	*Carbonaceous clastic material*			*Carbonaceous ferruginous sed. 1.59wt% Fe*					
Element (ppm)									
Al	520.650	155.450	7274.080	523.020	110.420	830.380	1128.190	892.830	199.920
Si	400128.630	400128.590	400128.560	381161.250	381161.250	381161.250	381167.840	381167.840	381167.840
Ca	373.440	226.680	432.860	397.700	290.410	287.620	217.570	167.260	130.970
Sc	1.216	0.824	0.977	0.847	0.669	0.724	0.773	0.662	0.665
Ti	11.150	5.350	23.000	2.930	2.470	2.630	65.280	38.030	0.623
V	0.891	0.212	9.960	0.410	0.114	0.758	2.090	1.310	0.137
Cr	3.170	1.244	42.850	1.208	0.892	1.653	19.050	10.460	1.100
Mn	32.660	7.060	34.290	16.570	29.930	139.140	0.289	0.185	26.270
Co	14.100	8.290	55.830	7.630	27.380	13.210	0.437	0.479	4.920
Ni	63.850	60.690	118.490	32.390	86.930	39.620	5.300	11.060	22.320
As	486.710	1958.010	756.310	1355.640	568.270	864.780	5.800	11.050	610.700
Rb	0.263	0.225	0.574	0.036	0.050	0.073	1.800	1.570	0.027
Sr	3.590	2.100	5.670	3.410	3.270	3.350	6.120	1.189	2.140
Y	0.483	1.126	0.145	0.299	0.144	0.476	0.233	0.144	0.066
Zr	0.128	0.067	0.312	0.087	0.083	0.063	1.430	1.380	0.041
Nb	0.021	0.006	0.012	0.003	0.005	0.004	0.100	0.053	0.001
Cs	0.141	0.109	0.134	0.061	0.068	0.073	0.137	0.109	0.054
Ba	83.260	58.050	1141.480	21.020	22.640	26.920	317.870	274.040	13.430
Hf	0.004	BDL	0.010	0.003	0.002	0.002	0.032	0.035	BDL
Ta	0.002	BDL	0.002	0.000	0.000	0.001	0.009	0.005	0.000
Pb	22.490	34.390	17.040	7.790	11.710	10.920	0.645	0.175	4.140
Th	0.006	0.004	0.019	0.012	0.007	0.007	0.035	0.022	BDL
U	0.010	0.014	0.017	0.060	0.005	0.006	0.047	0.046	BDL
La	0.8670	0.5560	0.0340	1.1280	0.7990	0.0374	3.1500	2.8400	0.0626
Ce	0.0671	0.0334	0.0877	1.5200	0.0476	0.0485	0.1700	0.0226	0.0179
Pr	0.0096	0.0067	0.0097	0.1960	0.0066	0.0048	0.0221	0.0024	0.0024
Nd	0.0518	0.0403	0.0387	0.9040	0.0337	0.0224	0.0871	0.0131	0.0103
Sm	0.0240	0.0247	0.0133	0.1960	0.0092	0.0119	0.0245	0.0045	0.0038
Eu	0.0207	0.0225	0.0080	0.0722	0.0076	0.0127	0.0109	0.0027	0.0033
Gd	0.0479	0.0660	0.0160	0.1690	0.0118	0.0229	0.0314	0.0091	0.0032
Tb	0.0080	0.0144	0.0022	0.0165	0.0025	0.0051	0.0049	0.0026	0.0011
Dy	0.0590	0.1057	0.0174	0.0719	0.0169	0.0430	0.0319	0.0172	0.0067
Ho	0.0133	0.0254	0.0038	0.0100	0.0045	0.0115	0.0077	0.0046	0.0017
Er	0.0377	0.0752	0.0129	0.0247	0.0154	0.0359	0.0200	0.0159	0.0056
Tm	0.0060	0.0111	0.0015	0.0029	0.0017	0.0051	0.0033	0.0023	0.0009
Yb	0.0357	0.0704	0.0130	0.0157	0.0131	0.0328	0.0245	0.0198	0.0048
Lu	0.0061	0.0119	0.0019	0.0017	0.0016	0.0043	0.0038	0.0038	0.0006
Y/Ho	36.32	44.33	38.59	30.02	32.03	41.54	30.14	31.10	38.16
Eu/Eu*	2.62	1.99	2.50	1.87	2.78	2.82	1.73	1.34	2.78

Slab ref.	MSA15-CQ-10_4-2			MSA15-CQ-10_4-2					
Sample code	***E41-1**	**E41-2**	***E41-3**	**E42-1**	**E42-2**	**E42-3**	**E42-4**	**E42-5**	**E42-6**
Description	*Inclusion rich clastic material*			*Fractured jaspilitic sed.*					
Element (ppm)									
Al	43680.870	101061.580	17586.700	147.050	74.160	76.360	456.330	53.000	272.150
Si	376077.440	376077.440	376077.410	387430.560	387430.530	387430.560	387437.630	387437.630	387437.630
Ca	853.390	1370.580	564.680	404.810	340.520	264.560	180.390	278.810	212.580
Sc	6.160	6.150	1.191	0.727	0.614	0.596	0.614	0.686	0.706
Ti	2013.960	1948.500	387.140	10.860	5.660	6.790	5.310	2.130	1.320
V	101.520	82.760	21.020	0.109	0.056	0.066	0.048	0.041	0.146
Cr	543.450	496.750	132.410	1.326	0.987	1.021	0.629	0.687	0.594
Mn	81.410	81.460	10.170	5.840	3.510	3.690	3.040	4.360	6.490
Co	3.390	9.820	47.990	0.249	0.867	0.640	0.115	0.125	0.155
Ni	134.410	536.680	180.150	4.350	5.720	3.870	3.710	5.240	2.810
As	9.620	15.520	172.530	7.100	12.160	8.110	5.300	4.390	6.250
Rb	29.030	25.920	6.820	0.091	0.048	0.049	0.465	0.021	0.034
Sr	26.800	80.450	3.630	3.740	3.230	3.210	3.500	3.280	3.340
Y	5.730	11.730	0.751	0.127	0.121	0.101	0.074	0.086	0.117
Zr	44.400	82.530	5.390	0.145	1.026	0.058	0.069	0.095	0.092
Nb	3.720	3.470	0.844	0.003	0.006	0.002	0.004	0.004	0.002
Cs	0.921	1.420	0.307	0.075	0.055	0.049	0.092	0.052	0.064
Ba	10763.740	57203.600	18342.130	34.820	26.010	24.640	243.520	13.250	17.560
Hf	1.120	2.210	0.142	0.004	0.002	0.001	0.002	BDL	BDL
Ta	0.336	0.371	0.071	0.000	BDL	BDL	0.001	BDL	0.000
Pb	0.920	2.010	9.330	0.395	0.337	0.222	0.220	BDL	0.215
Th	1.450	2.550	0.194	0.011	0.001	0.025	0.001	BDL	0.001
U	1.200	2.390	0.167	0.003	0.004	0.003	0.002	BDL	0.003
La	2.4500	2.9500	1.2710	6.5200	1.1920	1.1750	0.1380	0.4580	1.9100
Ce	4.4600	5.9900	0.3980	0.3010	0.1145	0.0834	0.0944	0.0483	0.0878
Pr	0.4540	0.5910	0.0451	0.0296	0.0155	0.0089	0.0103	0.0057	0.0132
Nd	1.7200	2.1400	0.1480	0.1168	0.0590	0.0401	0.0476	0.0238	0.0496
Sm	0.5585	0.5750	0.0392	0.0263	0.0146	0.0097	0.0129	0.0061	0.0132
Eu	0.2595	0.3290	0.0410	0.0116	0.0072	0.0069	0.0092	0.0069	0.0077
Gd	0.7670	1.0160	0.0761	0.0230	0.0144	0.0160	0.0088	0.0125	0.0180
Tb	0.1101	0.1940	0.0144	0.0033	0.0033	0.0022	0.0016	0.0018	0.0019
Dy	0.8290	1.6100	0.1071	0.0198	0.0163	0.0131	0.0106	0.0126	0.0185
Ho	0.1890	0.3700	0.0236	0.0041	0.0038	0.0024	0.0015	0.0026	0.0041
Er	0.5960	1.2010	0.0813	0.0123	0.0123	0.0085	0.0078	0.0070	0.0100
Tm	0.0942	0.1960	0.0146	0.0022	0.0013	0.0012	0.0011	0.0006	0.0017
Yb	0.6940	1.4500	0.0897	0.0114	0.0119	0.0131	0.0090	0.0081	0.0116
Lu	0.1020	0.2230	0.0142	0.0019	0.0041	0.0016	0.0011	0.0011	0.0016
Y/Ho	30.32	31.70	31.82	30.72	31.82	42.31	50.97	32.42	28.49
Eu/Eu*	1.81	1.74	3.03	2.01	1.83	2.61	3.28	3.67	2.56

Slab ref.	MSA15-CQ-10_4-2						MSA15-CQ-10_4-2			
Sample code	**E43-1**	**E43-2**	**E43-3**	**E43-4**	***E43-5**	**E43-6**	**E44-1**	**E44-2**	**E44-3**	**E44-4**
Description	*Ferruginous sed. 1.59wt% Fe*						*Jaspelitic lam.*	*Jaspelitic lam.*	*Grey lam.*	*Grey lam.*
Element (ppm)										
Al	286.810	305.440	49.630	1857.360	341.820	1235.780	323.010	262.330	BDL	BDL
Si	400762.410	400762.410	400762.410	400769.720	400769.750	400769.750	399333.470	399333.470	399333.470	399333.470
Ca	330.220	278.070	256.740	394.760	250.490	292.700	BDL	BDL	BDL	BDL
Sc	0.897	0.781	0.857	1.165	0.971	0.936	1.690	1.680	1.054	1.040
Ti	0.926	4.140	1.530	2.010	1.010	1.450	BDL	BDL	BDL	BDL
V	0.251	0.193	0.062	1.017	0.174	0.522	0.301	0.165	BDL	BDL
Cr	0.889	0.746	0.750	1.810	1.041	5.350	BDL	BDL	BDL	BDL
Mn	969.140	419.510	554.970	1935.160	1056.670	1332.020	68.020	105.860	BDL	BDL
Co	4.020	0.663	2.220	3.390	0.940	4.190	2.990	9.700	0.519	0.033
Ni	28.920	4.510	22.620	31.940	9.060	37.480	55.670	143.620	BDL	BDL
As	208.560	70.330	5069.530	185.530	171.120	242.890	310.290	793.140	97.740	16.780
Rb	0.053	0.562	0.008	1.071	0.036	0.031	BDL	BDL	BDL	BDL
Sr	3.840	3.890	3.510	4.840	4.230	3.550	7.470	9.110	BDL	BDL
Y	0.110	0.548	0.089	0.208	0.246	0.125	0.185	BDL	BDL	0.404
Zr	0.022	0.061	0.039	0.101	0.040	0.057	BDL	BDL	BDL	BDL
Nb	0.006	0.002	0.001	0.006	0.004	0.005	BDL	BDL	BDL	BDL
Cs	0.071	0.103	0.061	0.129	0.078	0.070	0.263	0.226	0.031	0.032
Ba	30.120	110.060	23.270	235.320	28.220	21.210	1.400	11.820	BDL	BDL
Hf	0.001	0.002	0.001	BDL	0.001	BDL	BDL	BDL	BDL	BDL
Ta	0.000	BDL	0.000	BDL	BDL	BDL	BDL	BDL	BDL	BDL
Pb	4.940	0.516	3.080	2.200	0.727	3.890	1.320	3.560	BDL	BDL
Th	0.002	0.003	0.002	BDL	0.002	BDL	BDL	BDL	BDL	BDL
U	0.005	0.029	0.009	0.015	0.003	BDL	BDL	BDL	BDL	BDL
La	0.1131	2.6600	0.0340	1.9200	1.8800	1.4400	BDL	BDL	BDL	BDL
Ce	0.0460	0.0283	0.0314	0.0673	0.0362	0.0318	BDL	0.3060	BDL	BDL
Pr	0.0064	0.0052	0.0045	0.0104	0.0063	0.0044	BDL	BDL	BDL	BDL
Nd	0.0316	0.0256	0.0261	0.0442	0.0339	0.0236	BDL	BDL	BDL	BDL
Sm	0.0119	0.0145	0.0092	0.0215	0.0114	0.0075	0.0130	0.0568	BDL	BDL
Eu	0.0079	0.0119	0.0066	0.0141	0.0070	0.0074	0.0115	0.0290	BDL	0.0065
Gd	0.0137	0.0426	0.0117	0.0273	0.0208	0.0141	0.0238	0.0563	BDL	0.0176
Tb	0.0024	0.0080	0.0017	0.0042	0.0036	0.0020	0.0037	0.0086	BDL	0.0026
Dy	0.0184	0.1219	0.0124	0.0277	0.0232	0.0184	0.0155	0.0561	BDL	0.0301
Ho	0.0044	0.0164	0.0025	0.0055	0.0068	0.0039	0.0027	0.0180	BDL	0.0078
Er	0.0104	0.0440	0.0078	0.0189	0.0190	0.0111	0.0100	0.0459	BDL	0.0254
Tm	0.0016	0.0054	0.0009	0.0024	0.0023	0.0021	0.0011	0.0059	BDL	0.0036
Yb	0.0138	0.0306	0.0076	0.0219	0.0174	0.0144	0.0122	0.0322	BDL	0.0066
Lu	0.0016	0.0060	0.0011	0.0040	0.0033	0.0023	BDL	0.0092	BDL	0.0026
Y/Ho	25.07	33.41	35.30	37.61	36.44	32.24	69.55			51.79
Eu/Eu*	2.54	1.86	2.91	2.57	1.93	3.43	2.93	2.20		4.72

Slab ref.	MSA15-CQ-10_4-2		MSA15-CQ-10_6.1			MSA15-CQ-10_6.1		
Sample code	**MATRIX-1**	**MATRIX-2**	***E45-1**	**E45-2**	**E45-3**	**E46-1**	***E46-2**	**E46-3**
Description			*Carbonaceous ferruginous sed. 5.83wt% Fe*			*Carbonaceous ferruginous sed. 11.29wt% Fe*		
Element (ppm)								
Al	263.600	138.540	584.490	346.030	541.740	318.420	749.220	283.210
Si	444067.340	444067.340	400672.220	400672.220	400672.220	392062.310	392062.310	392062.310
Ca	413.710	270.060	338.910	306.520	355.120	464.130	541.750	270.610
Sc	0.739	0.637	1.232	1.214	1.112	0.787	1.076	0.712
Ti	1.200	6.070	7.990	5.570	8.910	9.830	5.460	3.500
V	0.069	0.089	1.828	1.281	1.980	0.632	1.226	0.445
Cr	1.041	0.862	8.250	3.040	1.882	1.024	1.430	0.832
Mn	0.410	0.573	79.360	76.330	122.940	219.520	230.040	62.910
Co	0.433	0.032	2.810	4.100	4.470	8.100	8.350	3.280
Ni	4.290	3.640	23.900	43.940	35.480	97.480	96.740	44.550
As	5.040	2.050	50.720	52.770	92.250	1663.270	673.850	833.730
Rb	0.307	0.098	0.077	0.067	0.083	0.047	0.064	0.099
Sr	1.233	1.012	12.110	7.850	11.990	16.190	19.380	11.130
Y	0.054	0.044	1.162	1.930	2.160	16.800	1.240	0.186
Zr	0.275	0.154	0.278	0.326	0.291	0.430	0.266	0.264
Nb	0.005	0.003	0.041	0.033	0.052	0.045	0.031	0.030
Cs	0.074	0.046	0.369	0.269	0.235	0.284	0.303	0.209
Ba	68.750	33.700	57.520	44.280	72.530	50.760	65.420	48.230
Hf	0.007	0.006	0.007	0.004	0.007	0.004	0.004	0.004
Ta	0.001	0.002	0.003	0.002	0.004	0.001	0.001	0.000
Pb	0.061	0.140	1.750	1.130	1.680	15.860	13.300	7.290
Th	0.009	0.002	0.016	0.016	0.025	0.010	0.007	0.008
U	0.021	0.002	0.013	0.026	0.022	0.023	0.024	0.006
La	2.1900	4.5300	0.0972	0.3390	0.1932	0.0816	0.1540	0.0768
Ce	0.0104	0.0138	0.1538	0.3070	0.3280	0.2140	0.4080	0.1880
Pr	0.0007	0.0015	0.0200	0.0372	0.0410	0.0328	0.0583	0.0230
Nd	0.0030	0.0037	0.0917	0.1890	0.1940	0.2100	0.3240	0.1000
Sm	0.0018	0.0005	0.0379	0.0731	0.0796	0.2505	0.1015	0.0305
Eu	0.0013	BDL	0.0321	0.0602	0.0723	0.2210	0.0472	0.0144
Gd	BDL	BDL	0.0993	0.1670	0.2110	0.9190	0.1530	0.0247
Tb	BDL	BDL	0.0173	0.0310	0.0380	0.2030	0.0213	0.0043
Dy	0.0071	0.0009	0.1418	0.2430	0.3020	1.7800	0.1380	0.0274
Ho	0.0010	BDL	0.0316	0.0537	0.0636	0.4410	0.0316	0.0058
Er	0.0048	0.0002	0.0924	0.1640	0.1780	1.5200	0.0886	0.0195
Tm	0.0005	0.0001	0.0128	0.0219	0.0220	0.2410	0.0131	0.0035
Yb	0.0068	BDL	0.0855	0.1482	0.1422	1.7500	0.0745	0.0203
Lu	0.0011	0.0004	0.0150	0.0219	0.0204	0.2360	0.0107	0.0027
Y/Ho	51.83		36.77	35.94	33.96	38.10	39.24	32.29
Eu/Eu*	4.86	0.00	2.16	2.20	2.25	1.53	1.77	2.08

Slab ref.	MSA15-CQ-10_6.1			MSA15-CQ-1	MSA15-CQ-10_6.1			
Sample code	**E47-1**	***E47-2**	**E47-3**	**E50-1**	***E51-1**	***E51-2**	***E51-3**	***E51-4**
Description	*Carbonaceous ferruginous/jaspilitic sed. 3.765 wt% Fe*			*Translucent ci*	*Clastic material*			
Element (ppm)								
Al	380.810	61.320	73.150	24.450	282.510	1594.960	693.610	1320.360
Si	401126.590	401126.630	401126.590	393498.000	399513.410	399513.410	399513.410	399513.440
Ca	259.830	184.060	352.060	166.690	457.000	413.920	369.150	279.070
Sc	1.163	0.887	1.005	0.782	1.184	1.095	1.071	0.997
Ti	7.020	1.293	2.800	1.610	1.740	2.290	5.830	1.175
V	0.386	0.071	0.055	0.008	0.153	0.617	0.295	0.640
Cr	1.303	16.480	0.730	0.629	55.290	0.938	1.890	1.213
Mn	47.520	16.860	27.190	0.361	18.840	16.280	28.180	97.320
Co	1.550	0.941	1.468	0.217	0.107	0.055	0.095	0.104
Ni	6.320	4.870	5.830	4.200	1.960	6.770	4.970	6.240
As	11.810	7.920	12.380	162.610	9.200	3.510	3.650	5.380
Rb	0.041	0.028	0.031	0.027	0.055	0.018	0.032	0.024
Sr	12.250	4.440	4.340	1.579	2.620	2.910	2.660	2.410
Y	0.382	0.085	0.080	0.008	0.125	0.071	0.115	0.162
Zr	0.172	0.024	0.038	0.034	0.045	0.024	0.089	0.024
Nb	0.021	0.006	0.008	0.002	0.002	0.002	0.002	0.002
Cs	0.098	0.078	0.083	0.029	0.064	0.066	0.069	0.065
Ba	59.280	22.360	16.660	9.980	16.430	17.520	16.960	18.470
Hf	0.004	0.001	0.001	0.001	0.001	0.001	0.002	0.001
Ta	0.001	BDL	0.000	0.000	0.000	0.000	0.000	0.001
Pb	0.350	0.278	0.806	0.139	0.139	0.128	0.146	0.111
Th	0.007	0.001	0.002	0.002	0.001	0.006	0.002	0.001
U	0.021	0.006	0.006	0.001	0.002	0.011	0.003	0.001
La	0.0774	0.0258	3.9000	5.2100	0.0207	0.2650	0.0122	0.3110
Ce	0.1260	0.0484	0.0502	0.0316	0.0241	0.4540	0.0303	0.0166
Pr	0.0158	0.0057	0.0051	0.0036	0.0053	0.0579	0.0036	0.0030
Nd	0.0653	0.0240	0.0302	0.0116	0.0140	0.2710	0.0159	0.0118
Sm	0.0203	0.0082	0.0067	0.0012	0.0062	0.0620	0.0069	0.0051
Eu	0.0149	0.0075	0.0069	BDL	0.0048	0.0255	0.0048	0.0044
Gd	0.0385	0.0075	0.0110	0.0005	0.0088	0.0484	0.0070	0.0080
Tb	0.0061	0.0021	0.0013	0.0002	0.0025	0.0044	0.0022	0.0019
Dy	0.0460	0.0129	0.0130	0.0011	0.0143	0.0199	0.0116	0.0146
Ho	0.0101	0.0026	0.0021	0.0002	0.0031	0.0038	0.0028	0.0041
Er	0.0336	0.0070	0.0087	0.0009	0.0083	0.0068	0.0080	0.0119
Tm	0.0054	0.0008	0.0010	0.0002	0.0012	0.0008	0.0012	0.0023
Yb	0.0399	0.0100	0.0119	0.0011	0.0113	0.0041	0.0097	0.0136
Lu	0.0071	0.0018	0.0021	0.0001	0.0013	0.0006	0.0017	0.0028
Y/Ho	37.75	32.60	38.83	39.60	1.40	2.10	2.03	0.70
Eu/Eu*	2.37	3.19	4.06	0.00	2.13	2.17	2.15	2.49

Slab ref.	MSA15-CQ-10_6.1				
Sample code	**MATRIX-1**	**MATRIX-2**	***MATRIX-3**	**MATRIX-4**	**MATRIX-5**
Description					
Element (ppm)					
Al	143.130	302.940	220.280	59.740	139.580
Si	444067.440	444067.470	444067.470	444067.470	420695.560
Ca	325.390	221.170	249.860	234.160	117.710
Sc	0.957	0.911	0.866	0.853	0.591
Ti	1.810	1.600	21.280	3.720	9.800
V	BDL	0.009	0.416	0.014	0.014
Cr	0.721	1.129	1.484	0.816	0.677
Mn	0.568	1.095	0.273	0.525	0.159
Co	0.005	0.015	0.871	0.027	0.005
Ni	1.700	2.690	6.930	2.090	2.130
As	1.460	3.100	10.810	2.070	1.660
Rb	0.101	0.040	0.308	0.077	0.054
Sr	0.939	1.172	1.232	4.090	1.006
Y	0.003	0.002	0.154	0.010	BDL
Zr	0.037	0.070	0.252	0.083	0.014
Nb	0.001	0.004	0.031	0.004	BDL
Cs	0.059	0.061	0.060	0.077	0.049
Ba	176.480	526.250	125.090	31.600	268.140
Hf	0.004	0.004	0.009	0.002	0.001
Ta	0.000	0.000	0.005	0.000	BDL
Pb	0.053	0.052	0.068	0.037	0.052
Th	0.002	0.000	0.016	0.001	0.001
U	0.001	0.003	0.028	0.014	0.000
La	3.9500	1.6090	0.2790	0.0909	3.1700
Ce	0.0071	0.0053	0.0717	0.0074	0.0026
Pr	0.0004	0.0004	0.0102	0.0007	0.0038
Nd	0.0097	0.0004	0.0353	0.0035	0.0012
Sm	0.0005	0.0007	0.0115	0.0005	0.0002
Eu	0.0016	0.0029	0.0055	0.0011	0.0015
Gd	0.0005	BDL	0.0152	BDL	BDL
Tb	0.0011	0.0001	0.0027	BDL	BDL
Dy	0.0002	BDL	0.0205	0.0012	0.0005
Ho	0.0001	0.0042	0.0046	0.0005	0.0000
Er	0.0001	0.0001	0.0139	0.0012	BDL
Tm	BDL	BDL	0.0024	0.0001	BDL
Yb	BDL	BDL	0.0139	0.0011	BDL
Lu	BDL	BDL	0.0025	0.0002	BDL
Y/Ho	50.60	0.44	33.77	21.91	
Eu/Eu*	2.52	19.90	1.76	14.60	45.16

APPENDIX C

Individual LA-ICP-MS analyses for the chert and silica veins

BDL = below detection limit

* = measurements used for REE+Y and trace element profiles in the main text

UiB = measurements taken in the University of Bergen

Location	Puddingstone Hill						Puddingstone Hill
Sample code	***19-PS-04-1**	**19-PS-04-2**	**19-PS-04-3**	**19-PS-04-4**	**19-PS-04-5**	**19-PS-04-6**	***19-PS-01-1**
Description	*Grey/green chert close to barite*						*Black chert vein*
Element (ppm)							
Al	5237.020	9309.880	5905.270	9171.730	17947.560	7426.970	15881.380
Si	444067.470	444067.440	444067.470	444067.440	444067.440	444067.440	462526.630
Ca	317.920	493.750	584.660	3239.050	351.500	300.050	761.560
Sc	5.710	7.630	5.970	3.830	3.860	4.140	3.750
Ti	168.600	915.390	531.380	432.670	118.440	431.900	792.670
V	16.200	50.220	23.710	7.530	8.960	15.030	27.410
Cr	164.820	507.760	222.840	82.460	88.870	196.950	132.470
Mn	2.000	1.620	2.670	2.310	0.908	0.953	2.390
Co	27.760	47.520	20.100	10.600	14.930	19.350	2.010
Ni	155.090	372.460	126.620	62.320	32.240	77.420	9.600
As	97.440	121.470	81.390	52.600	35.110	68.300	48.260
Rb	8.220	16.150	10.250	2.630	17.010	5.360	25.490
Sr	9.610	13.010	13.160	2720.090	24.030	5.540	4.480
Y	0.664	0.946	0.752	0.352	0.159	0.483	1.680
Zr	4.830	7.060	5.510	1.580	0.937	4.090	8.300
Nb	0.181	2.680	0.815	0.561	0.159	0.562	1.007
Cs	0.316	0.510	0.374	0.289	0.246	0.284	0.488
Ba	1298.2600	4607.880	1979.160	372886.060	29093.900	11761.590	3559.480
Hf	0.131	0.192	0.159	0.117	0.031	0.098	0.201
Ta	0.029	0.231	0.088	0.061	0.032	0.056	0.077
Pb	0.916	0.584	0.767	0.578	1.640	1.014	0.846
Th	0.459	0.405	0.627	0.177	0.057	0.599	0.575
U	0.214	0.373	0.216	0.198	0.040	0.167	0.369
La	1.9400	2.4900	13.9600	10.4900	9.4400	1.7800	1.7200
Ce	2.1700	1.4430	3.3400	1.2150	0.1680	1.5610	2.4800
Pr	0.2180	0.1493	0.3360	0.1770	0.0244	0.1618	0.2970
Nd	0.8140	0.5150	1.2520	0.2600	0.0577	0.5980	1.1750
Sm	0.1325	0.1281	0.1910	0.0931	0.0168	0.1043	0.2505
Eu	0.0434	0.0737	0.0654	1.2690	0.0959	0.0671	0.1058
Gd	0.1220	0.1670	0.1650	0.1120	0.0294	0.0695	0.2220
Tb	0.0185	0.0240	0.0203	0.0072	0.0015	0.0107	0.0394
Dy	0.1107	0.1560	0.1370	0.0513	0.0179	0.0759	0.2630
Ho	0.0272	0.0349	0.0273	0.0095	0.0046	0.0185	0.0629
Er	0.0837	0.1094	0.0908	0.0336	0.0156	0.0533	0.1880
Tm	0.0148	0.0178	0.0146	0.0083	0.0025	0.0077	0.0293
Yb	0.0948	0.1264	0.0988	0.0372	0.0167	0.0680	0.2250
Lu	0.0171	0.0196	0.0166	0.0075	0.0036	0.0131	0.0368
Y/Ho	24.41	27.11	27.55	37.05	34.79	26.11	26.71
Eu/Eu*	1.45	2.29	1.64	70.49	28.48	3.11	1.79

Location	Barite Valley										
Sample code	**18-BV-26-1**	**18-BV-26-2**	**18-BV-26-3**	**18-BV-26-4**	**18-BV-26-5**	**18-BV-26-6**	**18-BV-26-7**	**18-BV-26-8**	**18-BV-26-9**	**18-BV-26-10**	**18-BV-26-11**
Description	*Green/white chert close to barite*										
Element (ppm)											
Al	672.960	2501.080	340.530	904.420	685.960	906.620	808.330	461.570	522.920	294.030	239.930
Si	443973.970	443974.000	443973.970	443974.000	443974.000	443973.970	443973.970	443973.970	443974.000	443974.000	443974.000
Ca	228.980	1155.620	117.610	202.000	271.190	217.380	584.280	430.190	413.950	312.090	277.900
Sc	3.000	2.680	2.760	2.650	2.400	2.220	1.582	1.810	1.510	1.520	1.580
Ti	8.500	10.290	1.600	3.160	2.670	3.880	24.970	BDL	0.410	BDL	BDL
V	0.117	0.231	0.152	0.116	0.104	0.139	1.181	0.298	0.379	0.170	0.178
Cr	1.449	1.480	0.920	1.152	6.110	1.479	6.580	0.742	0.608	0.456	0.352
Mn	1.420	0.458	0.194	0.347	0.233	0.524	0.204	0.160	0.121	0.095	0.083
Co	0.089	0.028	0.011	0.094	0.047	0.131	0.226	BDL	BDL	BDL	BDL
Ni	BDL	356.600	BDL	BDL	BDL	BDL	0.730	0.630	BDL	BDL	BDL
As	0.799	2.870	0.502	0.687	0.806	0.904	2.760	0.422	0.448	0.342	0.420
Rb	0.953	0.316	0.574	1.278	0.943	1.223	1.127	1.027	0.961	0.725	0.778
Sr	2.920	1182.240	3.380	3.390	3.750	3.430	6.470	1.800	1.930	1.640	1.990
Y	0.002	0.098	0.002	0.005	0.002	0.007	0.061	0.002	BDL	BDL	0.002
Zr	0.025	0.067	0.015	0.480	0.014	0.230	1.044	BDL	BDL	BDL	BDL
Nb	0.003	0.001	BDL	0.012	0.002	0.003	0.021	BDL	BDL	BDL	BDL
Cs	0.087	0.183	0.078	0.095	0.099	0.093	0.102	0.095	0.089	0.092	0.091
Ba	321.500	260336.360	337.520	326.330	237.670	565.930	434.470	185.180	166.880	135.820	147.680
Hf	BDL	0.044	BDL	0.004	0.003	0.008	0.019	0.002	0.007	BDL	BDL
Ta	BDL	0.001	BDL	0.001	BDL	BDL	0.004	0.001	0.001	BDL	0.001
Pb	BDL	2.260	BDL	0.010	0.022	0.022	0.207	0.029	BDL	BDL	BDL
Th	BDL	0.101	BDL	BDL	0.001	BDL	0.013	BDL	BDL	BDL	BDL
U	0.003	0.005	BDL	0.017	0.002	0.006	0.130	0.004	0.003	0.001	0.001
La	7.3100	28.2700	3.5500	19.7900	7.0200	9.5600	7.7100	BDL	3.3400	0.0819	BDL
Ce	0.0189	0.4390	BDL	0.0074	0.0025	0.0405	BDL	BDL	BDL	BDL	BDL
Pr	0.0027	0.0807	BDL	0.0418	0.0010	0.0025	BDL	BDL	BDL	BDL	BDL
Nd	0.0052	0.0509	BDL	BDL	BDL	0.0047	BDL	BDL	BDL	BDL	BDL
Sm	BDL	0.0187	0.0025	BDL	0.0008	BDL	0.0066	BDL	BDL	0.0003	BDL
Eu	BDL	0.7900	BDL	BDL	BDL	BDL	0.0042	BDL	0.0499	0.0031	0.0045
Gd	0.0074	0.0589	BDL	BDL	BDL	BDL	0.0044	BDL	0.0025	BDL	0.0027
Tb	0.0004	0.0017	BDL	BDL	BDL	0.0005	BDL	0.0004	0.0024	BDL	BDL
Dy	BDL	0.0044	BDL	BDL	BDL	0.0005	0.0066	0.0002	0.0022	BDL	BDL
Ho	BDL	0.0003	BDL	BDL	BDL	0.0003	0.0018	BDL	0.0070	BDL	BDL
Er	BDL	0.0039	BDL	BDL	BDL	0.0003	0.0081	BDL	0.0186	BDL	BDL
Tm	BDL	0.0027	BDL	BDL	0.0002	BDL	0.0015	BDL	0.0003	BDL	BDL
Yb	BDL	0.0038	BDL	BDL	BDL	BDL	0.0073	BDL	BDL	BDL	BDL
Lu	0.0006	0.0008	BDL	BDL	BDL	BDL	0.0012	0.0003	0.0011	BDL	BDL
Y/Ho		350.71				20.00	34.29				
Eu/Eu*		210.74									

Location	Barite Valley					
Sample code	**18-BV-15-1**	***18-BV-15-2**	***18-BV-15-3**	**18-BV-15-4**	***18-BV-15-5**	***18-BV-15-6**
Description	*Middle part main chert vein*					
Element (ppm)						
Al	80348.230	47417.050	17659.040	24179.960	181573.470	18376.960
Si	443973.970	443973.970	443973.940	443973.970	443974.000	443973.970
Ca	1593.780	1096.760	905.140	836.790	2599.970	876.410
Sc	9.060	5.910	4.600	5.230	14.120	4.270
Ti	803.720	1139.840	767.820	4844.310	749.040	838.170
V	135.900	62.550	26.650	43.910	231.550	33.120
Cr	2012.790	354.630	145.700	244.380	1116.630	278.480
Mn	1.610	1.720	0.807	0.692	4.640	0.626
Co	0.416	0.279	0.291	1.980	0.224	0.205
Ni	8.190	6.790	5.620	4.700	13.440	1.900
As	2.750	2.100	2.790	5.190	1.680	1.420
Rb	84.230	49.230	18.760	27.570	183.880	20.810
Sr	88.520	53.260	21.310	30.330	213.180	24.280
Y	1.670	4.040	4.470	22.470	3.240	4.860
Zr	7.670	13.380	17.890	18.640	14.460	15.940
Nb	0.715	1.640	1.214	6.020	0.417	1.162
Cs	2.220	1.519	0.579	0.884	4.520	0.656
Ba	28866.720	13910.710	5866.460	8058.480	59451.040	6034.870
Hf	0.257	0.457	0.407	0.530	0.864	0.487
Ta	0.076	0.151	0.254	0.398	0.106	0.097
Pb	0.419	1.080	0.741	3.330	1.022	0.558
Th	0.473	0.580	0.716	0.946	0.798	1.149
U	0.316	0.456	0.587	0.982	0.449	0.580
La	1.0290	1.8100	1.3260	5.8300	1.0290	3.9500
Ce	1.8700	1.9600	2.4500	4.9600	1.6400	5.3400
Pr	0.2120	0.2430	0.2900	0.8380	0.1990	0.6070
Nd	0.5820	0.9530	1.2390	4.3600	0.7050	2.4800
Sm	0.1545	0.2560	0.3325	1.2860	0.1545	0.4890
Eu	0.1002	0.1112	0.1086	0.4475	0.1750	0.1509
Gd	0.1240	0.3500	0.4460	2.6300	0.2170	0.5290
Tb	0.0207	0.0561	0.0738	0.4010	0.0386	0.0776
Dy	0.1450	0.4370	0.5530	2.6200	0.3500	0.5930
Ho	0.0353	0.0798	0.1201	0.5980	0.0903	0.1345
Er	0.0990	0.3660	0.4080	2.0900	0.2820	0.4450
Tm	0.0161	0.0554	0.0593	0.2220	0.0485	0.0695
Yb	0.1420	0.4300	0.4130	1.4600	0.3490	0.4480
Lu	0.0211	0.0569	0.0600	0.2410	0.0464	0.0667
Y/Ho	47.31	50.63	37.22	37.58	35.88	36.13
Eu/Eu*	2.91	1.62	1.21	1.10	3.99	1.31

Location	Barite Valley						Barite Valley				
Sample code	***18-BV-13-1**	***18-BV-13-2**	**18-BV-13-3**	***18-BV-13-4**	**18-BV-13-5**	**18-BV-13-6**	**18-BV-18-1**	***18-BV-18-2**	**18-BV-18-3**	**18-BV-18-4**	**18-BV-18-5**
Description	*Upper part main chert vein*						*Lower part main chert vein*				
Element (ppm)											
Al	26530.720	8328.250	1033.210	9014.380	3477.530	39144.890	27268.320	20770.350	39242.360	27019.220	25888.780
Si	443974.000	443973.970	443973.970	443973.970	443973.970	443974.000	443974.000	443974.000	443973.970	443973.970	443974.000
Ca	857.140	715.500	551.620	833.130	588.420	1006.590	1083.220	887.310	958.520	1055.400	989.810
Sc	3.850	2.940	1.870	2.580	2.140	10.480	4.750	3.430	5.010	3.870	3.790
Ti	1310.480	767.630	4.270	360.740	10.660	1853.000	960.910	876.660	2226.860	815.620	1236.430
V	31.110	13.910	1.830	17.940	4.560	58.470	43.890	37.480	67.350	63.480	46.540
Cr	173.540	91.320	8.470	106.150	22.510	395.660	274.110	211.790	508.210	380.810	276.760
Mn	0.633	0.785	BDL	0.913	BDL	2.920	2.360	0.923	2.550	1.680	2.380
Co	2.050	3.240	0.116	0.431	1.193	0.514	0.258	0.540	0.352	0.332	1.470
Ni	8.650	10.050	1.720	6.430	6.400	6.320	5.610	4.920	5.090	3.750	17.520
As	7.630	4.940	3.550	1.570	23.050	5.810	66.690	7.280	18.130	8.740	23.860
Rb	29.320	10.510	1.181	12.720	4.170	40.340	29.610	21.390	40.730	31.880	32.320
Sr	35.370	15.180	3.970	12.480	6.080	64.560	33.960	21.160	40.610	25.190	25.340
Y	2.560	1.720	BDL	0.600	0.081	35.790	26.440	1.620	9.080	1.290	2.730
Zr	10.080	9.170	0.608	3.890	1.156	609.530	7.590	8.030	11.360	8.610	12.990
Nb	2.100	1.379	0.011	0.499	0.008	3.140	1.113	1.134	8.530	0.829	1.550
Cs	1.232	0.432	0.224	0.570	0.283	1.900	0.862	0.879	1.220	0.946	1.392
Ba	7192.130	2391.060	189.150	1832.140	733.460	19714.750	9166.080	7132.920	13379.720	8078.860	7880.630
Hf	0.315	0.239	0.006	0.117	0.036	15.010	0.241	0.250	0.379	0.284	0.384
Ta	0.150	0.138	0.002	0.051	0.006	0.243	0.093	0.104	0.603	0.071	0.132
Pb	0.606	0.691	0.055	0.257	0.144	1.410	1.970	0.122	0.546	0.259	0.360
Th	1.173	1.920	BDL	0.415	0.072	4.620	1.480	0.593	1.700	0.793	0.962
U	0.515	0.462	0.053	0.188	0.065	3.670	0.644	0.254	0.334	0.255	0.313
La	1.7300	10.4600	9.5600	1.0910	4.2100	5.3700	70.3100	2.1000	13.4300	5.4800	6.5200
Ce	3.0100	19.2000	BDL	1.4110	0.5070	10.2000	24.2500	2.6300	7.9700	3.8800	4.9200
Pr	0.3470	2.0700	BDL	0.1402	0.0643	1.2460	16.3700	0.3810	2.0500	0.8660	0.6970
Nd	1.2370	7.6000	BDL	0.5320	0.2090	5.3400	67.4500	1.4600	8.1800	2.9600	2.5800
Sm	0.2180	1.1775	BDL	0.0957	0.0327	1.6125	13.8100	0.3065	1.5700	0.5045	0.5100
Eu	0.0813	0.2575	BDL	0.0381	0.0091	0.7215	3.9050	0.1000	0.4385	0.1326	0.1510
Gd	0.2330	0.7040	BDL	0.1203	0.0148	2.8400	16.4500	0.3050	1.4700	0.3840	0.4530
Tb	0.0370	0.0599	BDL	0.0146	0.0014	0.5350	1.8100	0.0708	0.2130	0.0479	0.0707
Dy	0.3010	0.2910	BDL	0.0860	0.0066	4.0400	8.8500	0.2910	1.4700	0.2590	0.4480
Ho	0.0801	0.0543	BDL	0.0182	0.0034	0.9190	1.2280	0.0636	0.3130	0.0518	0.0964
Er	0.2610	0.1600	0.0031	0.0651	0.0042	3.0100	2.1800	0.1710	0.8760	0.1550	0.2990
Tm	0.0414	0.0186	BDL	0.0080	0.0013	0.4630	0.1780	0.0253	0.1290	0.0216	0.0444
Yb	0.2620	0.1540	BDL	0.0531	0.0069	3.1200	0.7820	0.1700	0.8030	0.1610	0.2730
Lu	0.0487	0.0195	BDL	0.0094	BDL	0.5100	0.0853	0.0277	0.1136	0.0237	0.0428
Y/Ho	31.96	31.68	#VALUE!	32.97	23.54	38.94	21.53	25.47	29.01	24.90	28.32
Eu/Eu*	1.54	1.22	#VALUE!	1.71	1.59	1.37	1.28	1.19	1.25	1.30	1.31

Location	Barite Valley				Barite Valley						
Sample code	**18-BV-30-1**	***18-BV-30-2**	***18-BV-30-3**	***18-BV-30-4**	***18-BV-32-1**	***18-BV-32-2**	***18-BV-32-3**	**18-BV-32-4**	**18-BV-32-5**	**18-BV-32-6**	**18-BV-32-7**
Description	*Green chert close to barite*				*Grey chert below barite*						
Element (ppm)											
Al	7642.810	3702.870	3389.010	3086.940	5516.540	6910.260	4082.550	6117.880	83002.160	11657.870	6997.930
Si	443973.970	443973.970	443973.970	443974.000	443974.000	443974.000	443973.970	443973.970	443974.000	443973.970	443974.000
Ca	654.900	637.260	649.090	535.880	551.830	589.410	561.240	652.130	1431.930	685.150	1009.230
Sc	3.070	2.320	2.430	2.670	1.640	1.500	1.309	1.930	9.980	4.090	3.490
Ti	885.670	154.230	144.160	614.010	591.440	284.910	251.270	392.450	604.350	840.900	623.370
V	14.820	15.600	13.960	9.870	8.820	11.430	7.970	9.870	231.190	38.470	15.440
Cr	81.310	445.950	441.910	432.850	51.490	79.270	46.310	49.570	803.220	167.360	58.370
Mn	1.290	1.770	1.990	5.440	0.983	1.135	0.626	1.210	15.760	3.740	1.880
Co	0.144	0.971	0.572	1.386	0.125	0.171	BDL	0.182	0.519	0.957	0.408
Ni	4.890	14.660	6.170	12.100	4.010	3.600	3.560	4.030	44.130	8.850	7.460
As	3.870	34.640	73.470	128.340	2.820	1.330	0.630	3.100	0.203	69.340	30.080
Rb	12.980	6.080	6.150	5.940	9.280	10.490	6.870	10.260	162.160	21.480	14.180
Sr	3.220	3.870	23.780	6.390	3.670	3.520	3.770	4.050	6.020	58.320	693.510
Y	4.260	0.031	0.063	0.346	0.521	0.504	0.528	0.781	0.041	1.290	0.713
Zr	32.220	0.753	1.183	3.900	3.530	3.740	4.010	5.920	0.371	6.980	6.060
Nb	0.863	0.031	0.035	0.193	1.400	0.447	0.219	0.293	0.372	0.984	0.498
Cs	0.349	0.153	0.154	0.156	0.186	0.207	0.170	0.247	2.400	0.493	0.361
Ba	1259.510	1120.430	3414.270	777.840	992.250	1108.350	966.900	1370.110	17735.750	29363.320	47569.840
Hf	0.838	0.017	0.027	0.080	0.100	0.105	0.114	0.181	0.039	0.209	0.174
Ta	0.085	0.005	0.004	0.009	0.150	0.049	0.016	0.028	0.058	0.106	0.044
Pb	0.960	0.611	1.920	5.410	0.851	1.092	BDL	0.345	BDL	2.830	0.451
Th	0.993	0.008	0.013	0.045	0.230	0.162	0.200	0.255	0.023	0.471	0.326
U	0.587	0.021	0.026	0.118	0.116	0.096	0.171	0.207	0.012	0.287	0.245
La	BDL	2.6100	1.4500	0.4890	0.3310	BDL	BDL	0.3640	0.0065	7.8400	0.9300
Ce	BDL	0.0749	0.1590	0.2710	0.6150	0.5760	0.1490	0.3460	0.0373	9.9800	1.3500
Pr	0.0780	0.0139	0.0228	0.0526	0.0745	0.0578	0.0149	0.0316	0.0068	1.0080	0.1360
Nd	0.3840	0.0547	0.1032	0.2630	0.2200	0.2400	0.0501	0.0853	0.0072	2.7600	0.4040
Sm	0.1605	0.0114	0.0174	0.0539	0.0801	0.0847	0.0152	0.0278	0.0029	0.4200	0.0970
Eu	0.0691	0.0111	0.0194	0.0253	0.0340	0.0297	0.0102	0.0141	0.0403	0.2275	0.3675
Gd	0.3110	0.0063	0.0183	0.0661	0.1019	0.1045	0.0409	0.0429	0.0035	0.3640	0.0950
Tb	0.0766	0.0012	0.0011	0.0092	0.0137	0.0113	0.0098	0.0127	0.0011	0.0495	0.0178
Dy	0.6310	0.0076	0.0118	0.0584	0.0981	0.0858	0.0746	0.1032	0.0058	0.2780	0.1220
Ho	0.1460	0.0010	0.0022	0.0127	0.0197	0.0166	0.0178	0.0173	0.0016	0.0477	0.0278
Er	0.4480	0.0053	0.0054	0.0372	0.0610	0.0275	0.0575	0.0905	0.0055	0.1450	0.0945
Tm	0.0695	0.0005	0.0009	0.0055	0.0060	0.0061	0.0107	0.0127	BDL	0.0211	0.0153
Yb	0.4740	0.0031	0.0058	0.0391	0.0618	0.0476	0.0697	0.0956	0.0020	0.1300	0.0891
Lu	0.0739	0.0008	0.0006	0.0059	0.0075	0.0075	0.0096	0.0145	BDL	0.0176	0.0147
Y/Ho	29.18	30.10	29.12	27.24	26.45	30.36	29.66	45.14	25.40	27.04	25.65
Eu/Eu*	1.07	4.68	6.00	1.94	1.75	1.57	1.37	1.29	40.17	2.52	15.22

Location	Barite Valley							
Sample code	**19-BV-08-1**	**19-BV-08-2**	**19-BV-08-3**	**19-BV-08-4**	**19-BV-08-5**	**19-BV-08-6**	**19-BV-08-7**	**19-BV-08-8**
Description	*Jasper lam.*	*Jasper lam.*	*Jasper lam.*	*Jasper lam.*	*Grey lam.*	*Grey lam.*	*Grey lam.*	*Grey lam.*
Element (ppm)								
Al	263.350	352.130	328.110	180.660	95.280	BDL	BDL	21.900
Si	443974.000	443973.970	443973.970	443974.000	443973.970	443973.970	443973.970	443973.970
Ca	420.800	569.210	467.130	339.080	215.160	113.890	449.770	337.570
Sc	1.630	2.080	1.740	1.590	1.319	1.203	1.410	1.247
Ti	9.400	35.910	36.310	7.570	0.730	0.610	BDL	BDL
V	0.544	0.734	0.713	0.621	0.040	BDL	BDL	BDL
Cr	1.490	3.430	4.950	1.640	0.766	0.636	0.513	0.535
Mn	16.350	31.810	27.740	9.900	7.360	1.300	4.320	4.830
Co	0.151	0.256	0.572	0.124	0.149	0.044	0.047	0.047
Ni	5.420	13.670	7.830	3.950	1.290	BDL	30.190	0.408
As	17.900	35.570	88.310	14.790	12.740	9.010	3.840	27.900
Rb	0.026	0.040	0.041	0.028	0.044	BDL	0.023	0.021
Sr	10.190	12.860	12.940	8.540	2.860	1.049	1.540	1.350
Y	0.435	0.559	0.380	0.342	0.147	0.058	0.066	0.072
Zr	0.046	0.250	0.355	0.080	0.014	0.062	BDL	BDL
Nb	0.018	0.058	0.054	0.024	0.001	BDL	BDL	0.004
Cs	0.117	0.125	0.238	0.098	0.110	0.070	0.113	0.077
Ba	23.040	29.100	36.970	22.470	16.550	7.260	10.780	8.110
Hf	0.002	0.008	0.009	0.003	BDL	BDL	BDL	BDL
Ta	0.001	0.003	0.004	0.001	BDL	BDL	BDL	BDL
Pb	0.780	1.690	1.410	0.683	3.090	0.458	1.130	0.710
Th	0.008	0.013	0.021	0.008	0.002	0.001	0.001	0.001
U	0.004	0.017	0.014	0.005	0.003	0.004	0.002	0.002
La	0.4640	1.1640	0.3600	1.1230	4.8700	BDL	0.0099	1.0380
Ce	0.4590	0.4300	0.3790	0.2880	0.0377	0.0135	0.0149	0.0256
Pr	0.0368	0.0589	0.0643	0.0406	0.0040	0.0013	0.0026	0.0026
Nd	0.1400	0.2160	0.2150	0.1300	0.0194	0.0067	0.0061	0.0114
Sm	0.0276	0.0330	0.0320	0.0271	0.0083	0.0045	0.0041	0.0066
Eu	0.0135	0.0174	0.0194	0.0106	0.0076	BDL	0.0027	0.0036
Gd	0.0390	0.0548	0.0440	0.0385	0.0145	0.0088	0.0091	0.0114
Tb	0.0120	0.0062	0.0058	0.0041	0.0024	0.0010	0.0021	0.0027
Dy	0.0379	0.0534	0.0399	0.0342	0.0161	0.0090	0.0053	0.0049
Ho	0.0082	0.0103	0.0084	0.0080	0.0032	0.0011	0.0022	0.0013
Er	0.0278	0.0316	0.0234	0.0199	0.0074	0.0051	0.0031	0.0029
Tm	0.0035	0.0043	0.0036	0.0034	0.0011	0.0006	0.0006	0.0007
Yb	0.0262	0.0313	0.0241	0.0232	0.0023	0.0033	0.0065	0.0035
Lu	0.0032	0.0054	0.0039	0.0029	0.0011	0.0010	0.0003	0.0006
Y/Ho	52.98	54.27	45.29	42.91	46.08	53.43	29.86	57.01
Eu/Eu*	1.28	2.09	2.45	1.69	2.98	#VALUE!	1.56	1.50

Location	Masenjane									
Sample code	**19-MB-19-1**	**19-MB-19-2**	**19-MB-19-3**	**19-MB-19-4**	**19-MB-19-5**	**19-MB-19-6**	**19-MB-19-7**	**19-MB-19-8**	**19-MB-19-9**	**19-MB-19-10**
Description	*Grey chert vein*						(UiB)	(UiB)	(UiB)	(UiB)
Element (ppm)										
Al	376.080	243.310	404.120	1511.450	737.970	357.900	397.044	389.049	637.200	633.157
Si	467018.750	467018.750	467018.720	467018.750	467018.750	467018.720	467000.000	467000.000	467000.000	467000.000
Ca	542.100	310.680	246.470	401.260	316.040	470.600	125.030	155.356	205.732	90.178
Sc	1.840	1.820	1.650	1.529	1.463	1.570	1.314	1.255	1.410	1.227
Ti	BDL	BDL	0.390	BDL	0.710	BDL	BDL	BDL	BDL	BDL
V	0.121	0.059	0.028	1.121	0.170	0.057	0.106	0.159	0.243	0.048
Cr	0.503	0.442	0.461	3.340	0.971	0.612	6.180	6.664	6.285	5.811
Mn	3.280	0.182	BDL	3.040	2.230	0.487	47.978	85.518	219.608	14.917
Co	BDL	0.373	0.116	0.038	1.079	0.362	0.015	0.030	0.110	0.010
Ni	0.244	0.790	BDL	1.060	2.380	1.000	0.220	0.316	0.358	0.214
As	0.269	1.410	0.506	0.267	4.640	1.770	0.172	0.202	0.221	0.172
Rb	0.635	0.428	0.095	0.313	0.160	0.546	0.819	0.791	0.698	0.649
Sr	2.660	0.939	0.807	82.230	2.080	1.550	2.473	3.527	4.822	1.306
Y	0.132	0.010	0.177	0.107	0.612	0.099	0.326	0.445	0.619	0.333
Zr	BDL	BDL	0.223	BDL	2.680	BDL	0.389	0.289	0.584	0.310
Nb	0.006	0.006	0.004	BDL	0.001	0.004	0.008	0.008	0.009	0.007
Cs	0.348	0.325	0.324	0.284	0.294	0.290	0.434	0.442	0.431	0.418
Ba	201.360	175.510	872.320	5635.230	1388.410	185.220	155.234	159.512	133.574	129.504
Hf	BDL	BDL	0.003	BDL	0.042	BDL	0.018	0.014	0.033	0.015
Ta	BDL	0.001	BDL	0.001	0.001	0.001	0.001	0.001	0.000	0.001
Pb	BDL	0.156	0.075	0.705	1.087	0.298	0.043	0.049	0.061	0.030
Th	BDL	BDL	0.001	BDL	0.002	0.000	0.002	0.002	0.003	0.001
U	0.002	BDL	0.006	0.019	0.068	0.005	0.015	0.014	0.021	0.011
La	1.6000	5.9700	0.0040	0.5960	4.2000	BDL	0.0075	0.0069	0.0139	0.0026
Ce	BDL	BDL	BDL	0.1151	BDL	BDL	0.0117	0.0107	0.0297	0.0041
Pr	BDL	BDL	0.0005	0.0144	0.0010	BDL	0.0017	0.0021	0.0037	0.0009
Nd	BDL	BDL	BDL	0.0236	BDL	BDL	0.0122	0.0082	0.0200	0.0045
Sm	0.0020	BDL	0.0030	0.0065	0.0046	0.0014	0.0025	0.0049	0.0075	0.0031
Eu	BDL	BDL	BDL	0.0221	0.0082	BDL	0.0040	0.0073	0.0082	0.0055
Gd	0.0060	BDL	0.0065	BDL	0.0312	0.0062	0.0152	0.0186	0.0282	0.0168
Tb	0.0017	0.0003	0.0011	0.0016	0.0051	0.0012	0.0047	0.0064	0.0091	0.0046
Dy	0.0172	0.0020	0.0211	0.0120	0.0617	0.0083	0.0345	0.0486	0.0653	0.0340
Ho	0.0032	0.0004	0.0381	0.0024	0.0156	0.0027	0.0108	0.0142	0.0185	0.0095
Er	0.0105	0.0013	0.0144	0.0107	0.0625	0.0098	0.0349	0.0476	0.0652	0.0357
Tm	0.0021	0.0001	0.0016	0.0015	0.0077	0.0011	0.0053	0.0068	0.0087	0.0034
Yb	0.0111	0.0005	0.0075	0.0153	0.0777	0.0080	0.0320	0.0488	0.0587	0.0359
Lu	0.0015	BDL	0.0024	0.0019	0.0130	0.0015	0.0052	0.0080	0.0086	0.0042
Y/Ho	41.38	26.58	4.65	45.66	39.23	36.97	30.28	31.26	33.48	35.06
Eu/Eu*				12.02	2.42		1.40	1.77	1.39	1.91

Location	Masenjane		Masenjane		
Sample code	**19-MB-19-11**	***19-MB-19-12**	***19-MB-24-1**	***19-MB-24-2**	***19-MB-24-3**
Description	(UiB)	(UiB)	*Grey feeder chert crossing barite*		
Element (ppm)					
Al	6337.553	5810.211	9531.960	8603.260	7275.390
Si	467000.000	467000.000	463888.750	463888.750	463888.720
Ca	460.662	126.314	274.110	1414.560	2635.800
Sc	1.353	1.152	3.420	2.240	2.630
Ti	BDL	BDL	2705.960	699.280	1326.090
V	0.541	0.128	120.490	21.020	22.330
Cr	6.050	5.821	1298.820	141.980	152.890
Mn	404.262	82.109	1.710	6.670	50.760
Co	1.120	0.084	4.360	0.687	25.320
Ni	2.161	0.412	42.840	BDL	55.660
As	4.137	0.292	48.460	1.520	45.450
Rb	0.627	0.700	9.450	7.790	6.940
Sr	11.302	2.644	121.880	1584.180	66.810
Y	0.946	0.876	0.286	0.901	0.396
Zr	3.519	0.713	0.844	BDL	4.020
Nb	0.005	0.007	2.670	0.908	1.394
Cs	0.425	0.410	0.847	0.690	0.609
Ba	141.083	144.185	77925.610	290718.410	12252.370
Hf	0.112	0.025	0.012	0.253	0.143
Ta	0.001	0.001	0.158	0.082	0.101
Pb	0.624	0.067	0.602	0.266	1.980
Th	0.007	0.004	0.161	0.662	0.321
U	0.044	0.031	0.181	0.478	0.235
La	0.0263	0.0090	0.1950	0.4480	1.1240
Ce	0.0619	0.0170	0.5740	0.5020	1.7400
Pr	0.0075	0.0026	0.1022	0.2440	0.2240
Nd	0.0382	0.0123	0.3040	0.6140	0.7090
Sm	0.0137	0.0068	0.0530	0.1200	0.0807
Eu	0.0156	0.0126	0.1431	0.7880	0.0145
Gd	0.0452	0.0317	0.0741	0.1400	0.0603
Tb	0.0169	0.0115	0.0078	0.0146	0.0075
Dy	0.1147	0.0961	0.0362	0.1330	0.0615
Ho	0.0320	0.0237	0.0083	0.0281	0.0116
Er	0.1000	0.0849	0.0271	0.0955	0.0465
Tm	0.0162	0.0124	0.0040	0.0200	0.0091
Yb	0.1029	0.0869	0.0317	0.1490	0.0596
Lu	0.0177	0.0109	0.0037	0.0216	0.0101
Y/Ho	29.54	37.05	34.38	32.06	34.14
Eu/Eu*	1.42	1.78	11.73	30.32	0.89